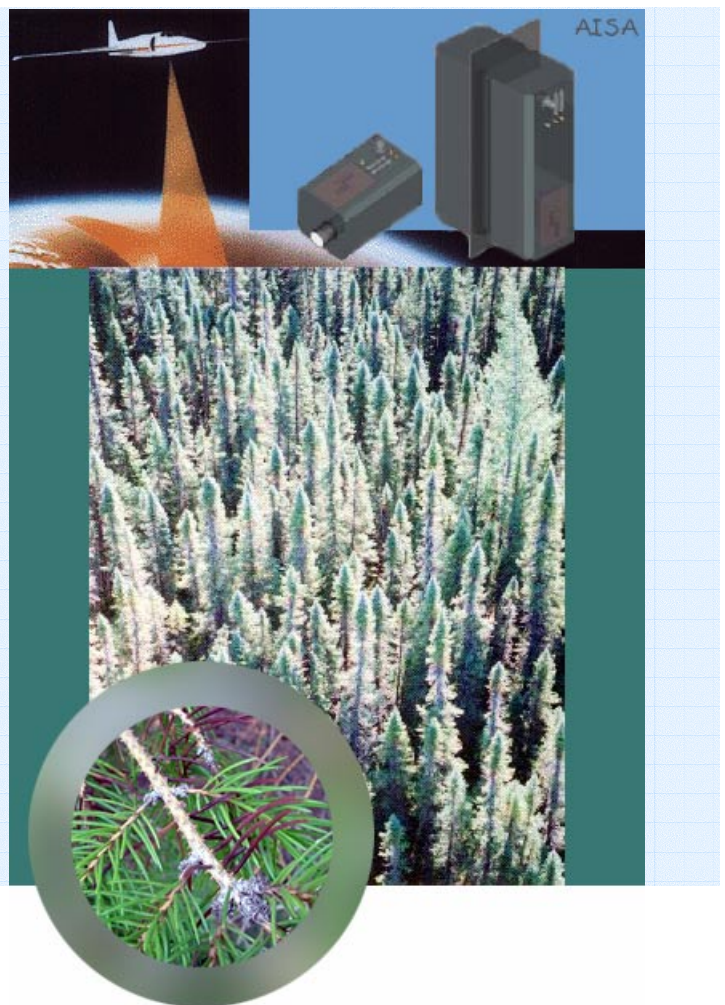# Investigation of Functional Parts and Status of Norway Spruce Crowns Using Spectral Remote Sensing Information

Zbyněk Malenovský

March 2002

WAGENINGEN UNIVERSITY

WAGENINGEN UR

Investigation of Functional Parts and Status of Norway Spruce Crowns Using Spectral Remote Sensing Information

Zbyněk Malenovský[*]

Thesis Report GIRS-2002-25 of the Laboratory of Geo-Information Science and Remote Sensing, Wageningen University, Wageningen (The Netherlands), and a project report submitted to the Remote Sensing Laboratory of the Geological Survey of Finland (GTK), Espoo (Finland)

March 2002

Supervisor: Jan G.P.W. Clevers (WUR)
Consultants: Hilkka Arkimaa (GTK), Viljo Kuosmanen (GTK)

[*] email: ZSf@seznam.cz
    web: http://ZSf.hyperlink.cz

Abstract

In this research two AISA (Airborne Imaging Spectrometer) hyperspectral images (17 spectral channels from 452.6 to 870.3 nm) with high spatial resolution of 1.1 meter were used for an investigation of different functional parts and status of Norway spruce (*Picea abies (L.) K a r s t.*) crowns. Two main objectives were defined for this study. First task was to explore the possibilities to distinguish the juvenile and production part of a spruce crown on the base of their spectral properties, in particular the red-edge inflection point (REIP) calculated from the hyperspectral image. As second task the estimations of chlorophyll content and general health-state were done in frame of spruce crown status assessment. The PROSPECT- SAIL vegetation reflectance model was used to estimate the required attributes for the spruce canopy. Combination of the theoretically derived chlorophyll content and the REIP values defined four categories of spruce forest damage.

Interpretation of one-sample T – test results showed the spectral disparity of the production part and highly damaged juvenile part of the spruce crown. However, the hypothesis about the spectral difference of the juvenile and production crown part at early stress transformation stages was not approved. After all, further research in the field of spruce crown functional part spectrometric characteristics is recommended.

In general a very low multiple stress impact was assessed for the Norway spruce stands of the first AISA image. The analysis of 75 trees from three randomly selected research places showed a slightly more negative crown status (theoretical chlorophyll content of 40 - 100 μg.cm^{-2}; health-state between low damage and very low or no damage) than results of the analysis with coniferous pixels of the whole AISA image (estimated chlorophyll concentration $\geq$ 60 μg.cm^{-2} for 83.5% of the coniferous pixels; spruce crowns with very low or without damage). In case of the second AISA image occurrence of a Cu-Zn sulphide mine partly influenced the crown status of the neighbouring spruce ecosystems. Crowns of 50 spruces, growing in the zone affected by the mining activities, were evaluated as low and/or moderately damaged (estimated chlorophyll content 35 - 70 μg.cm^{-2}). A more positive average crown status was obtained from the evaluation of spruce pixels of seven forest stands chosen at different distances from the strip mine (assessed chlorophyll content $\geq$ 60 μg.cm^{-2} for 49.3% of the observed pixels; crowns with low and very low or no damage).

Acknowledgements

Table of Contents

List of Figures

List of Tables

Glossary of Acronyms

AISA	Airborne Imaging Spectrometer
ASAS	Airborne Solid-state Array Spectroradiometer
CET	Central European Time
CIR	Colour Infrared
CLAPAS	CLAssement de PAysages et Segmentation
DEM	Digital Elevation Model
df	degree of freedom
DN	Digital Number
ENVI	The Environment for Visualizing Images
FWHM	Full-Width-Half-Maximum
FS #	Forest Stand No.
GIS	Geographic Information System
IGN	Inverted Gaussian Model
LAI	Leaf Area Index
LAD	Leaf Angle Distribution
LIDF	Leaf Inclination Distribution Function
MIR	Middle Infrared
NDVI	Normalized Difference Vegetation Index
NE	North-East
NIR	Near Infrared
par	Photosynthetically Active Radiation
PROSPECT	PROpriétés SPECTrales
REIP	Red Edge Inflection Point
REIP_RAD	Red Edge Inflection Point computed from Radiance
REIP_REF	Red Edge Inflection Point computed from Reflectance
RGB	Red Green Blue
RP #	Research Place No.
SAIL	Scattering from Arbitrarily Inclined Leaves
SAM	Spectral Angle Mapper
TTA	Training and Test Area
VIS	Visible part of spectra
WDVI	Weighted Difference Vegetation Index

1. Introduction and Objectives

1.1. Investigation of the Stress Response of Spruce Forest Ecosystems

A lot of research has been done to determine the causes of forest decline in Europe and North America during the last 20 years (Ulrich, 1994). The results show that no single causal factor is responsible for the forest decline and that a synergistic effect of a number of natural and anthropogenic stress factors is probably involved (Innes, 1987). This chronic stress impact (a long term effect with a variable intensity) is from time to time raised by acute biotic and/or abiotic stress events (a short term and extremely intensive attack).

The response of plants to changing environmental factors or stress impacts involves both short term physiological responses and long term physiological, structural, and morphological modifications (Dickson and Isebrands, 1991). Cudlin et al. (2001) developed a method of retrospective evaluation of the response of a mountain Norway spruce ecosystem to multiple stress. This method is based on the crown structure transformation, i.e. formation of secondary shoots of different orders in successive series on damaged and/or defoliated branches (Gruber, 1994). This is a very sensitive indicator for long term tree damage processes (30 – 40 years back) and for the subsequent regenerative processes. The proposed approach traces the retrospective stress response of spruce forest ecosystems during a long time-period to a non-mortal acute and chronic stress action. Limits of this method are an impossibility to distinguish individual stress factors and a necessity to observe the crown structure of each tree separately; therefore it enables us to evaluate relatively small areas of forest stands. Consequently, if the characteristic spectral properties of crown transformation processes would be uncovered, the spruce forest stress response in a larger area could be evaluated through the analysis of high spectral resolution, i.e. hyperspectral, remotely sensed image data.

1.2. Norway Spruce Crown – Structure and Stress Response

During its life cycle the Norway spruce (*Picea abies (L.) K a r s t.*) tree goes through the following three modes of bud-shoot formations (Gruber, 1994):

- *Proleptic shoot formation:* shoot is formed in season *x* from a meristem or developing bud, which is initiated at the beginning of the same season *x*.
- *Regular shoot formation:* shoot is created in year *x*+1 from a winter bud, which is initiated and entirely developed in season *x*. This regular formation, placed at the periphery of the crown, has the function to occupy and maximize the crown space and to defend it against the crown expansion from neighbouring trees, beside a function of assimilate production.
- *Proventitious (secondary;* Cudlín et al., 2001*) shoot formation:* shoot is formed earliest in the season *x*+2 (or later *x*+*n*) of a so-called proventitious bud, which was initiated and developed in season *x*. These secondary shoots are able to establish a highly efficient needle biomass especially in the inner part of the crown, which suffers permanently from high biotic or abiotic stresses, including light deficiency. After complete primary shoot defoliation, secondary shoots can form a new top of the branch. Through the proventitious bud formation the spruce crown possesses a highly developed repair and regeneration system for replacing damaged or lost needles and branches. Therefore, increased formation of secondary shoots should be considered as a powerful tool for spruce tree regeneration after pollutant effects (Gruber, 1994).
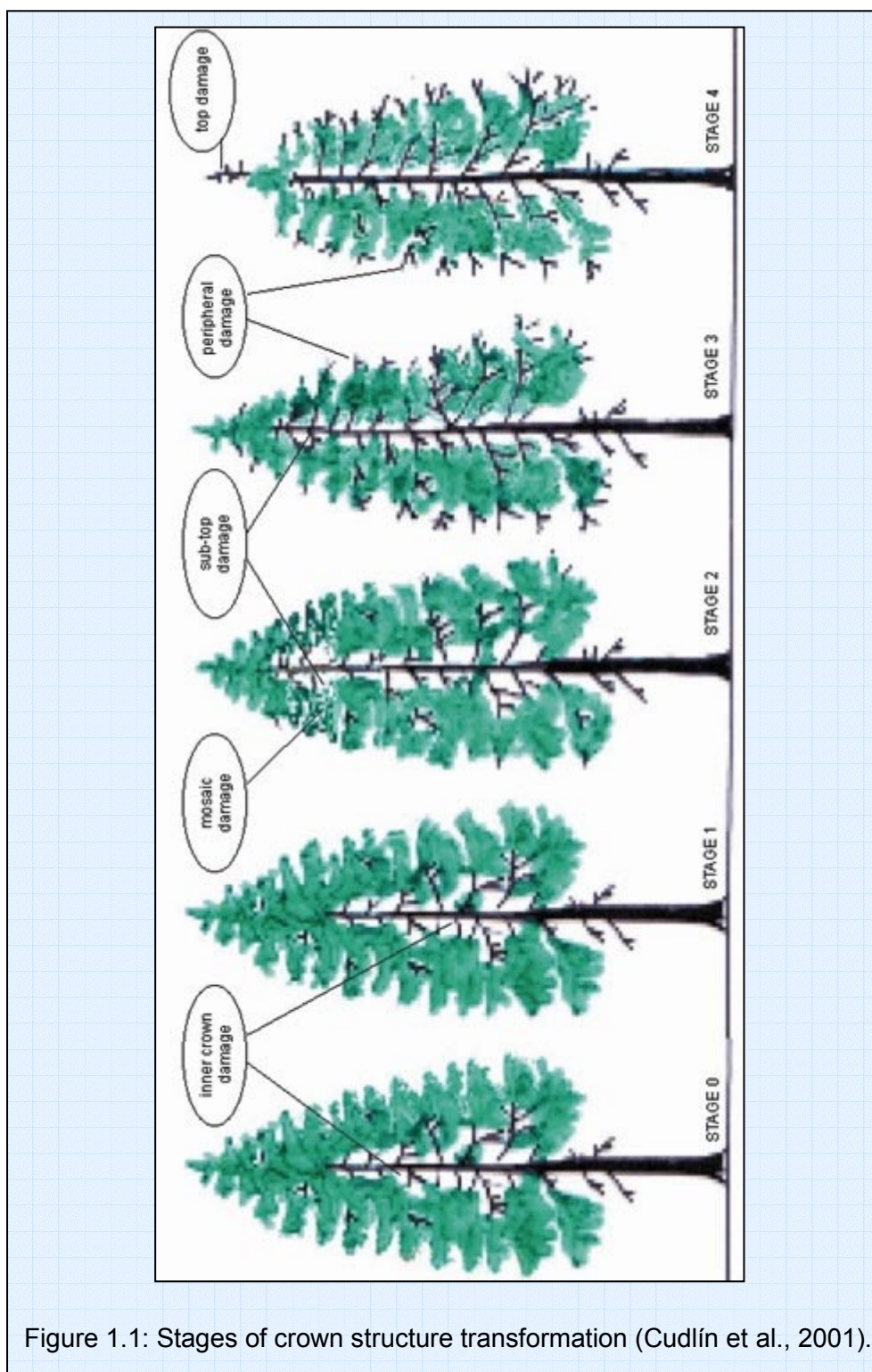
Figure 1.1: Stages of crown structure transformation (Cudlín et al., 2001).

The upper part of the spruce crown, named "juvenile part", is consisting often of proleptic shoot formation. It has as dominant function to colonize new space, and for this reason, the tree protects this part preferentially, even under long-time stress influence. This part shows a strong damage only at the last crown structure transformation stage (see Figure 1.1). The middle part of the crown is named "production part", and supplies most of the tree assimilate production. There the secondary shoots are formed at a different rate according to the ratio of degradation and regenerative processes of this crown part, therefore this part is most

important for observation of spruce damage and stress responses. The last basal part of the crown, called "saturation part", suffers mostly from the lack of light. Its primary structure is almost completely replaced by secondary shoots (Cudlin et al., 2001). A detailed description and illustration of all these crown parts can be found in Appendix 1.

Spruce crown under chronic stress influence changes its architecture according to the impact intensity and its duration. Cudlín et al. (2001) established five progressive stages of crown transformation (see Figure 1.1):

Stage 0 – small defoliation of the stem and/or mosaic type (estimated for branches of the second order), percentage of secondary shoots less than 20 %.

Stage 1 – defoliation of the stem and/or mosaic type, counteracted by scattered secondary shoot formation, percentage of secondary shoots from 21 to 50 %.

Stage 2 – incipient peripheral (ends of primary branches) injury, sometime sub-top injury, often in combination with stem and/or mosaic type, percentage of secondary shoots from 51 to 80 %.

Stage 3 – peripheral injury prevailing, sometime top injury, often in combination with previous injury types, percentage of secondary shoots from 81 to 99 %.

Stage 4 – peripheral injury occurring by all branches of the middle part of the crown, sometime top injury, often in combination with previous injury types, percentage of secondary shoots 100 %.

1.3.   Monitoring of Norway Spruce Ecosystems by Remote Sensing

From a historical point of view colour infrared (CIR) aerial photography was very popular among foresters for monitoring forests. In 1991 the European Community proposed in its manual a complete forest health status assessment based on the visual interpretation of airborne CIR images. The interpretation keys for spruce (*Picea abies*), beech (*Fagus sylvatica*), oak (*Quercus sp.*), pine (*Pinus sylvestris*), and Silver fir (*Abies alba*) have been created on the base of individual tree crown colour, shape, and texture (Commission of the European Communities and Directorate-General for Agriculture, 1991). Although, the CIR images might have a fine spatial resolution, the richness of their spectral resolution is not comparable with multispectral images, which consist of several separate bands taking into account visible and infrared parts of the spectrum (VIS, NIR, MIR, etc.). Since the eighties a lot of studies using multispectral images for evaluation of forest damage have been carried out, particularly for coniferous mountain forests (Ardö et al., 1997; Vogelmann and Rock, 1988). For instance, Lambert et al. (1995) distinguished 3 health categories (Light, Moderate, and Heavy damage – accuracy 83-95 %) for Norway spruce stands of the Ore Mts. (Krušné Hory, Czech Republic) using a Landsat TM image. In general, a disadvantage of multispectral data is represented by broad spectral bands, which only allow identification of visible forest damage. At present, a hyperspectral type of RS data has enabled the observation of initial subtle "pre-visual" tree reactions against stress impacts (Entcheva, 2000). These initial stress changes at the level of cellular tissues invoke a spectral response effect of vegetation called "blue shift of the chlorophyll red edge", which is the shift of the reflectance curve of a leaf at the red-edge region (680-740 nm) towards shorter wavelengths (Horler et al., 1983; Rock et al., 1988). It can be measured by the wavelength position of an optical index called red-edge inflection point (REIP), determined by the level of red and NIR reflectance (Hoshizaki et al., 1988; Moos and Rock, 1991, Vogelmann et al., 1993). Entcheva (2000) used ASAS (Advanced Solid-state Array Spectroradiometer) aerial hyperspectral images of Norway spruce stands from Ore Mts. (spatial resolution: 1.5 – 2 m; spectral resolution: 62 bands from 417.0 – 1025.2 nm, full-width-half-maximum c. 12 nm) to distinguish 5 classes of damage (combination of percent defoliation and chlorosis) through reflectance and derivate indices (e.g. REIP). Besides the main influencing factor, represented by the amount of foliar pigments (chlorophyll a+b), the reflectance indices were able to describe the bio-chemical cellular properties (concentration of cellulose, lignin,

tannins, starch, sugar, etc.) that could be used as bio-indicators of vegetation damage too (Kokaly and Clark, 1999).

Fine spectral resolution remotely sensed data might be statistically analysed to estimate the concentration of biochemical constituents in a forest canopy (Johnson et al., 1994; Wessman et al., 1989). Such information has been used to drive simulation models for estimation of photosynthetic efficiency and the degree of vegetation stress (Curran, 1994).

Remote sensing uses spectral modelling, that consists of an abstract and simplified version of reality, to simulate the vegetation reflectance at leaf and canopy level, respectively. At leaf level, a radiative transfer model for individual leaves called PROSPECT (Jacquemoud and Baret, 1990) has been successfully used in a lot of studies. The conifer leaf model LIBERTY was designed by Dawson et al. (1998) to model accurately the spectral response of pine needles. At canopy level more reflectance models have been created. One of the most popular models is the SAIL model (Verhoef, 1984), which was followed by the IAPI model (Iaquinta and Pinty, 1994), KUUSK model (Kuusk, 1995), and NADI model (Gobron et al., 1997). 3-D spatial distribution of canopy architecture has been taken in consideration in the 3-D canopy model DART (Demarez and Gastellu-Etchegorry, 2000). The simulated reflectance of some vegetation models (SAIL, IAPI, KUUSK, NADI) and their sensitivity to their input parameters has been compared and the results proved their reciprocal coherency (Bacour et al., 2002). Radiative transfer models for vegetation serve as a basis for extracting vegetation variables using directional/spectral data from modern sensors (Kimes et al., 2002). However, laboratory analysis of the relationships between vegetation reflectance and biochemical concentrations are still important to verify the interpretation of the remotely sensed spectral information (O'Neil et al., 2002). Thus, reflectance models play an important role in the interconnection of field and/or laboratory vegetation reflectance and presently also for chlorophyll fluorescence observations of vegetation obtained from remote sensing image data (Zarco-Tejada et al., 2000).

1.4.   Objectives

1.4.1. *Spectral Response of Spruce Crown Functional Parts*

The functional crown parts of Norway spruce are built by different bud-shoot formations and, moreover, their bio-chemical processes differ from each other (intensity of photosynthesis, assimilate flow, etc.). Therefore, there is a valid assumption that their spectral characteristics (reflectance) could be different, too. The tree especially protects and supports growth of the juvenile crown part (3-5 latest whorls), which is responsible for vertical increment and colonisation of new space. For this reason, this crown part reflects the long-term stress impacts only after long influence duration. The stress response of the saturation part is usually strongly influenced by the lack of direct sunlight (it has low photosynthetic activity). Consequently, the production part of the crown is expected to be the more appropriate and significant section for long term (chronic) multiple stress response detection due to the strongest reactions at the leaf and shoot level, as well within crown architecture changes.

On that account, the first objective of this study was to test the hypothesis that the juvenile and production part of a stressed (damaged) and an unstressed spruce crown have a different spectral response in the Red and NIR part of the electromagnetic spectrum and that this spectral disparity can be observed with high spatial resolution hyperspectral data. The red edge inflection point (REIP) was used as a spectral tool for analysing the stress response of the crown of spruces.

1.4.2. *Status of Norway Spruce Crowns*

The canopy chlorophyll concentration is one of the main factors determining plant photosynthetic capability. Together with the REIP it can be used as an indicator for the evaluation of canopy status, particularly the health-state of vegetation. Maps of those relatively simple vegetation attributes (chlorophyll content and the REIP) may be combined to infer and monitor the spatial distribution of complex vegetation attributes as for instance the level of vegetation damage.

The second aim of this study was to investigate and evaluate the status of Norway spruce crowns of a forested area close to Pyhäsalmi (Finland) using two hyperspectral AISA images. A map of the chlorophyll amount of spruce crowns was created through simulations with a PROSPECT-SAIL vegetation reflectance model. This map, with considerable contribution of the REIP map, should provide the base for a general damage assessment of the Norway spruce forest stands, which can finally be visualised as the map of estimated health-state of observed spruce crowns.

1.5.   Set-up of the Report

In chapter 1 an overview of the present scientific knowledge about the stress response of the Norway spruce forests, the spruce crown structure, and remote sensing methods used for the monitoring of the forest ecosystems was presented. Also both scientific objectives of this study were described here.

Chapter 2 explains the methodological approach of the study. It starts with the input data description and continues through pre-processing of the images to the classification procedures used for the two AISA images. Also an alternative accuracy assessment of the classifications is described, which we introduced due to the lack of ground truth data. Basic information about the used vegetation indices (REIP and WDVI) is available there. Finally, an inversion method for estimation of the chlorophyll content and health-state of the spruce crowns from the hyperspectral images using the PROSAIL reflectance model is depicted in this chapter.

Chapter 3 shows the results of the visual and automatic classifications. The error matrices for each classification are presented. Three statistical analyses were provided to test the behaviour of the REIP values within selected spruce crowns and to explore a potential spectral difference of two spruce crown functional parts. In the end an evaluation of spruce crown status (i.e. estimation of the chlorophyll content and health-state assessment) was done for both AISA images at two levels.

Several comments concerning the weak points of the image processing (especially about the classifications and multi-resolution image segmentation) are discussed in chapter 4. The potential interpretations of the results from accomplished statistical tests about the REIP are given there. At last, recommendations about the spruce canopy reflectance modelling and remarks about the maps of chlorophyll content and spruce health-state are stated in this chapter.

The conclusions, declared in chapter 5, give the direct answers on the scientific questions and hypothesis defined in chapter 1 as the objectives of this study.

2. Material and Methods

2.1. Overall Methodology

Figure 2.1 provides a flowchart illustrating the overall methodology applied in this study. Each step of this methodological approach is discussed in the subsequent sections of this chapter.

Figure 2.1: Flowchart illustrating the overall methodological approach.
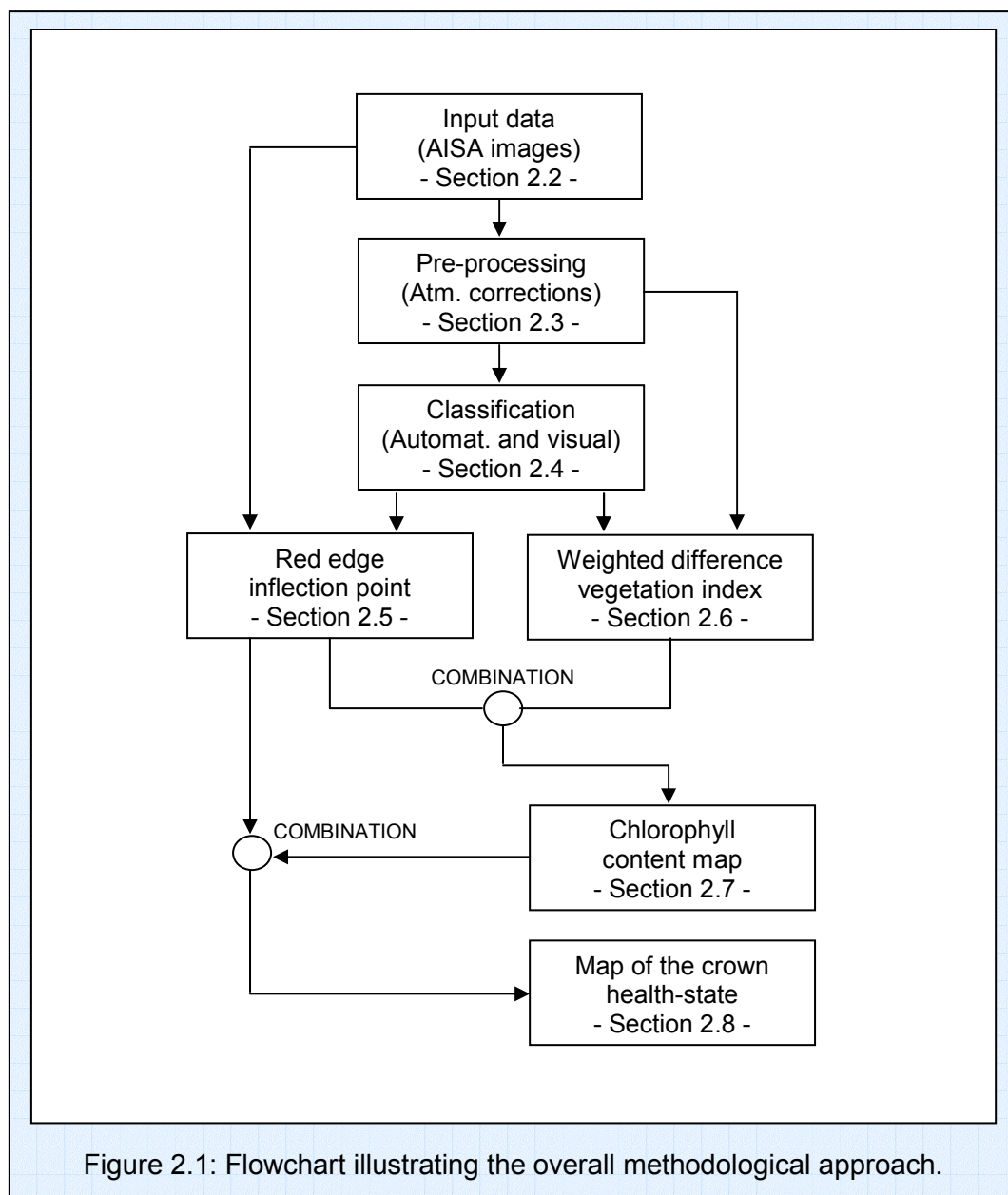
2.2. Input Data

The input data available for this study were two AISA (Airborne Imaging Spectrometer) hyperspectral image mosaics of the area lying south-eastern of a small city called Pyhäsalmi, almost in the middle of Finland, from September 7th 1999 (see Figure 2.2).

AISA is a low-cost imaging spectrometer that was designed from the beginning for both research and operational work. It uses a CCD sensor matrix with 384 columns and 286 rows. The CCD sensor and the optical system limit the wavelength range, which for the AISA of Metla (Finnish Forest Research Institute) is 450 - 870 nm. The spatial mode of the AISA sensor was used during the campaign over Pyhäsalmi. It was possible to collect 17 spectral channels with the exposure time used during the flights. The channel configuration used in this study is shown together with a vegetation spectrum collected using the spectral mode of the AISA in Figure 2.3 and Table 2.1. At an altitude of 1100 meters used during the flights a spatial resolution of 1.1 m was reached.

When imaging a target area, the aircraft typically flies in several adjacent lines over the site. This resulted into image strips, which have been orthorectified using a digital elevation model (DEM) of 25 m pixel size into one geo-coded image mosaic. For geo-coding the Finnish KKJ (Uniform Zone [27°E]) map projection system was used.

The radiometric correction performed on the image transformed the raw data into units of radiance as "seen" by the instrument. To compensate the effects due to the elevation of the Sun, the radiance data was normalised to the same solar time using a Lambertian model. The atmospheric corrections were performed only for the AISA image no. 2 – "West".

Figure 2.2: Location of the "East" and "West" AISA image covering the study area.
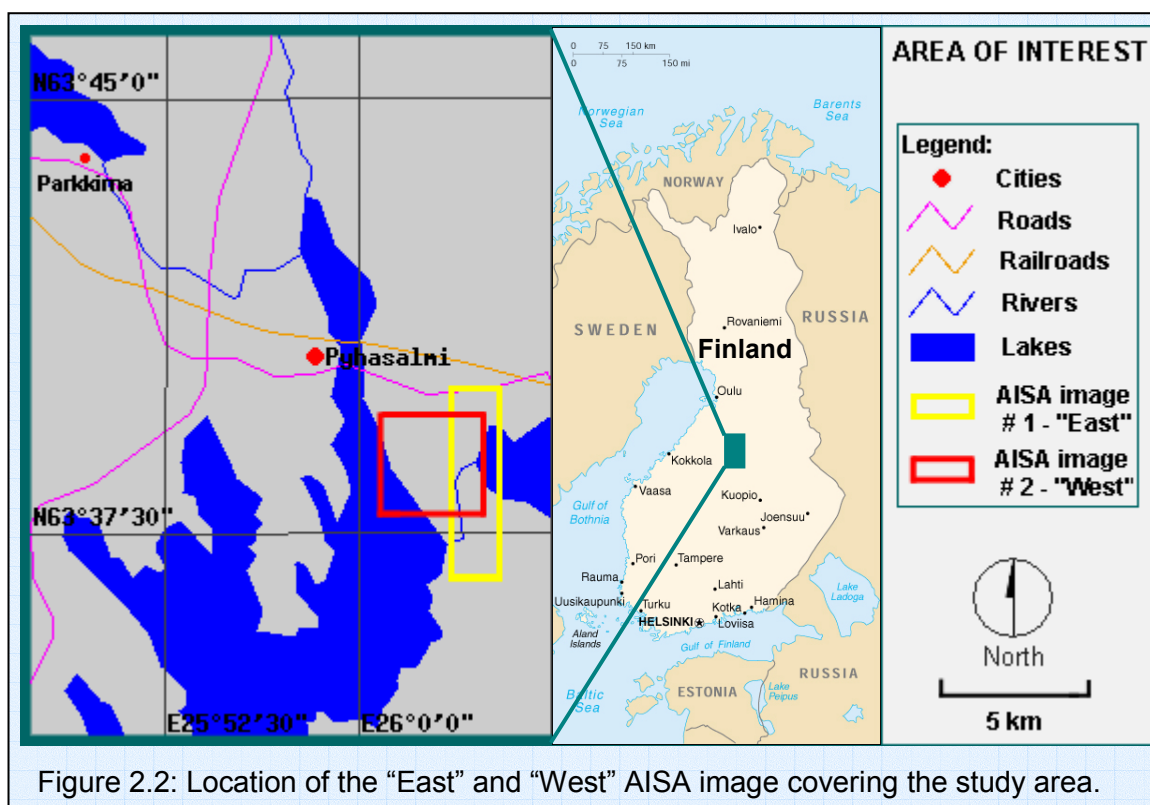
The AISA sensor owned by the Finnish Forest Research Institute was used in this campaign carried out for the Geological Survey of Finland in 1999. All image pre-processing described above was done in the frame of the flight campaign, not in the frame of this study.
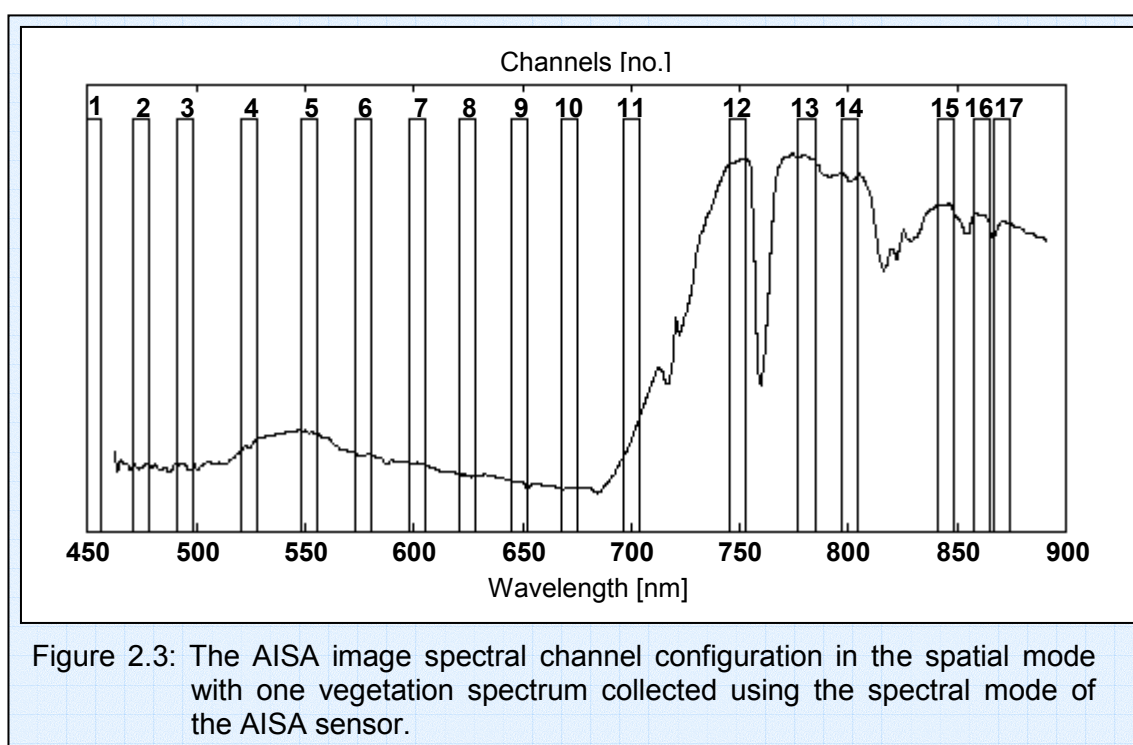
Figure 2.3: The AISA image spectral channel configuration in the spatial mode with one vegetation spectrum collected using the spectral mode of the AISA sensor.

Table 2.1: The spectral band positions of the AISA images.

No.	Centre [nm]	Width [nm]	No.	Centre [nm]	Width [nm]	No.	Centre [nm]	Width [nm]
1	452.6	7.3	7	601.2	7.3	13	780.7	7.6
2	474.5	7.3	8	624.6	7.3	14	800.4	7.6
3	494.9	7.3	9	648.5	7.6	15	844.5	7.6
4	524.0	7.3	10	671.3	7.6	16	861.2	7.6
5	551.7	7.3	11	700.2	7.6	17	870.3	7.6
6	576.5	7.3	12	748.8	7.6			

Realization of the whole study was split up in two separate blocks due to the different level of pre-processing and background information of the input AISA images.

There was no ground truth information about forest ecosystems for the AISA image no. 1 (working name "East") available at the time of this study. Remote sensing analysis without any ground truth terrain exploration, and without ancillary maps (for instance map of land use, map of forest stands, etc.) is very hard and almost impossible. On this account, the results of some analysis over this image have got a relatively high uncertainty.

The AISA image no. 2 (working name "West") contained Norway spruce stands damaged by a nearby Cu-Zn sulphide mine. Its harmful influence on the forest stands has been directly observed during the terrain exploration and the damage of forest stands has been mapped and recorded into a vector polygon file. The vector file contained the polygon limits of the spruce trees where the damage had been found, and a second polygon draws the boundary of the Cu-Zn sulphide dust spread. Unfortunately, the terrain ancillary data showed just damage and/or dust occurrence, but not a qualitative evaluation of spruce stress response nor quantitative values of dust distribution from the Cu-Zn sulphide mine were mentioned. Therefore, the interpretation of the Norway spruce injury type, which was found on the AISA image, was very difficult.

2.3. Pre-processing – Atmospheric Corrections

To be able to compare the contents of remote sensing images, taken at different observation dates and times, meaning during different atmospheric conditions, at different altitudes with different sensor systems, with one other, atmospheric corrections must be performed (Clevers, 2001).

To grant this ability the Empirical Line atmospheric calibration (Kruse et al., 1990) was applied to the "East" AISA image using the ENVI 3.4 software. This correction uses a linear regression for each band to equate DN and reflectance. This is equivalent to removing the solar irradiance and the atmospheric path radiance. The following regression equation shows the relationship between reflectance and radiance (ENVI User's Guide, 2000):

Reflectance (field spectrum) = offset coefficient + gain coefficient x radiance (DN - input data)

A laboratory measured reference spectrum of two targets, a black and a white target (panel), in combination with their spectral response from AISA imagery, was used to fit the regression line and to compute offset and gain coefficient values for each band separately. Then the gain and offset coefficients were applied to the radiance spectra for each pixel of the "East" AISA image to produce apparent reflectance on a pixel-by-pixel basis.

The values for solar irradiance E_0 and atmospheric "path" radiance L_a, for each channel of the AISA imagery, computed during the Empirical Line procedure are depicted in Figure 2.4.
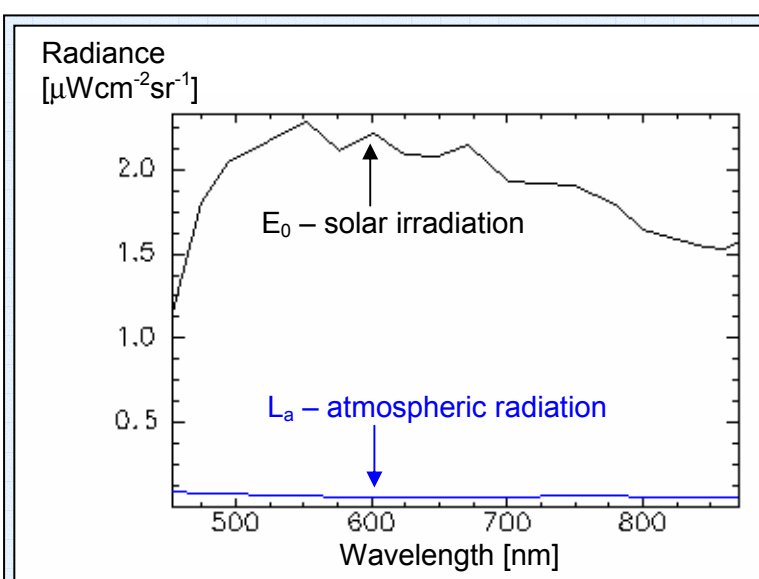
Figure 2.4: Solar irradiation and atmospheric radiation for channels of the "East" AISA image.

Processing of the AISA image no. 2 – "West" was a little easier due to the advanced level of its pre-processing and more available background information. This image has been atmospherically corrected at the Remote Sensing Laboratory of the Geological Survey of Finland.

2.4. Classification of Land Use and Forest Categories

This study was focused on the observation of the Norway spruce (*Picea abies (L.) Karst.*) crowns. Therefore, first a selection of Norway spruce forest stands, as the objects of research, had to be performed through a classification. An assumption was that all coniferous forest stands of the AISA image no. 1 – "East" were supposed to be composed mainly of the Norway spruce trees. If there were some other coniferous species inside the coniferous stands, for instance Scotch pine (*Pinus sylvestris L.*), we supposed that those species were in minor occurrence and we did not take them in consideration, because their classification without any ancillary information would be impossible.

The whole classification process of the "East" image contained the following steps: a visual classification of the main land use categories and some homogenous forest patches, an automatic classification of forest classes, evaluation of the automatic forest classification, and generalization of the forest class's map. Finally, the visual classification map was overlaid with the generalized forest map to obtain a thematic map of land use and forest categories (see Figure 2.5).

Figure 2.5: Flowchart of the AISA image no. 1 classification process.
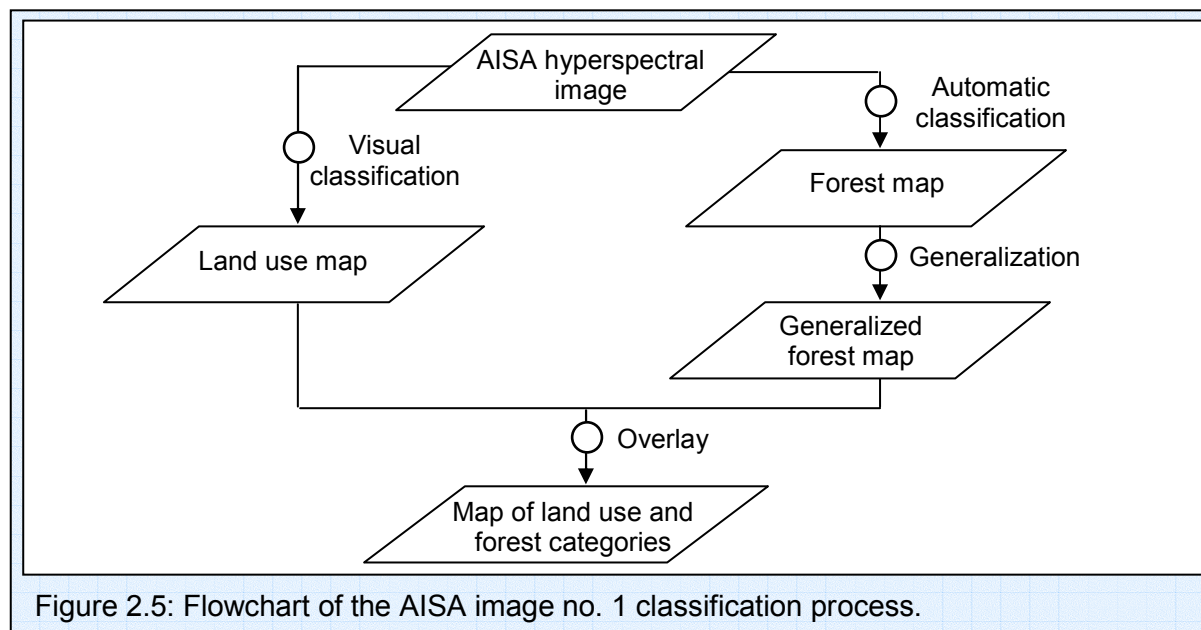
2.4.1. Visual Classification

By visual interpretation of coloured RGB composites of the AISA image the following classes were distinguished: urban area, agriculture area, open water (lake), river, main roads, and no data (data gaps after orthorectification). Beside these categories, visually distinguishable homogenous forest patches like clear cuts, forest breaks, tree plantations, and young trees were classified. For visual interpretation we used the natural coloured RGB composition of AISA channels 8, 5, and 3 and also 12, 10, 7 RGB composition in unnatural colours.

2.4.2. Automatic Classification

<u>"EAST" AISA Image</u>

An automatic processing is a very quick and effective tool in the field of classification. The automatic classification of the image is a universal method for sorting pixels of the image to the classes of ground occupation, in accordance with their reflectance characteristics. In general, classifications are divided into unsupervised or supervised ones (Schowengerdt, 1983). The supervised Maximum Likelihood classifier was chosen for our purpose as a main classification method.

Regrettably for automatic classification, the "East" AISA image was produced as a mosaic of several flight lines. Once combined into a single large image, there were remarkable differences in reflectance values between crowns of the same tree species as one can see in Figure 2.6. These differences are a result of the bidirectional reflectance factor inherent to forest canopies, and the geometric relationship among the sensor, sun and target positions (Fish et al., 1995). Different reflectance levels of the same tree species are due to the combined effect of the looking angle of the sensor and the sun zenith angle. The AISA

instrument recorded the shadow side of trees within one flight line and the sunny side of the trees in the next flight line. This is a natural and unavoidable effect in areas of low sun zenith angles like Finland (Kuosmanen, personal communication).

Figure 2.6: A comparison of two Norway spruce crown reflectance profiles from the different flight lines of the "East" AISA image mosaic.
The reflectance curves of the central ("top") pixels of two Norway spruce crowns placed in two different flight lines were carried out. As one can see, the maximum NIR reflectance of a crown from the right-up part of AISA image slide is about 40%, it means significantly higher than the peak of NIR reflectance of the second left-down tree crown, which is only about 25%.

For this reason, the original channels of the "East" AISA image mosaic could not be directly used for automatic classification of forest categories, and therefore five transformed bands were created from it. The transformations were in general based on spectral rationing of channels, because this is an appropriate way for compensating the undesirable reflectance differences within an AISA image (Lillesand and Kiefer, 2000). First band was computed as a ratio of channels 12 (NIR) / 10 (Red). Second band was the ratio of channels 5 (Green) / 7 (Red). The Normalized Difference Vegetation Index (NDVI = (NIR-Red)/(NIR+Red)) was computed from channels 12 (NIR) and 10 (Red), and considered as the third transformed band. Next two bands were computed for the edge sharpening and isolation via a Roberts high-frequency filter. The Roberts filter is a non-linear edge detector filter similar to the Sobel filter. It is a special case filter that uses a preset 2 x 2 approximation of the true Roberts function, a simple two-dimensional differencing method (ENVI User's Guide, 2000). To build up the fourth band the Roberts filter of band 1, the ratio of channels 12 and 10, was used with 60% of "adding back" part of the original band, which helps to preserve the spatial context of the image. It means that 60% of the original image is added to 40% of the convolution filter image to produce the final result. The fifth band was made through Roberts filtering of the NDVI image with 20% of "adding back" part of the original image. All these transformed bands represented the input to the Maximum Likelihood Classification.

Before the classification a mask of already classified areas was generated from results of the visual interpretation. This mask was laid over the transformed bands. The supervised classification requires training of the reflectance of homogenous sets corresponding with the

defined classes. The following classes were trained over the transformed "East" AISA image: deciduous trees, coniferous trees, roads, bare soil (partly covered by low vegetation) and shadows. Finally, the Maximum Likelihood classification with a probability threshold of 75% was provided.

The AISA image was captured in autumn (September) 1999, when some of the deciduous trees started the discolouring process. These discoloured trees were easily identified in the image as a special class by the Spectral Angle Mapper (SAM) classification (Kruse et al., 1993). SAM is a minimum-angle procedure that was specifically designed for use of hyperspectral images in combination with a spectral curve library. The spectral curve of discoloured vegetation is significantly different from the spectral profile of green vegetation especially in the red (chlorophyll absorption) part of the electromagnetic spectrum (see Figure 2.7), which allowed easy classification of discoloured deciduous trees using the SAM classifier. The classified discoloured trees were finally joined to the Maximum Likelihood classification as a new category.
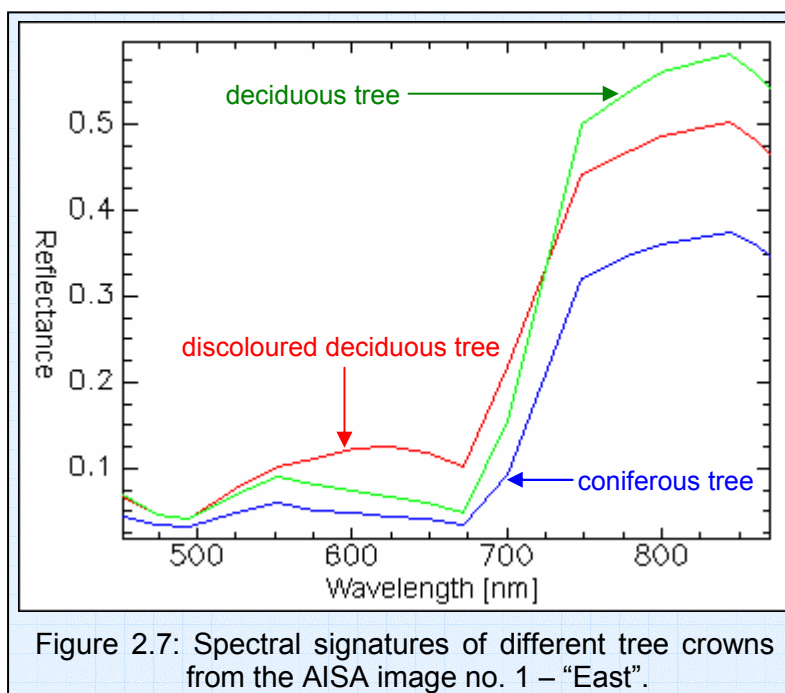
Figure 2.7: Spectral signatures of different tree crowns from the AISA image no. 1 – "East".

"WEST" AISA Image

Unlike the "East" AISA image ground truth data was supplied by the Remote Sensing Laboratory of the Geological Survey of Finland for the "West" AISA image. Therefore, during the terrain investigation seven relatively homogeneous Norway spruce forest stands were chosen in different distances from the Cu-Zn sulphide mine as study objects (see Appendix 10).

For the study aims, it was necessary to eliminate non-spruce and shadowed pixels of forests stands and to identify just the pure Norway spruce pixels inside the forest stands (FSs). For this purpose we used the Spectral Angle Mapper (SAM) classifier (Kruse et al., 1993). A spectral library of four present spectral signatures (deciduous trees, coniferous trees, discoloured vegetation, and shadows) was generated from the "West" AISA image (see Figure 2.8). Because there was not a significant difference in spectral behaviour of the same tree species caused by the effect of sensor looking angle and sun zenith angle (see Figure 2.6) inside of the FSs, the original AISA band could be taken as the classification inputs.

2.4.3. Evaluation of Automatic Classification

"EAST" AISA Image

As was stated by Lillesand and Kiefer (2000), a classification is not concluded when its exactness and success is not evaluated. Because of lack of terrain data the ordinary method for this assessment, i.e. an error matrix of classification results against ground truth classes, could not be used. An alternative solution has been chosen to evaluate the results of the

Maximum Likelihood classification. A second automatic classification of the same categories based on a completely different approach was executed. If the results of both classifications are identical, then the classification could be declared as approved.
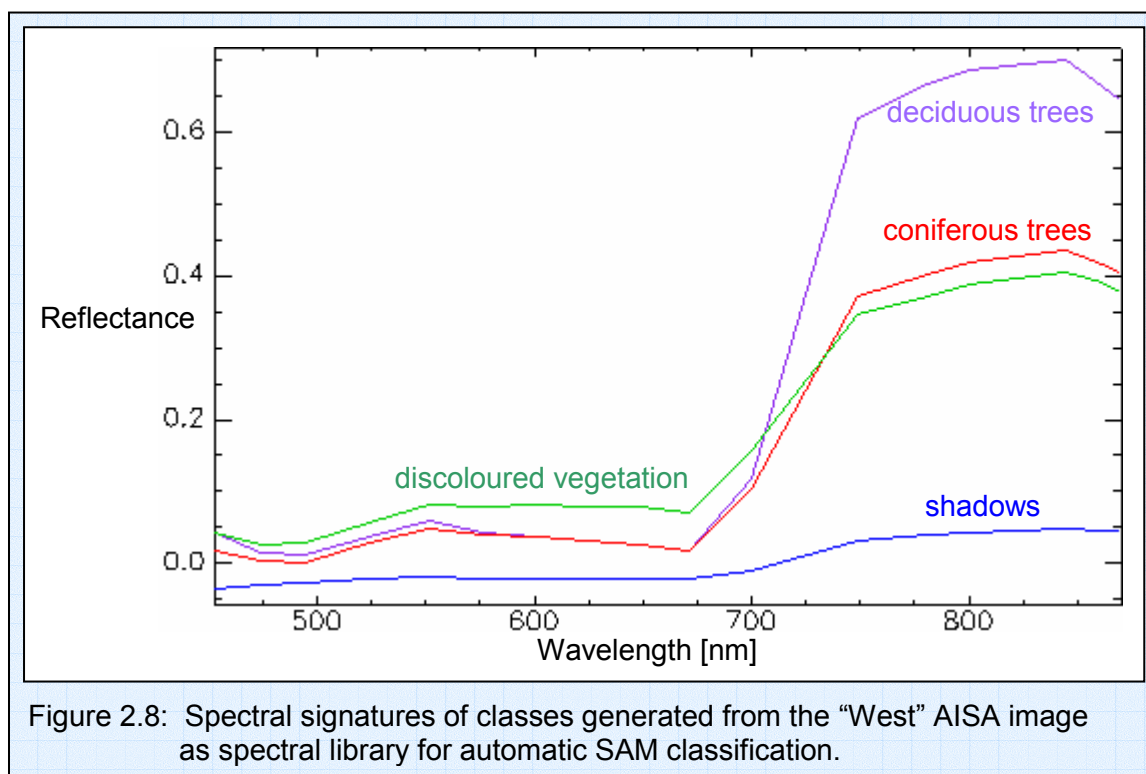
Figure 2.8: Spectral signatures of classes generated from the "West" AISA image as spectral library for automatic SAM classification.

To compare results of different classification logics, the object-oriented image processing provided by eCognition software was used for a second classification. This treatment has two main steps. First, a multiresolution segmentation of homogeneous image objects is performed on base of colour, texture and form of image objects. In the second step classification of these objects is done, in our case supervised classification called Nearest Neighbor. Nearest Neighbor classifies image objects in a given feature space and with given samples for the classes of concern. The algorithm looks for the closest sample objects for each image object in the determined feature space (Baatz et al., 2000).

Unfortunately only a demo version of the eCognition software, with some functional limits, was available during this project. Due to the limit of maximal processed image size, a raster of 545 x 1035 pixels from the "East" AISA transformed image (5 transformed bands) was selected as input into the object-oriented analysis. For segmentation of homogenous objects the scale parameter 2 and normal segmentation mode were used. Homogeneity criteria for the segmentation were set as follows: colour 80%, shape 20% (smoothness 60% and compactness 40%). After segmentation we have got 169 504 homogenous objects, from 564 075 incoming pixels, with an average object size of 3.33 pixels. Then the supervised Nearest Neighbor classification was performed for the segments of the categories: discoloured vegetation, deciduous trees, coniferous trees, roads, bare soil (partly covered by low vegetation) and shadows. The defined raster, cut from the result of the Maximum Likelihood classification, was uploaded to eCognition as a Training and Test Area (TTA) Mask. This TTA Mask usually represents the ground truth data sets in the evaluation process. In the end the error matrix of the Nearest Neighbor classification against the Maximum Likelihood classification was computed to compare their correlation.

"WEST" AISA Image

Because of lack of ground truth data, an alternative classification accuracy assessment was used again. The Nearest Neighbor classification of the same categories based on the

object-oriented image processing including a multi-resolution segmentation of homogeneous image objects (criterions: colour 40%, shape 60% - smoothness 60%, compactness 40%; 22897 homogenous objects with an average size of 3.39 pixels) was performed for the FS #1. Then the resultant map of the Nearest Neighbor classifier was used in an error matrix against the SAM classification as ground truth information. In case of comparable results we can declare the classification as approved.

2.4.4. *Generalization of the Forest Map – "East" AISA Image*

Because we used as the main automatic classification procedure for the high spatial resolution AISA image a pixel-by-pixel based procedure, the resulting classification map had a heterogeneous structure (see Figure 3.1). That means there are many isolated pixels, or small groups of pixels, whose classification is different from that of their neighbours at the thematic map. These pixels posed "noise" for the perception and interpretation of features at the resultant map composition, and therefore it is necessary to eliminate them through a method of generalization (Malenovský, 2001).
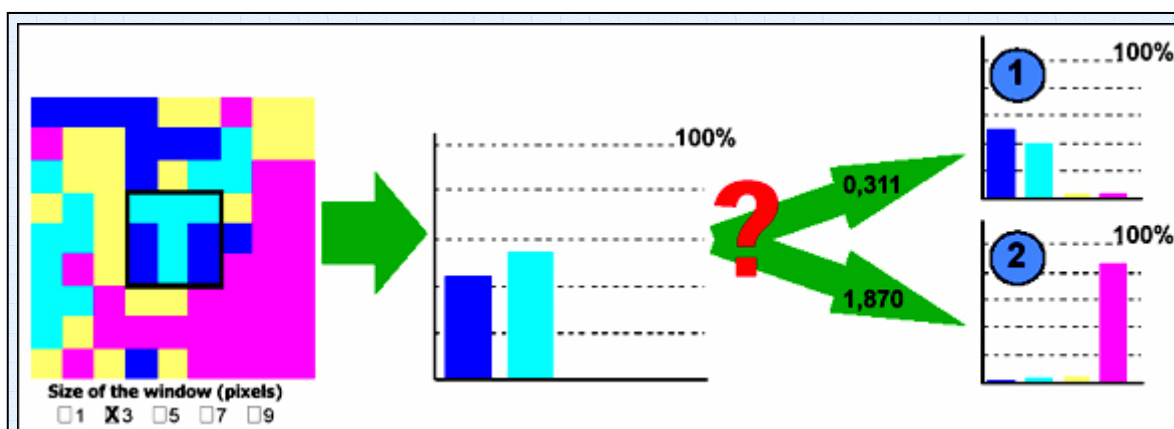
Figure 2.9: Calculation and classification of a pixel within the distance vector during the CLAPAS processing.
For a centre cell point of the image having 4 classes (left) the frequency histogram is calculated (centre) from the defined square-window of 3x3 pixels. In this sample, the investigated pixel will be placed in the class of Reference Landscape ① (right-up), because that distance vector value of 0.311 is smaller than the distance vector of 1.870 for the second Reference Landscape ②.

For this purpose we used a modal majority filter in combination with a specific method called CLAPAS (*CLAssement de PAysages et Segmentation* – Classifying landscapes) developed by Robbez-Masson (1994).

CLAPAS is a technique to achieve classification of pixels of an image under a particular cover frequency algorithm. This program is useful for processing, at each cell point, to which category of so-called Reference Landscapes the point must be classified, taking into account the composition of its neighbourhood. This neighbourhood of a pixel point is a variable sized square-window centred at this point. The indispensable elements of the proceeding are Reference Landscapes defined by their frequency histograms. CLAPAS computes a mathematical cover-frequency distance vector between the frequency histogram of the observed pixel point neighbourhood (for every defined size of the square-windows) and all assigned Reference Landscape histograms. Finally, it places the investigated pixel into the class of the Reference Landscape, which has the shortest cover-frequency vector distance (for all sizes of square-windows). This is illustrated in Figure 2.9. This process is repeated for each pixel of an image. More detailed information about CLAPAS can be found in Robbez-

Masson et al. (1996) and Meunier-Caldairou (1999) or at the ENSA de Montpellier web site: http://sol.ensam.inra.fr/Clapas/Default.asp.

Because this study was focused on properties of coniferous forest stands, Norway spruce crowns in particular, the number of input categories to CLAPAS could be reduced from originally seven to four, when the shadows and roads joined the unclassified category and discoloured deciduous vegetation was merged with deciduous trees. Our frequency histograms of Reference Landscapes were developed through vector polygons delimited from the reclassified Maximum Likelihood map. Finally, we established four Reference Landscapes: deciduous forest, coniferous forest, mixed forest and bare soil with low vegetation. The particular percent composition of all these Reference Landscape histograms is given in Table 2.2. In CLAPAS we used the Manhattan distance method to compute the cover-frequency vectors, with as size of minimum investigated neighbourhood 13 and as maximum 15 pixels. A low pass Mode filter, choosing for the central pixel the most frequently occurring value in a kernel, with a 7 x 7 kernel followed the CLAPAS execution to delete the isolated pixels and improve the resulting forest map.

Table 2.2: Frequency histograms for the Reference Landscapes created from categories of the Maximum Likelihood classification.

CLASS Ref. Landsc.	unclassified [%]	deciduous [%]	coniferous [%]	bare soil [%]
deciduous forest	38.54	47.40	13.99	0.06
coniferous forest	56.91	4.88	38.18	0.03
mixed forest	50.73	14.43	34.73	0.11
bare soil with low veg.	45.53	16.25	4.49	33.73

2.5. Red Edge Inflection Point

The Red Edge Inflection Point (REIP) is defined as the inflection point of the Red Near-infrared reflectance curve slope. Its accurate determination requires measurement of a large number of very small spectral bands in this region (Clevers, 1994). Clevers applied three procedures for estimating the REIP values. First, a polynomial function may be fitted to the data (Clevers and Büker, 1991). Secondly, an inverted Gaussian fit to the Red Near-infrared slope (Bonham-Carter, 1988), working with an Inverted Gaussian Model (IGM) introduced by Hare et al. (1984) and Miller et al. (1985), could be applied. Finally, the third method is a simple linear model of Guyot and Baret (1988) using only four wavelength bands.

Due to the low number of AISA channels in the Red and NIR part of the electromagnetic spectrum (see Table 2.1), we were able to use only the last so-called "method of Guyot" to compute REIP values. This method uses reflectance measurements at about 670, 700, 740 and 780 nm. First of all, the reflectance value at the inflection point halfway minimum (at 670 nm) and maximum (at 780 nm) reflectance is estimated. Secondly, a linear interpolation method is applied between the measurements at 700 and 740 nm for estimating the wavelength corresponding to the estimated reflectance value at the inflection point. In our case the reflectance measurements at 670, 700, 740 and 780 nm were substituted by the measurements at 671.3, 700.2, 748.8 and 780.7 nm (AISA channels no. 10, 11, 12 and 13). The "method of Guyot" was used via following equations:

Calculation of the reflectance at the inflection point:

$$R_{REIP} = \frac{(R_{671.3} + R_{780.7})}{2} \qquad [1]$$

Calculation of the REIP wavelength:

$$\lambda_{REIP} = 700.2 + 48.6 * \left(\frac{(R_{REIP} - R_{700.2})}{(R_{748.8} - R_{700.2})} \right) \qquad [2]$$

where R_{REIP} is the estimated reflectance value at the main inflection point.
$R_{671.3}$, $R_{748.8}$, $R_{700.2}$ and $R_{780.7}$ are the reflectance values at 671.3, 700.2, 748.8 and 780.7 nm.

According to the previous studies, focused on the influence of leaf and plant properties and external factors on the position of the REIP (Clevers, 1994), the main influence is represented by varying Leaf Area Index (LAI) and amount of chlorophyll. Mesophyll structure causes a small shift of the REIP position to longer wavelengths up to value N=3, whereas higher N values do not change the REIP position. The leaf inclination angle has only a small influence on the REIP position, as well as the solar zenith angle above 60°. Finally, the soil reflectance has hardly any influence on the REIP wavelength, and also atmospheric conditions do not change the position of the REIP (Guyot et al., 1988).

2.6.   Weighted Difference Vegetation Index

Clevers (1989) described a simplified reflectance model for estimating the LAI of a green canopy based on a "corrected" NIR reflectance. This reflectance, called WDVI (weighted difference vegetation index), is ascertained as a weighted difference between the measured NIR and Red reflectance, assuming that the ratio between NIR and Red reflectances for bare soil is constant, independent of soil moisture content (this assumption is valid for many soil types). The values of WDVI are given by:

$$WDVI = r_{NIR} - C * r_{Red}$$

where r_{NIR} is total measured NIR reflectance
       r_{Red} is total measured Red reflectance
and

$$C = r_{s,\ NIR} / r_{s,\ Red}$$

with $r_{s,\ NIR}$ = NIR reflectance of the bare soil
       $r_{s,\ Red}$ = Red reflectance of the bare soil.

2.7.   Chlorophyll Content Map

The decrease in vegetative chlorophyll concentration during the growth cycle has been shown to cause a "blue shift" effect of the REIP (Horler et al., 1983). The so-called PROSAIL model, a combination of the leaf reflectance model PROSPECT (Baret et al., 1992) and the canopy radiative transfer model SAIL (Verhoef, 1984) modified to include the hot spot effect (Kuusk, 1991), was used in this study for the theoretical estimation of chlorophyll content within the spruce crowns at the area of interest. Four categories of Norway spruce damage were specified through combination of the REIP and WDVI values computed from the AISA images and connected with the PROSAIL canopy reflectance simulations.

2.7.1. SAIL and PROSPECT Reflectance Models

SAIL is a one-layer radiative transfer model (Verhoef, 1998) and it simulates canopy reflectance as a function of the parameters: canopy properties (leaf reflectance and transmittance, LAI and LAD - leaf angle distribution), soil reflectance, ratio diffuse/direct irradiation and solar-view geometry characteristics (solar zenith angle, zenith view angle, and sun-view azimuth angle). The SAIL model has been extended with the hot spot effect by introducing a hot spot size-parameter, which equals the ratio of horizontal correlation length

and canopy height (Kuusk, 1985). Verhoef and Bunnik (1981) introduced the leaf inclination distribution functions (LIDF) used by the SAIL model.

The PROSPECT reflectance model for individual leaves, developed by Jacquemoud and Baret (1990), is based on the generalized "plate model" of Allen et al. (1969), which considers a compact theoretical plant leaf as a transparent plate. The "plate model" described diffuse reflectance and transmittance of a compact leaf by two parameters: n – refractive index, and k – absorption coefficient showing improvements upon the Kubelka-Munk formulation. An actual leaf is supposed to be composed of a pile of N homogenous compact layers separated by N-1 air spaces. The thickness of the air spaces of layer separation was taken as infinitesimal. The compact leaf (N=1) has no intercellular air spaces of the mesophyll or the water has infiltrated them. The PROSPECT model allows computing the reflectance and transmittance spectra from 400 to 2500 nm for different kinds of leaves using as input variables: leaf mesophyll structure parameter N, chlorophyll content and water content. Since the output of the PROSPECT model equals the input for the SAIL model, a combined PROSAIL model was made from them (Clevers et al., 1994).

2.7.2. PROSAIL Parameter Assumptions

First of all, the PROSAIL input of leaf and canopy parameters, sun-view geometric properties and radiation characteristics had to be estimated.

Leaf and canopy parameters included the mesophyll structure parameter N, the leaf angle distribution functions, hot spot parameter and water content. Dicotyledons leaves, which are characterized by a spongy parenchyma with air cavities on the abaxial face, have N values ranging from 1.5 to 2.5 (Jacquemoud and Baret, 1990). Monocotyledon leaves with a compact mesophyll, including also the spruce needles, have N values between 1 and 1.5. For our study the upper limit of N = 1.5 was used. LAD was set as spherical (Verhoef and Bunnik, 1981), what is the most heterogeneous combination of leaf inclination distributions close to the natural distribution of spruce needles. The hot spot parameter for a Norway spruce tree was assumed 0.001. The water content (equivalent water thickness) was an unimportant variable, because the absorption features of water and foliar pigments are clearly spectrally separated. The water domain is 800-2500 nm, but we were focused on the reflectance of pigments from 400 to 800 nm. However, as a model requirement the equivalent water thickness of 0.008 cm was estimated for the spruce needle, by expert judgement.

AISA is a hyperspectral pushbroom type of sensor with an instrument field of view of 21°. Concerning the sun-view geometric variables, the viewing zenith angle was set for nadir view of the sensor at 0°. The solar zenith angle θ_s on September 7th was computed for the central point of the "East" AISA image mosaic with the latitude φ = 63° 38' 24.77'' N and longitude λ = 26° 04' 37.63'' E by the equation of Hykš and Hraška (1990):

$$\theta_s = 90° - (arc\ sin\ (sin\ \varphi\ .\ sin\ \delta - cos\ \varphi\ .\ cos\ \delta\ .\ cos\ \tau)) \qquad [3]$$

where φ is the latitude

δ is the sun declination computed by:

$$\delta = 23.45°\ sin\ (29.7°\ M + 0.98°\ D - 109°) \qquad [4]$$

M ...... ordinal number of month in year
D ...... ordinal number of day in month

τ is the clock angle computed by:

$$\qquad [5]$$

$$\tau = 15° (H - 12)$$

H ...... real sun time given by:

$$H = \left(CET + \frac{4 * (\lambda - 15°)}{60°} - \eta \right) - 1 \qquad [6]$$

CET ...... Central European Time (in summer period – 1)
λ .... the longitude
η............. a time correction between central and real sun time given by:

$$\eta = 0.125 \sin (0.98° \ D + 29.7° \ M - 32°) + 0.165 \sin (1.96° \ D + 59.4° \ M - 38°) \ [7]$$

The values of the solar zenith angle θ_s on September 7th from 7.00 till 19.00 CET are shown in Table 2.3. For the PROSAIL modelling of both AISA images we used the value for real sun noon: $\theta_s = 58°$.

Table 2.3: Solar zenith angle θ_s on September 7th from 7.00 till 19.00 CET.

CET [hour]	H [hour]	τ [°]	θ_s [°]
7.00	6.0962	-88.5572	84.0
8.00	7.0962	-73.5572	77.4
9.00	8.0962	-58.5572	71.1
10.00	9.0962	-43.5572	65.6
11.00	10.0962	-28.5572	61.2
12.00	11.0962	-13.5572	58.5
13.00	12.0962	1.4428	57.6
14.00	13.0962	16.4428	58.9
15.00	14.0962	31.4428	61.9
16.00	15.0962	46.4428	66.5
17.00	16.0962	61.4428	72.3
18.00	17.0962	76.4428	78.6
19.00	18.0962	91.4428	85.3

Next parameter was soil reflectance in the Red and NIR part of the spectrum. This variable was computed directly from the AISA images as the NIR reflectance average of a bare soil training set with a matrix size of 100 x 100 pixels. Consequently, the resulting soil reflectance was set to 18% for the "East" and 29% for the "West" AISA image. The last demanded variable was the ratio diffuse/direct (total) irradiation. As shown by Clevers and Verhoef (1993) this ratio has only minor influence on the WDVI, which was a main objective of our spectral simulation modelling. For that reason, we used a value of zero (100% of direct irradiation) for our purpose.

2.7.3. PROSAIL Model Inversion

First step of the PROSAIL reflectance modelling was a simulation of the REIP as a function of different chlorophyll contents (5 - 80 μg cm^{-2}) and for various values of LAI (0.5 – 8) (see Table 2.4). In the next step simulated reflectance curves of the spruce canopy were determined for each combination of chlorophyll content and LAI. From these reflectance values, corresponding with 10th and 12th AISA channels, the WDVI was computed for all chlorophyll – LAI combinations (see Table 2.5). Constant C was obtained from the AISA images as a reflectance ratio of the channel 12 and 10 for a bare soil matrix of 150 x 150 pixels (C = NIR / Red = 18.20% / 13.13% = 1.386 for the "East" AISA image; C =

29.10% / 20.21% = 1.440 for the "West" AISA image). Finally, both simulations were merged into a nomogram illustrating the relationship of the REIP position and WDVI values through several combinations of LAI and chlorophyll content for both AISA images separately. The values of differently assumed or computed parameters (Red and NIR soil reflectance, constant C) had such minor influence on the modelling process that we obtained the same resultant REIP-WDVI nomogram for both AISA images (see Figure 2.10). This nomogram can now be used as a simple tool for PROSAIL model inversion.

Table 2.4: Matrix of the REIP values for several combinations of LAI and chlorophyll content.

REIP [nm]		LAI				
		0.5	1	2	4	8
Chlorophyll content [$\mu g\ cm^{-2}$]	5	696.5	698.4	701.2	704.3	706.3
	10	701.8	703.5	705.8	708.3	710.1
	15	704.7	706.2	708.3	710.6	712.5
	20	706.6	708.0	710.0	712.4	714.5
	30	709.3	710.5	712.6	715.3	718.0
	40	711.1	712.4	714.6	717.9	721.0
	60	713.9	715.4	718.1	722.5	726.6
	80	716.1	717.9	721.4	726.9	731.9

Table 2.5: Matrix of the WDVI values for several combinations of LAI and chlorophyll content.

WDVI [%]		LAI				
		0.5	1	2	4	8
Chlorophyll content [$\mu g\ cm^{-2}$]	5	2.11	9.12	19.05	29.77	36.65
	10	5.53	14.33	25.58	36.60	43.36
	15	7.14	16.61	28.22	39.19	45.82
	20	8.02	17.82	29.54	40.41	46.89
	30	8.85	18.92	30.66	41.30	47.55
	40	9.19	19.34	31.00	41.43	47.45
	60	9.37	19.49	30.96	41.01	46.62
	80	9.33	19.38	30.66	40.37	45.64

2.8.   Map of the Crown Health-state

The REIP-WDVI nomogram, obtained from the PROSAIL reflectance modelling using the AISA images, was split into 20 sectors for chlorophyll content estimation of spruce crowns (see Figure 2.10). These sectors were reclassified into nine categories of chlorophyll content, which were then combined into four health-state classes of Norway spruce crowns based on the REIP ranges (see Table 2.6).

Table 2.6: Categories of chlorophyll amount and health-state for spruce crowns.

Combination of REIP-WDVI	Chlorophyll content ch [$\mu g.cm^{-2}$]	REIP [nm]	Health-state
I.A, I.B, I.C, I.D	ch < 20	REIP < 706	High damage
II.C, II.D	5 - 30	706 - 711	
II.A, II.B, III.D	10 - 40	706 - 718	Moderate damage
III.C	15 - 60	711 - 718	
III.B, IV.D	20 - 80	711 - 727	Low damage
III.A	30 - 100	711 - 718	
IV.C	40 - 100	718 - 727	Very low or no damage
IV.B, V.C, V.D	60 - 120	718 - 727 or REIP $\geq$ 727	
IV.A, V.A, V.B	ch $\geq$ 80	718 - 727 or REIP $\geq$ 727	

Figure 2.10: Nomogram of the REIP and WDVI relation for several combinations of LAI and chlorophyll content, how it was simulated by PROSAIL model. *20 sectors of the REIP-WDVI combinations (right) were specified for a chlorophyll amount estimation of Norway spruce crowns from the AISA images.*
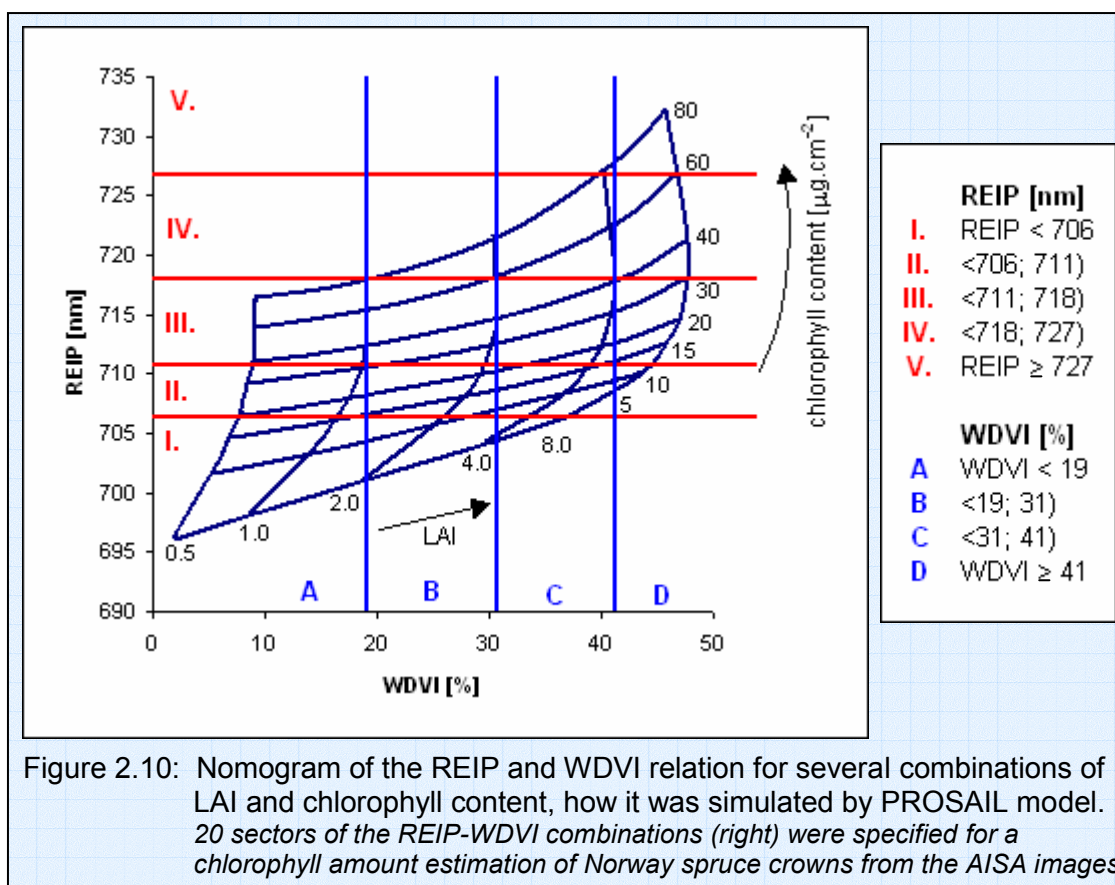
3. Results

3.1. Classification Results and Accuracy Assessment

<u>"EAST" AISA Image</u>

The resultant map composition of the Maximum Likelihood as well as Nearest Neighbor automatic classification for part of the whole image is depicted in Figure 3.1.

Figure 3.1: The windows cut out from results of the Maximum Likelihood classification (right) and the Nearest Neighbor classification after the segmentation of homogenous objects (left).
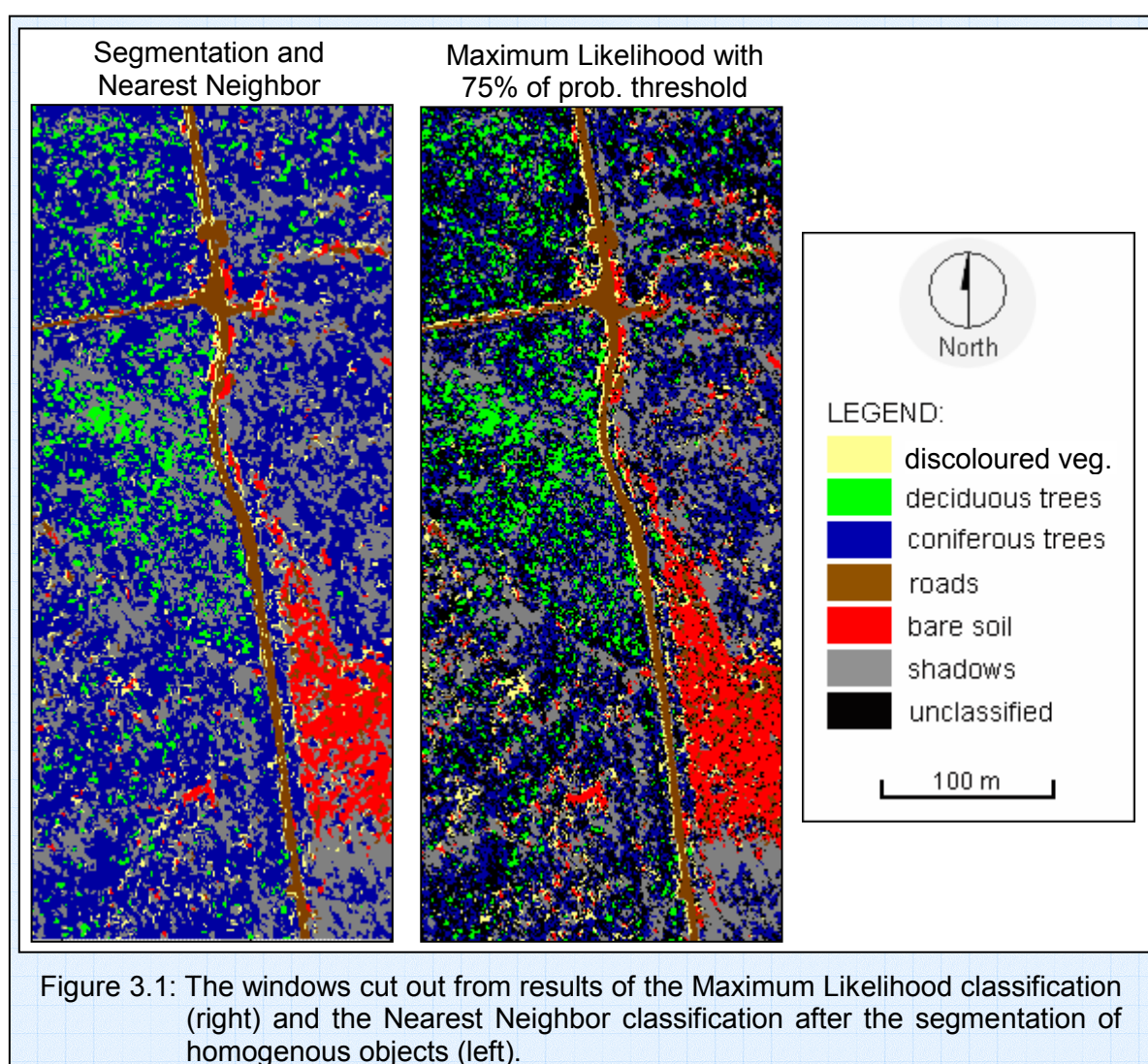
Table 3.1 shows the results of the automatic classification accuracy assessment. In general there was significant correlation between both classification results in all classes, except for discoloured vegetation. The mean correspondence of all categories was 64.0%. The main problematic class was discoloured vegetation with a recognition rate of only 21.4%. 62.7% of the pixels of this class from Nearest Neighbor classification were in the case of the Maximum Likelihood classifier assigned to coniferous trees, 7.8% to roads, 4.5% to bare soil, and 3.4% to shadow. Most interesting for our purposes was a substitution of deciduous and coniferous trees. 37.2% of deciduous objects from Nearest Neighbor were identified as coniferous by the Maximum Likelihood method. Important is also the trade-off between

coniferous trees and shadows, where 24.2% of the coniferous pixels from Nearest Neighbor were assigned to the shadows class during Maximum Likelihood. Other replacements of classes are not so much important for our study, besides 13.6% shadows and 5.7% bare soil objects placed in Maximum Likelihood to the coniferous category.

Table 3.1: Error matrix of the Nearest Neighbor classification (columns) against the Maximum Likelihood classification (rows).

CLASS [%]	discoloured veg.	deciduous	coniferous	roads	bare soil	shadows	SUM [%]
discoloured veg.	**21.4**	0.2	62.7	7.8	4.5	3.4	100.0
deciduous	0.1	**60.7**	37.2	0.0	0.0	1.5	100.0
coniferous	0.3	0.2	**75.3**	0.0	0.0	24.2	100.0
roads	10.5	0.0	0.0	**70.5**	13.4	5.6	100.0
bare soil	0.8	0.0	5.7	0.8	**72.2**	20.5	100.0
shadows	1.5	0.0	13.6	0.9	0.0	**83.9**	100.0

In the last step of the whole classification process the generalized forest map was superimposed by the land use map of visual interpretation to make a final map of land use and forest categories (see Figure 2.5). This final map of the "East" AISA image classification can be found in Appendix 2.

"WEST" AISA Image

Figure 3.2 shows the results of the SAM and Nearest Neighbor classification for the forest stand no. 1.

Figure 3.2: The results of SAM classification (left) and Nearest Neighbor classification including the segmentation of homogenous objects (right) – FS #1.
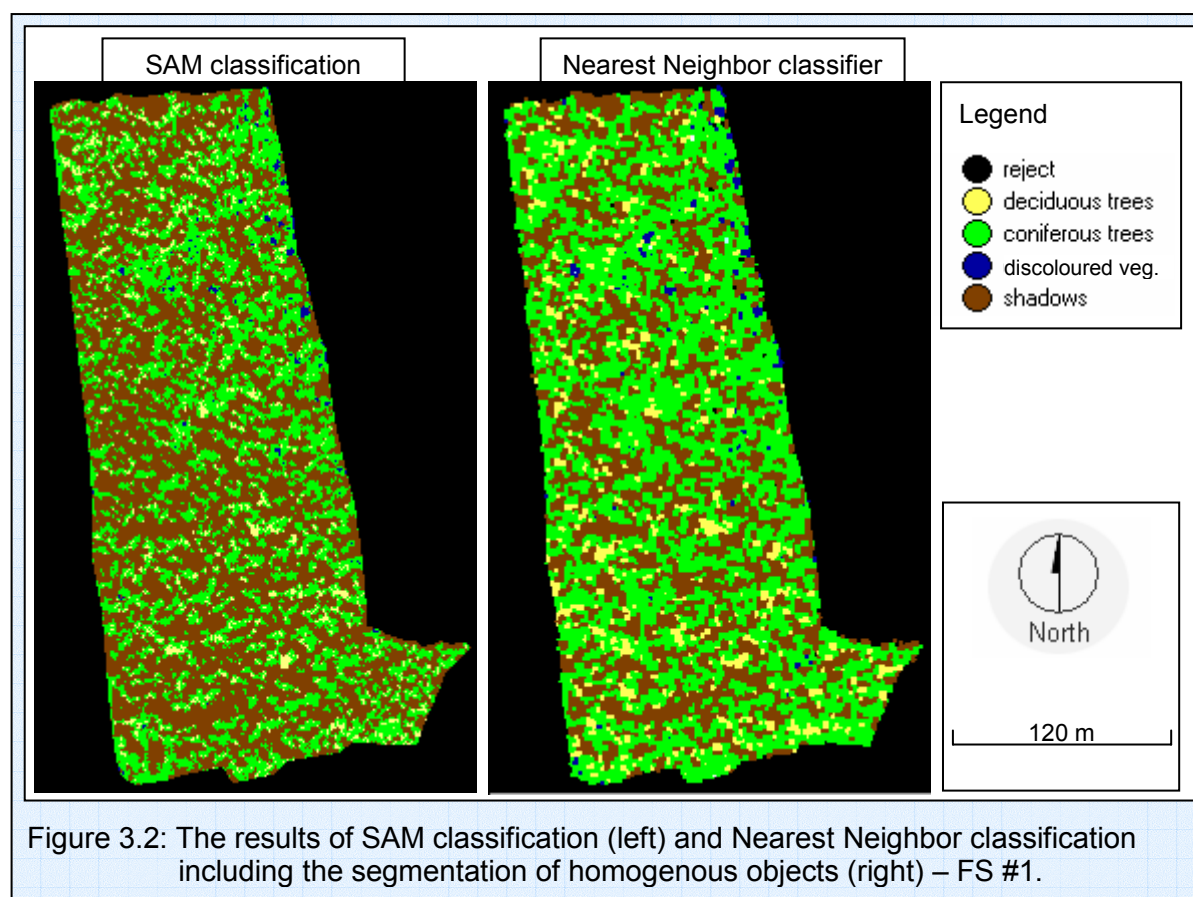
According to the error matrix (see Table 3.2) one can conclude that the SAM classification distinguished significantly more shadow pixels against less coniferous pixels than the Nearest Neighbor classifier. This fact can be explained by a multi-resolution segmentation,

provided in frame of the Nearest Neighbor classification, where the dark pixels of Norway spruces and shadowed pixels were taken on account of the same segment. There is also a discrepancy concerning deciduous trees, discoloured vegetation and the coniferous class, but the number of these pixels is low, thus unimportant from a general point of view. Finally, there is a high correspondence for the category of coniferous trees (spruce crowns) which is the objective of this study, therefore we decided to use the pixels of Norway spruces classified by the SAM algorithm in the next procedures as fully proved.

Table 3.2: Error matrix of the SAM classification (columns) against the Nearest Neighbor classification (rows) of forest stand #1.

CLASS [pixels]	deciduous	coniferous	discoloured veg.	shadows	SUM
deciduous	**464**	1933	1	1023	3421
coniferous	1825	**12415**	123	8764	23127
discoloured veg.	0	299	**118**	31	448
shadows	32	660	1	**15642**	16335
SUM	2321	15307	243	25460	43331

3.2. Results of the REIP Analyses

3.2.1. Comparison of the REIP Values Computed from Radiance and from Reflectance after Atmospheric Corrections

Guyot et al. (1988) stated that the position of the REIP is unaffected by atmospheric conditions. It means the REIP computed from radiance before atmospheric corrections should correspond with the REIP computed from reflectance of the AISA image no. 1 – "East" after atmospheric correction.

Two sets of 80 REIP values of pixels representing the Norway spruce crowns were selected to verify this statement for the case of our image. The first set of the REIP was computed from the "East" AISA image before providing the atmospheric corrections and the second set from the same imagery after these corrections. The paired T - test was used to test correspondence of the REIP values of the same pixels.

In the sample, the REIP computed from reflectance is 718.11 nm on average and the REIP from radiance is on average 716.43 nm. The mean difference between the REIP from reflectance and radiance is 1.69 nm.

The null hypothesis of this test states that there is no difference between the mean REIP from these two AISA images. A difference of 1.69 nm departs significantly from zero with value of $t = 47.74$ at the probability level equal to 0.05. Therefore, the null hypothesis can be rejected. From Figure 3.3 one can see that the REIP computed from reflectance (REIP_REF) is systematically higher than the REIP from radiance (REIP_RAD).
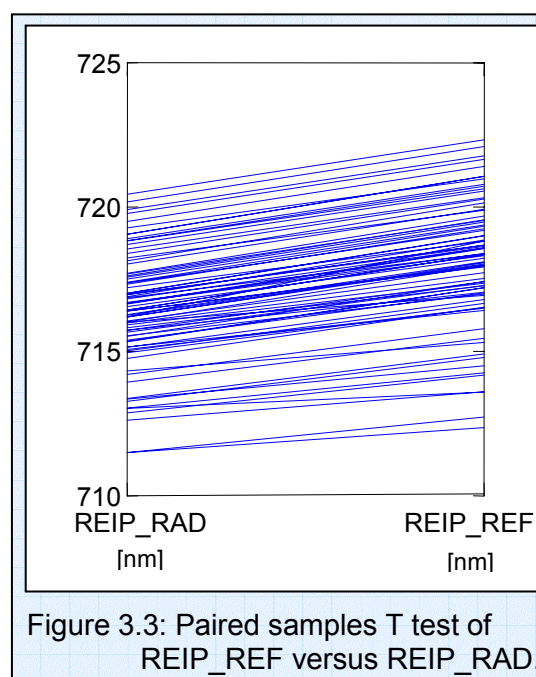
Figure 3.3: Paired samples T test of REIP_REF versus REIP_RAD.

The reason of this systematic shift of the REIP positions may be the atmospheric corrections of the "East" AISA imagery, in this case the Empirical Line calibration. A constant shape of a spectral curve must be retained to preserve equality of the REIP values before

and after linear atmospheric corrections. Unfortunately, during the atmospheric corrections the shape of the reflectance curve was changed due to non-linear growing of the gain values in the regression equation for each band of the AISA image. Therefore, the difference between the values of REIP_REF and REIP_RAD appeared.

As Bonham-Carter (1988) stated, bias in the reflectance measurements may cause false "blue shifts" (shift of reflectance curve to the shorter wavelengths) that might be confused with real "blue shifts" because of vegetation stress. There is not a significant shift to the shorter wavelengths, but an opposite effect, i.e. shift to the longer wavelengths in our case. In spite of this, the REIP values computed from radiance were used for the following analysis regarding estimation of status (health-state) of Norway spruce crowns. Figure 3.3 shows that similar trends in the REIP values are expected to be found for both REIP_RAD and REIP_REF.

3.2.2. *Influence of Decreasing Brightness of Crown Pixels on REIP Values*

For a detailed investigation of functional parts and the status of Norway spruce crowns, matrices of 3 x 3 pixels of 25 spruce crowns for three research places (RPs), in total 75 samples, were selected from the coniferous forest of the AISA image no. 1 – "East" (see Figure 3.4). There were specific requirements for the selection of those trees. First, the crown matrix of each of them should be composed just of pure inner crown pixels, i.e. pixels where the reflectance is not mixed with reflectance of the surrounding understorey vegetation (see Appendix 3). Secondly, each crown was supposed to stand separately to avoid a potential overlapping of the production part of a tree with the juvenile part of the neighbouring tree. Thirdly, only sun-lit crown pixels without deep shadow were used, to reduce the negative influence of shadows.
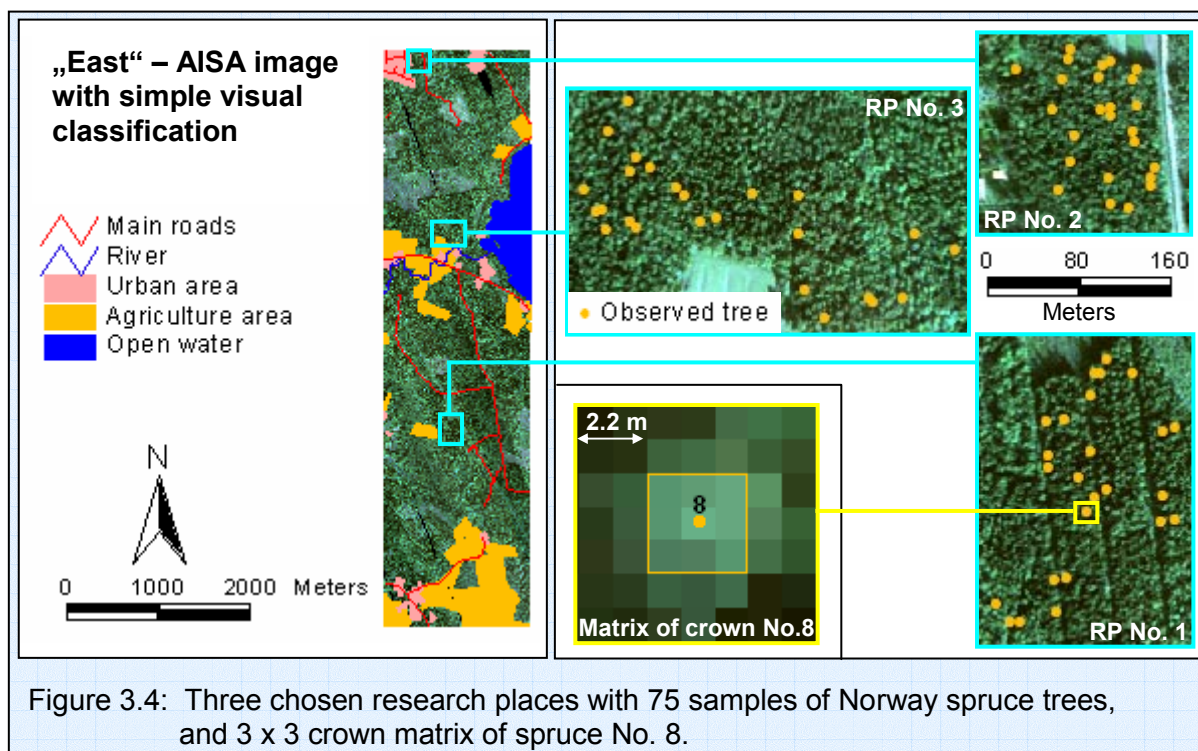
Figure 3.4: Three chosen research places with 75 samples of Norway spruce trees, and 3 x 3 crown matrix of spruce No. 8.

The analysis provided by Entcheva (2000) over the Norway spruce crowns from ASAS hyperspectral images revealed that the shadow within the tree crown causes changes in the amplitude and position of the first derivate (i.e. REIP). As the amount of shadow within a pixel increases, the noise within the spectra also increases. Even if we selected mostly sun-lit pixels of crowns for our analysis to avoid deep shadow and noise, still there was a

brightness decrease within the crown matrix. Therefore, a statistical linear regression test for the influence of this brightness-decreasing trend on the REIP values was accomplished.

The brightness of pixels, the independent variable, was expressed for 3 x 3 crown matrices per research place as an average of Blue (AISA channel no. 3), Green (AISA channel no. 5) and Red (AISA channel no. 8) reflectance. A high value formed light pixels, a low value formed dark pixels. Those matrices were crossed with the appropriate REIP values, the dependent variables. The null hypothesis of simple linear regression stated that values of the REIP are not dependent on the brightness of the pixel (H_0: $\beta = 0$, where REIP = $\alpha + \beta*$Brightness). Results of the regression test for all research plots are in Table 3.3.

Table 3.3: Results of the linear regression test for hypothesis: the REIP values inside of crown matrix are independent on the pixel Brightness.

	Multiple R	R - squared	Std. Error	α	β	T (β)	Prob. level
RP #1	0.336	0.113	1.941	721.704	-0.462	-5.323	0.000
RP #2	0.012	0.000	2.211	719.241	-0.020	-0.176	0.861
RP #3	0.047	0.002	2.214	720.424	-0.071	-0.701	0.484

According to the results from RP #2 and RP #3 one could conclude that there is no relationship between the REIP values and the Brightness of crown pixels. The T – test did not show that the β value is significantly different from zero, thus there was no significant slope of the regression curve for RP #2 and RP #3. The R-squared for RP #2 was equal to zero and for RP #3 it was only 0.2%. Only results from RP #1 were different. In this case the null hypothesis was rejected, so the relationship between Brightness and the REIP values is significant (negative) at the probability level equal to 0.05. In spite of this, Brightness of pixels can explain only 11.3% of the REIP variability, which is a quite small amount. The scatter-plot of the residuals against the estimated values of the dependent variable does not suggest that data has another than linear trend (see Figure 3.5), so we can declare the linear relationship as approved but very slight.

Figure 3.5: Graph illustrating the linear regression of the REIP on Brightness of crown pixels for RP #1 (left) and scatter-plot of the residuals against predicted values of the REIP (right).
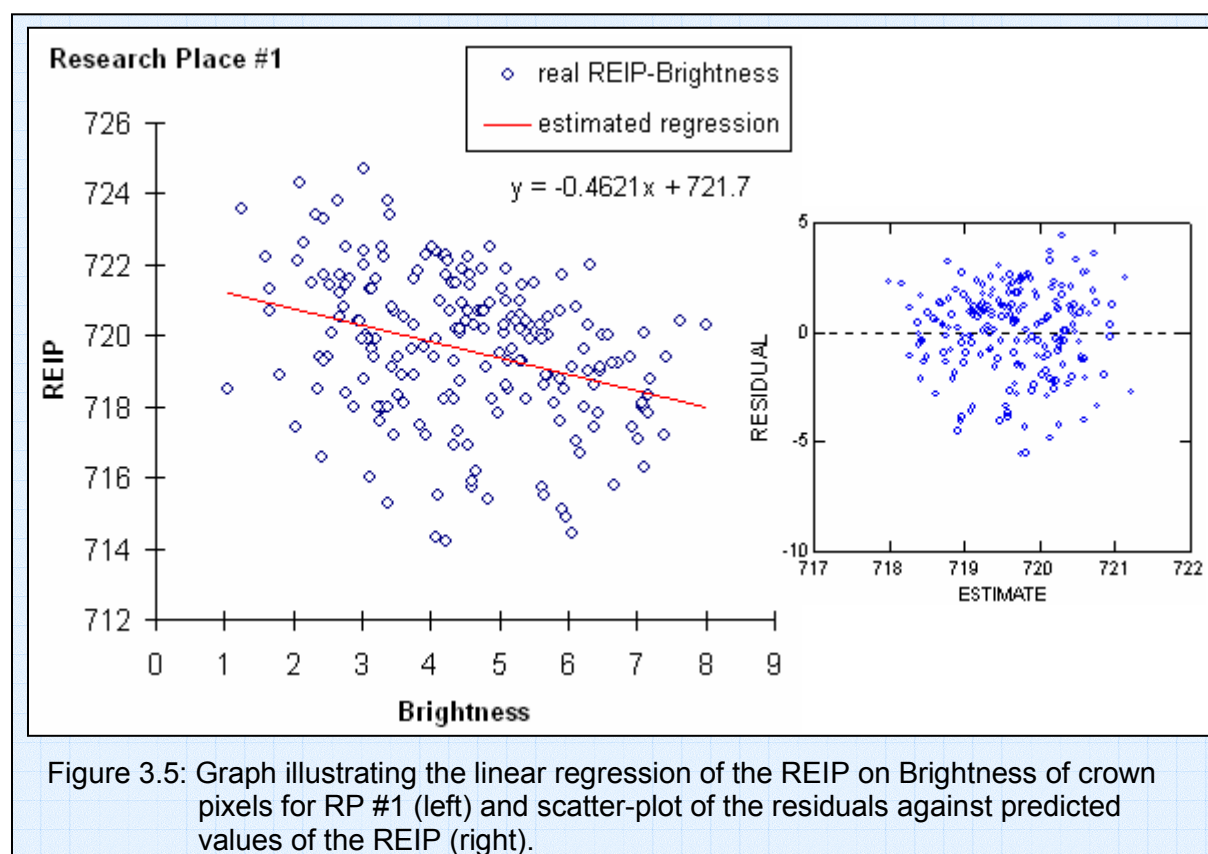
Finally, the overall conclusion of this statistical analysis is that the REIP values of selected spruce crowns of interest were unaffected or only slightly affected by the brightness decrease of the pixels within crown matrices.
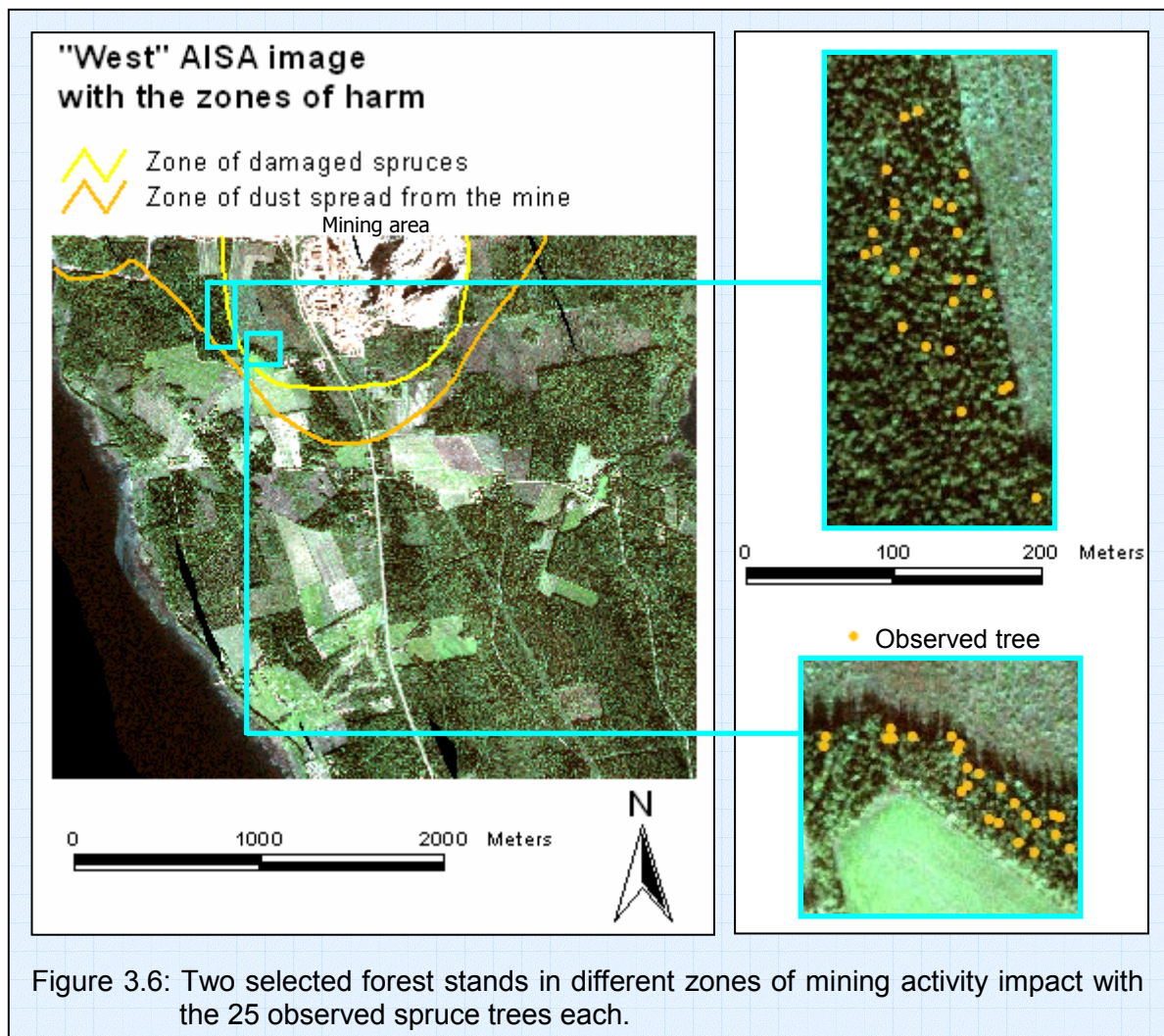
Figure 3.6: Two selected forest stands in different zones of mining activity impact with the 25 observed spruce trees each.

3.2.3. Test of the Disparity of Juvenile and Production Spruce Crown Parts through the REIP Values

In accordance with the theory about different parts of Norway spruce crowns (see section 1.2.) the disparity of the REIP of juvenile and production crown parts has been tested via statistical analysis. The one-sample T – test for each crown matrix was used to test the assumed difference. A null hypothesis expressed that the mean REIP of the production part pixels is equal to the REIP of the juvenile part pixel (H_0: $\mu = \mu_0$). We accepted the probability significance level of the one-sample T – test lower or equal to 0.1.

"EAST" AISA Image

The already selected pixel matrices of the 25 Norway spruce trees for 3 research places (75 samples in total) on the "East" AISA image were used for this test (see Figure 3.4). As a representative of the juvenile part one central (mostly sunlit) pixel of the crown was chosen, and 8 neighbouring pixels around represented the production part. For more details about the selection of juvenile and production part from the AISA image one is referred to Appendix 3. The overview of results per RP and for all observed trees together is depicted in Table 3.4. Detailed results of the one-sample T – test for each tree are in Appendix 4.

From the results of the "East" AISA image we can generally conclude that the null hypothesis can be approved for 75% of all cases. Only 25% of the observed trees significantly showed the difference between the REIP value of juvenile part and the mean REIP of the production part of crown. According to these findings we can state that the null hypothesis (H_0: $\mu = \mu_0$) was approved from a general point of view.

"WEST" AISA Image

25 spruce crowns (AISA matrices of size 3 x 3 pixels) for the FS #1 and FS #2 (in total 50 sample crowns) were selected from the "West" AISA image for investigation of spruce crown structure. The selection of forest stands was not random, but according to the damage found in the terrain. The FS #1 lies in the zone of the high Cu-Zn sulphide dust spread, and FS #2 belongs to the vegetation, where the symptoms of visible damage occurred (see Figure 3.6). The REIP values for the chosen 3 x 3 crown matrices were computed from the "West" AISA image in terms of radiance. An overview of results per FS and all the observed trees together is shown in Table 3.5. More detailed results of the one-sample T – test for each spruce crown are available in Appendix 5.

In general, the results show that the null hypothesis (H_0: $\mu = \mu_0$) was disapproved in 46% of the cases and it was not rejected for 54% of the cases. In spite of this, more than half of all trees (52%) from FS #2 significantly approved the alternative hypothesis about the disparity of the REIP values (H_A: $\mu \neq \mu_0$) of the juvenile and production crown parts. If one takes a deeper look at the result in Appendix 9, then one can figure out that the REIP of the juvenile part is always lower than the REIP of the production part in the cases of significantly confirmed inequality.

Table 3.4: Results of the one-sample T – test for the null hypothesis: mean REIP of production part pixels is equal to the REIP of juvenile part pixel – „East" AISA image.

	H_0: $\mu = \mu_0$			
	[trees]		[%]	
	no	yes	no	yes
RP 1	7	18	28	72
RP 2	7	18	28	72
RP 3	5	20	20	80
All RP	19	56	25	75

Table 3.5: Results of the one-sample T – test for the null hypothesis: mean REIP of production part pixels is equal to the REIP of juvenile part pixel – „West" AISA image.

	H_0: $\mu = \mu_0$			
	[trees]		[%]	
	no	yes	no	yes
FS 1	10	15	40	60
FS 2	13	12	52	48
Both FS	23	27	46	54

3.2.4. Verification of the REIP Dependence on North-East to South-West Direction - "NE trend" - within Norway Spruce Crown Matrices

During the selection of appropriate Norway spruce crown matrices for analysis with the REIP values, a trend of changing REIP from North-East to South-West ("NE trend") was discovered frequently within the crowns of sample trees. Therefore, a statistical linear regression analysis was performed to test this relationship for 75 selected spruce trees of the "East" and 50 sample trees of the "West" AISA image.

The pixels of the 3 x 3 matrix were numbered from 1 to 5 from North-East to South-West direction (see Figure 3.7). These values represented an independent variable NE. The created matrix was overlaid over the matrix of the dependent variable (the REIP values of spruce crown), and a simple linear regression between them was carried out. The null hypothesis expressed that values of the REIP are not dependent on "NE trend" (H_0: $\beta = 0$, where REIP = $\alpha + \beta*NE$).

The null hypothesis was rejected in cases, when the probability level of the T – test for regression coefficient β was lower than 0.05, which means that the slope of the regression line was significantly different from zero. In cases when the β coefficient T – test probability level was higher or equal to 0.05, the null hypothesis of the linear regression was accepted. The R-squared, explaining how many percent of the REIP variability can be explained by the "NE trend", was supposed to reach or exceed the value of 44.4% to confirm that the REIP values are dependent on the direction from North-East to South-West. Finally, the nature of the established regression equation was expected to be positive (β > 0).

Figure 3.7: Linear regression of the REIP on "NE trend".

"EAST" AISA Image

The overview of the simple linear regression results is shown in Table 3.6. Detailed results of the regression test for each tree are in Appendix 6.

The alternative hypothesis that the REIP values are dependent on the geographic direction from North-East to South-West was proved for 77% of all trees of interest from "East" AISA image (positive relationship for all the regression models). Only 23% of all cases showed no relationship between tested variables. We proved that the REIP values of the inner spruce crown matrices were growing from North-East to South-West direction.

"WEST" AISA Image

A summary of the statistical test results is depicted in Table 3.7, and all the linear regression outputs per investigated tree are given in Appendix 7.

The alternative hypothesis that the REIP values of spruce crowns are dependent on the "NE" trend" was proved for most trees of FS #1 and FS #2. 64% of the spruce trees from both forest stands of the "West" AISA image approved the positive relationship of the input variables. 36% of all investigated samples represented the cases of no relation between the tested variables.

Table 3.6: Results of the test of the null hypothesis: the REIP values inside the crown matrix do not depend on the direction from North-East to South-West – "East" AISA image.

	$H_0: \beta = 0$ where REIP $= \alpha + \beta*NE$			
	[trees]		[%]	
	no	yes	no	yes
RP 1	17	8	68	32
RP 2	23	2	92	8
RP 3	18	7	72	28
All RP	58	17	77	23

Table 3.7: Results of the test of the null hypothesis: the REIP values inside the crown matrix do not depend on the direction from North-East to South-West – "West" AISA image.

	$H_0: \beta = 0$ where REIP $= \alpha + \beta*NE$			
	[trees]		[%]	
	no	yes	no	yes
FS 1	18	7	72	28
FS 2	14	11	56	44
Both FS	32	18	64	36

3.3. Evaluation of Spruce Crown Status of the "East" AISA Image

The evaluation of the chlorophyll content and the health-state of Norway spruces of the AISA image no. 1 – "East" was done at two levels. First level was represented by the selected trees of interest in frame of the three research places (see Figure 3.4). At the second level, all the pixels of the "East" AISA image classified as a coniferous (Norway spruce) forest were used.

Using the 10th and 12th AISA channels a raster of WDVI was calculated. The required constant C has been derived from a bare soil training set as 1.386. The 3 x 3 matrices of investigated spruce crowns were isolated and their average WDVI and REIP values were computed. The values of WDVI and REIP, respectively, were drawn into the REIP-WDVI nomogram obtained by PROSAIL modelling (Figure 2.10). The REIP-WDVI nomograms for all research places are depicted in Appendix 8.

- RP 1 – the chlorophyll content of spruce crowns was between 35 – 100 μg.cm^{-2}. Approximately 50% of the crowns lay in the sector IV.B, the rest in sectors III.B and III.C. On that account, four crowns (16%) showed moderate damage, nine of them (36%) can be classified as low damaged and the other twelve crowns (48%) show very low or no damage.
- RP 2 – the amount of crown chlorophyll ranged between 40 and 80 μg.cm^{-2}. More than half of the crowns occupied sector III.B, the rest was in sectors III.A, III.C and IV.B. Only one crown (4%) belonged to the moderate damage class. Sixteen of them (64%) were low damaged and eight crowns (32%) were low damaged or undamaged.
- RP 3 – the chlorophyll content of crowns was estimated from 50 to 100 μg.cm^{-2} (maybe even more). 68% of crowns were located in sectors III.B and IV.B, the other 28% in sectors IV.A, IV.C, III.C. Again only two trees (8%) can be evaluated as moderately damaged. Seven crowns (28%) fell into the category of low damage, and finally sixteen spruces (64%) fell into the category of very low or no damage.

If we compare all three RPs with each other, the best crown status, i.e. the highest chlorophyll content and health-state, had RP #3, then RP #1 and at the last position would be for RP #2. In general, the amount of chlorophyll within all RPs varied from 35 to 100 μg.cm^{-2}, and the health-state of the RPs could be assessed as low damage and very low or no damage.

At the second level, an estimation of chlorophyll content as well as health-state was done for all pixels of the AISA image classified during the classification procedure as Norway spruce crowns. The class of coniferous trees from the Maximum Likelihood classification was overlaid by the map of spruce forest after generalization with CLAPAS. To reduce the classification errors and confusion of coniferous trees with the other classes during automatic classification, only accordant coniferous pixels of both raster maps were taken and a mask image was prepared from them. This mask was applied on the already computed images of the REIP and WDVI values to disguise the other categories of land use. Through crossing of the REIP and WDVI image matrices, reclassified to the categories presented in Figure 2.10, a raster with the REIP-WDVI combinations was obtained. Finally, this REIP-WDVI map was converted into a thematic map of chlorophyll content and also in a map of health-state of spruce crowns in accordance with Table 2.6. The results of this process are illustrated for a slit of the "East" AISA Image in Appendix 9. A statistical overview of results can be found in Tables 3.8 and 3.9.

From the results it can be concluded that about 83% of the selected Norway spruce pixels had a theoretical amount of chlorophyll pigments as simulated by the PROSAIL reflectance model higher or equal to 60 μg.cm^{-2}. Regarding the health-state 84.9% of those pixels represented very low or no damaged trees, 14.4% low damaged and only 0.7% moderately damaged spruce forest.

Table 3.8: Chlorophyll content for classified spruce pixels of the "East" AISA image.

Combination of REIP-WDVI	Chlorophyll content ch [$\mu g.cm^{-2}$]	Number of pixels	Frequency [%]
I.A, I.B, I.C, I.D	ch < 20	8	0.0
II.C, II.D	5 - 30	8	0.0
II.A, II.B, III.D	10 - 40	587	0.1
III.C	15 - 60	5592	0.7
III.B, IV.D	20 - 80	67537	7.9
III.A	30 - 100	54900	6.4
IV.C	40 - 100	12253	1.4
IV.B, V.C, V.D	60 - 120	223261	26.2
IV.A, V.A, V.B	ch $\geq$ 80	488522	57.3
	SUM	852698	100.0

Table 3.9: Health-state of Norway spruces classified from the "East" AISA image.

Health-state	Number of pixels	Frequency [%]
High damage	16	0.0
Moderate damage	6179	0.7
Low damage	122437	14.4
Very low or no damage	724066	84.9
SUM	852698	100.0

3.4.   Evaluation of Spruce Crown Status of the "West" AISA Image

The assessment of chlorophyll amount and health-state of Norway spruces of the AISA image no. 2 - "West" was also done at two levels. First level was represented by the crowns of 50 chosen trees of interest taking place in two harmed forest stands (see Figure 3.6). At the second level we evaluated the pixels of seven spruce forest stands (see Appendix 10) classified by the SAM classifier as coniferous trees.

From the selected 3 x 3 crown matrices the mean values of WDVI and REIP were computed. Relevant values of these indices were drawn in the REIP-WDVI nomograms per forest stand. Both nomograms are available in Appendix 11.

- FS #1 – the chlorophyll content of observed spruce crowns was estimated between 40 and 70 $\mu g.cm^{-2}$. Only one crown (4%) occurring in sector IV.B represents none or very low damaged trees. Sixteen trees (64%), which belong to the sectors III.A and III.B, were evaluated as low damaged, and eight spruces (32%) in sector III.C signified moderate damage.

- FS #2 – the chlorophyll content ranged between 35 and 65 $\mu g.cm^{-2}$. All the observed spruces showed some damage that means no one appeared in the category of very low or no damage. Nineteen trees (76%) fell into the sectors III.A and III.B, i.e. low damage, and finally six spruce crowns (24%) occupied the sector III.C of moderate damage.

By a mutual comparison we can say that both FSs had a very similar spruce crown health-state. According to chlorophyll content FS #2 had lower estimated concentrations of this foliar pigment than FS #1.

At the second level, a mask image was prepared from the pixels of the seven forest stands classified by the SAM classification as coniferous spruce crowns. This mask was applied on the images of the REIP and WDVI computed for the "West" AISA imagery. Through REIP-WDVI combinations a thematic map of chlorophyll content and also a map of health-state of spruce pixels (in accordance with Table 2.6) were obtained. A common statistical overview of the chlorophyll estimation and evaluation of the health-state for Norway spruces for all seven

forest stands is available in Table 3.10 and Table 3.11, respectively. The resultant map compositions as well as statistics per forest stand are depicted in Appendix 12.

Table 3.10: Chlorophyll content for classified spruce pixels of seven forest stands of the "West" AISA image.

Combination of REIP-WDVI	Chlorophyll content ch [μg.cm^{-2}]	Number of pixels	Frequency [%]
II.A, II.B, III.D	10 - 40	1058	1.9
III.C	15 - 60	4234	7.4
III.B, IV.D	20 - 80	10637	18.6
III.A	30 - 100	5992	10.5
IV.C	40 - 100	7000	12.3
IV.B, V.C, V.D	60 - 120	19493	34.2
IV.A, V.A, V.B	ch $\geq$ 80	8627	15.1
	SUM	57041	100.0

Table 3.11: Health-state of Norway spruces from seven forest stands of the "West" AISA image.

Health-state	Number of pixels	Frequency [%]
High damage	0	0.0
Moderate damage	5292	9.3
Low damage	16629	29.1
Very low or no damage	35120	61.6
SUM	57041	100.0

On one hand, estimated chlorophyll content for 49.3% of the observed spruce crown pixels within seven forest stands of interest was equal or higher than 60 μg.cm^{-2}. For 12.3% of them it was between 40 and 100 μg.cm^{-2} which together results into 61.6% of spruce pixels of the very low or none damage category. On the other hand, there is 29.1% of spruce pixels with an estimated chlorophyll content in interval 20 - 80 μg.cm^{-2} and even 7.4% of them with a potential chlorophyll amount between 15 and 60 μg.cm^{-2} and 1.9% of them in the interval 10 - 40 μg.cm^{-2}. These low chlorophyll concentrations in combination with lower REIP values resulted in 29.1% of low damage and 9.3% of moderate damage of spruce crowns, which could be caused by the mining activities of heavy metals nearby.

A more detailed look at the separate forest stands can help to better understand the potential influence of the Cu – Zn sulphide mine on the status of its neighbouring Norway spruces. On one side the results for spruce forest stands no. 1 and 2, which are close to the mine, show a lower chlorophyll content and a higher damage at the parts toward the mining area (see Appendix 12). One can even try to draw the border line of trees influenced by pollution, using visual interpretation of the health-state map containing a high percentage of low and moderate damaged trees. On the other side the forest stand no. 3, which is the closest stand to the mine, is demonstrated as the healthiest stand of all, with estimated chlorophyll contents higher or equal to 40 μg.cm^{-2} for 83.6% of its spruce pixels. Then the forest stands no. 4 and 6 are following. They are small and their estimations for chlorophyll content and health-state are close to (a little under) the average values. Finally, for the remaining forest stands no. 5 and 7, far off from the mining area, again a decreasing trend of assumed chlorophyll amount and increasing damage of trees can be observed. It is very hard to discover what the reasons for this spruce stress are without other ancillary data.

4. Discussion and Recommendations

4.1. Input Data

The AISA images were developed as a mosaic of several hyperspectral flight lines. As a result regular reflectance distortions within the mosaic could be observed, which represented a bottleneck for the processing of the "East" image. An effective procedure or tool should be developed to correct this negative influence of radiometric differences for subsequent automatic treatment. Another possibility is to process all flight lines separately and merge their resulting thematic maps in one mosaic at the end of the whole processing. However, this approach would be more time demanding.

4.2. Atmospheric Corrections of the "East" AISA Image

The weak points of the Empirical Line atmospheric corrections were the calibration by black and white panels (targets) captured by the AISA sensor during the flight campaign. The difficulty in using these panels was that they were not true Lambertian surfaces, and we had to use our own deduction to find the "darkest" and "lightest" pixel inside the panels, which were used for the atmospheric corrections. This problem could also be a potential cause of a systematic shift of the REIP values before and after atmospheric calibration as we showed in section 3.2.1.

4.3. Classification of the AISA Images

4.3.1. Visual Interpretation

The visual interpretation of the "East" AISA image has been completely based on the experiences of its providing person. No other ancillary data (e.g. topographic maps or GIS layers) was available, no terrain observation was possible to support and verify this process. Therefore, mistakes or, at least, commutations of classified categories (e.g. forest clear cut & agriculture area or young trees & tree plantation) may be found in the result.

4.3.2. Automatic Classification

Unfortunately, the transformations of the original "East" AISA channels did not only offset the reflectance differences within flight lines, but also "smoothed" the information content of the input data, which could bring about potential errors in a following automatic classification.

The training sets of classes for supervised automatic classification were prepared as vector polygons over the colour composition of the AISA image. We did our best to prepare a high quality homogenous training set, but unfortunately we had no opportunity to verify their homogeneity and suitability within a direct terrain investigation. Also the accuracy assessment of the Maximum Likelihood classification was not done by a standard way, but only through an alternative method, i.e. direct comparison with another classification (object oriented Nearest Neighbor classification). Therefore, the confidence in the automatic classification results may be lower.

After the random visual verification of the classification of the AISA image no. 1 and from the error matrix of the Nearest Neighbor classification against Maximum Likelihood

classification we recognized that the class of coniferous forest, Norway spruces in our case, contained an unspecified amount of deciduous trees. This result was also supported by the relatively high values of the REIP of some pixels for the Norway spruce category, which in reality probably belong to the class of broadleaf trees. How big the share of deciduous trees is in the coniferous category and how precise the result of automatic classification is, can only be properly estimated after a specific ground truth campaign.

The automatic classifiers used for identification of spruce crown pixels within the forest stands of the "West" AISA image produced different results for different types of algorithms. As one can see from the classification results of this study, classification including segmentation of pixels into homogeneous objects (Nearest Neighbor) gave a significantly higher number of coniferous pixels and a lower number of shadowed pixels than classification per pixel (SAM classification). This was explained as a consequence of the multi-resolution segmentation of homogeneous objects. The objects formed by segmentation occasionally contained pixels of tree canopy and shadowed pixels together, which caused this lower accuracy of classification results. Segmentation of an image to the objects of the forest environment could improve the subsequent automatic classification process only if the segmentation will be able to separate the tree crowns as separate objects.

It is also necessary to mention that high damaged spruce trees could not be distinguished through an automatic classification. These trees could be either completely yellow coloured (high LAI but low chlorophyll content) and thus classified as discoloured vegetation, or be defoliated (low LAI but high chlorophyll content and/or low LAI and low chlorophyll content) and then classified as deciduous trees due to the prevailing reflectance of understorey vegetation in pixels. This fact partly explains why there was no occurrence of Norway spruce crowns of the high damage category present in our health-state results.

4.4. Structure of Norway Spruce Crowns

4.4.1. Disparity of Spectral Properties of Juvenile and Production Spruce Crown Parts

On the one hand we did not prove through the REIP values a spectral disparity between the juvenile and the production parts for the spruce trees of the "East" AISA image. On the other hand the results of this test for the "West" AISA image showed the REIP disparity of juvenile and production spruce crown parts in case of the FS #2 (52% of observed trees). The key factor seems to be the harm of Norway spruces. The results of the spruce crown status investigation estimated in general a low influence of stress agents on the spruce forest stands of the "East" AISA image. It can be possible that their damage is too low and their crown transformations are in earlier stages to make a spectral difference between observed crown parts possible. It could also be that the crowns are in advanced transformation stages, but the spatial resolution of the input image data of 1.1 m is insufficient, or other stronger phenomena are overruling the assumed structure of crowns. On this account, the spatial distribution of the REIP values within the chosen crown matrices was observed, and an increasing gradient of the REIP from North-East (NE) towards South-West (SW) direction was discovered (see section 3.2.4.). The health-state of the trees observed in the "West" AISA image was evaluated as low or moderate damage. The spectral disparity was clearly proved especially for the crowns of low REIP values and in most cases the REIP of the juvenile part was lower than the mean REIP of the production part. These facts drive us to the conclusion that the spruces, where this disparity was statistically demonstrated, have a damaged top part of the crown. According to multiple stress response theory (Cudlín et al., 2001) these trees could be in the 4th stage of crown transformation (see Figure 1.1), but this conjecture needs direct evidence via terrain verification.

The spatial resolution of the AISA image (1.1 m) seems to be sufficient for observation of the spruce crown part differences in the case of tree top injury. However, our original hypothesis about higher chronic stress resistance of the juvenile crown part was neither confirmed nor disapproved. Therefore, for a next study on functional crown structures a finer spatial resolution of hyperspectral data (about 0.5 m) and thus a larger matrix of interest than 3 x 3 pixels is recommended. Only one pixel of the juvenile part and eight pixels of the production part could be inadequate representatives. Crown top (juvenile part) may take a role in not only one central pixel, but also share a place in two or four top pixels, and then its reflectance is mixed up with the reflectance of the production part. Or the juvenile part could not be large enough to fill fully one pixel of 1.1 x 1.1 m size. Also a larger number of pixels will be more suitable for the statistical tests. Ground observation is absolutely necessary for a further study! A more effective way should be to use Norway spruce trees with known crown structure, which are evaluated from direct visual assessment. Afterwards the reflectance properties (e.g. the REIP) of those trees from hyperspectral images in combination with field spectral measurements of their functional crown parts should be investigated.

4.4.2. Dependence of the Spruce Crown REIP Values on North-East to South-West Direction

For both AISA images the dependence of the REIP on the particular geographical direction was observed. There are, at least, two interpretations of the "NE trend" of the REIP values occurring for about half of the selected trees. The position of the REIP is strongly dependent on Leaf Area Index (LAI) and total amount of chlorophylls a+b. First explanation assumes that the crowns of the trees are stressed mostly at the North-East (NE) side, for instance by the regular NE winds or other stress agents (silver storms, imissions, etc.). That is why there is a lower number of green needles on the NE side. Secondly, the spruce trees are so "smart" that they distribute more needles and chlorophyll pigments on the SW side of crowns, because there is more photosynthetically active radiation (PAR) available during the day period, especially in the early afternoon. However, verification of both these hypothesis needs additional information either from remote-sensed data (e.g. very high spatial resolution airborne images), or terrain observation (assessment of tree damage, systematic laboratory analysis of leaf pigments and other chemical compounds, etc.).

4.5.   Investigation of Status of Norway Spruce Crowns

4.5.1. PROSPECT – SAIL Modelling

The PROSAIL modelling was provided for the purpose of canopy reflectance simulations for Norway spruces on the AISA images. From these simulations the values of the REIP and WDVI were computed for several combinations of LAI and chlorophyll content. Both factors have a clear relationship with these vegetation indices, so they can be estimated through the REIP and WDVI by inversion.

The PROSAIL input variables can be ordered according to their influence on the REIP and WDVI and consequently used for an estimation of chlorophyll amount and health-state of spruce crowns. The water content has no influence on the REIP and WDVI values, because they are derived from Red and NIR wavelengths. The following factors have only a minor influence on both indices: ratio diffuse/direct irradiation, soil reflectance and hot spot parameter for NADIR viewing (Clevers, 1994; Clevers and Verhoef, 1993). The influence of solar zenith angle becomes clear beyond a zenith angle of 60°. The influence up to a solar zenith angle of 60° is insignificant. Although the leaf angle distribution has a small influence on the REIP, it has a huge influence on the regression of LAI on WDVI. Even if the spherical LIDF was used as a most heterogeneous combination of LAD, a more intensive investigation

of the needle distribution in the frame of a spruce crown should be recommended for future study. The influence of the mesophyll structure parameter N on WDVI was found to be small (for "standard crop"; Clevers et al., 1994) up to LAI values of about 4.0. However, the N parameter has a significant influence on the REIP, especially for high values of chlorophyll content (about 80 μg cm^{-2}). A lower value of the N parameter would mean lower values of the REIP, which could cause a greater participation of the spruce crowns in health-state categories of higher damage.

For future research it should be recommended to focus more in detail on an estimation of the spruce mesophyll structure parameter and the leaf angle distribution, due to their significant influence on the simulation of canopy reflectance. Further important feature of the Norway spruce crown, regarding LIDF, is the type of branching (shoot angle distribution). There is the comb, brush, and plate type of spruce crown branching. This branching type has probably strong influence on the spectral behaviour of the spruce canopy, but it has not been included in a canopy reflectance model yet!

4.5.2. Estimation of Chlorophyll Content and Health-state of Spruce Crowns

The range of chlorophyll amount for the spruces of three research places on the "East" AISA image was computed as being between 40 - 100 μg.cm^{-2}. Also the health-state of the RPs was estimated to be half way between low damage and very low or no damage, but in case of the whole "East" AISA image 85% of the Norway spruce pixels were classified as very low damaged or undamaged and only 14% of them with low damage and 1% moderately damaged. From this brief recapitulation it is clear that simulation at the image level showed a more positive status of Norway spruces than analysis at the level of research places. On the one hand it is correct to assume that the status of trees of the randomly selected research plots was really worse than the average status of spruce crowns captured by the AISA image. On the other hand it also seems to be a realistic explanation that the class of coniferous trees could contain, due to the automatic classification, an amount of incorrectly classified pixels of deciduous trees or understorey vegetation. In addition to a higher reflectance of broadleaf vegetation mainly in the NIR part of the spectrum (see Figure 2.7 or Figure 2.8) their chlorophyll content and REIP values were higher, and consequently the status of observed crowns is overestimated.

A different interpretation of results must be used in case of the "West" AISA image. Here 50 separate spruce crowns were purposely selected in the zones of observed spruce damage and higher dust distribution. The results confirmed that crown status of these trees is generally worse than average values of all coniferous pixels within the seven forest stands of interest. Even if the estimated chlorophyll content interval for the 50 observed trees of 35 - 70 μg.cm^{-2} corresponds with the general chlorophyll content of the forest stands, their health-state is more negative. For 28% of them it is moderate damage, for 70% low damage, and only for 2% none or very low damage, while the average health-state ratio for coniferous pixels of the stands is 9% of moderate damaged trees, 29% of low damaged and about 62% of none or very low damaged trees. Of course, also in this case it is important to keep in mind that result of the automatic classification includes some portion of incorrectly classified pixels.

We tried to interpret the status of the seven spruce forest stands on the "West" AISA image using ancillary data about the area of interest. The bad health-state of the FS #1 and #2 is more likely caused by the direct influence of the close mining activities. Concerning the FS #5 and #7, which are quite far off from the Cu-Zn mine, the status of their spruce trees is not very positive. High geochemical anomalies of Cu, Zn, S and Cd have been found towards the South from the mine due to specific geological reasons. Also the soil type and water content varied more to the South from the mine (Arkimaa, personal communication). Those could be the main causal agents of the spruce injury at these forest stands far off the mine.

It is impossible to compare the results of the AISA "East" and "West" image quantitatively. At the first level the research plots of the "East" image were selected randomly, while the forest stands of the "West" image followed the places with the higher stress impacts on purpose. At the second level a different number of pixels classified as coniferous crowns was used for crown status evaluation (for the "East" AISA image 852 698 pixels were processed; for the "West" AISA image only 57 041 pixels). However, from a qualitative point of view we can state that the Norway spruce forest stands of the "East" AISA image are healthier and in better condition than the spruce ecosystems of the "West" AISA image. The most likely source of their harm is the strip mine of Cu-Zn sulphides in their neighbourhood.

5. Conclusions

5.1. Spectral Differences of Spruce Crown Parts

According to the results from the AISA images we confirmed the spectral difference of the juvenile and production part of the Norway spruce crown, but only for a number of the studied trees. The crown top damage (leaning to dry top) could be observed through REIP values computed from hyperspectral images at a spatial resolution of 1.1 m. However, the original hypothesis that the juvenile part is preferably supported by the tree during long time stress influence and thus the production part shows better multiple stress response was not proved. There can be more than one reason for this fact. If the cause is just a low intensity of stress influence on the production crown part, then the spatial resolution of about one meter could still be sufficient for observation of this effect from remote-sensed data. On the other hand this spatial resolution could be insufficient to provide pure reflectance information of the juvenile functional part, and consequently be unsuitable for this purpose. Finally, high Norway spruce crown heterogeneity or another stronger effect could defeat this attempt to distinguish different functional crown parts from the hyperspectral AISA images. In spite of this, the statistical test revealed the relation of the REIP values on the geographic direction from North-East to South-West within the Norway spruce crowns of the AISA images. To be able to explain this phenomenon, additional information obtained through terrain observation and ancillary GIS data is required.

5.2. Crown Status of Norway Spruces

At the level of research places of the "East" AISA image the analysis with the PROSAIL model estimated the theoretical spruce crown chlorophyll content between 40 - 100 $\mu g.cm^{-2}$, and the health-state of spruce trees on RPs was found between low damage and very low or no damage. At the more general level of the whole "East" AISA image the chlorophyll content of 83.5% of the spruce pixels was estimated to be equal or higher than 60 $\mu g.cm^{-2}$, for 57.3% of the spruce pixels even equal or higher than 80 $\mu g.cm^{-2}$. Concerning the health-state 85% of the observed pixels represented very low or no damage, 14% low damage and 1% moderately damaged spruce forest.

Estimated chlorophyll content of the fifty spruces taking place in two harmed forest stands of the "West" AISA image was between 35 - 70 $\mu g.cm^{-2}$. Their health-state was assessed as mainly low and/or moderate damage. A concentration of the chlorophyll pigments more than 60 $\mu g.cm^{-2}$ (up to a physiological limit of spruce needles) was estimated for 49.3% of the observed coniferous pixels from seven selected forest stands of the "West" AISA image. The assumed health-state of coniferous pixels of these forest stands was no or very low damage for about 62% of them, low damage for 29%, and moderate damage for 9%.

The high damage of Norway spruces can not be ascertained using the airborne AISA hyperspectral images from the autumn period due to a mix up of the senescent broadleaf vegetation and strongly stressed coniferous trees. From our research we can generally conclude that Norway spruces of the "East" AISA image have a very good crown status without abnormal damage caused by the biotic and/or abiotic stress agents, while the spruce forest stands of the "West" AISA image are languishing, partly due to the close mining activities of Cu-Zn sulphides.

Although the PROSPECT-SAIL vegetation reflectance model provided a useful and suitable tool for reflectance simulations and theoretical estimation of the canopy attributes, some of its input parameters should be verified and improved for the case of the Norway spruce tree. Finally, future research, as well as verification of its results, has to be connected with a terrain and laboratory investigation.

References

Allen, W., A., Gausman, H., W., Richardson, A., J., and Thomas, J., R., 1969: Interaction of isotropic light with a compact plant leaf; Journal Opt. Soc. Am., 59, 1376-1379.

Ardö, J., Lambert, N., J., Henžlík, V., Rock, B., N., 1997: Satellite-based estimation of coniferous forest cover changes: Krušné Hory, Czech Republic 1972-1989; Ambio, 26, 158-166.

Baatz, M., Heyen, M., Hofmann, P., Lingenfelder, I., Mimler, M., Schäpe, A., Weber, M., Willhauck, G., 2000: eCognition object oriented image analysis – Users Guide; DEFiNiENS, München, 361 pp.

Bacour, C., Jacquemoud, S., Tourbier, Y., Dechambre, M., Frangi, J.-P., 2002: Design and analysis of numerical experiments to compare four canopy reflectance models; Remote Sensing of Environment, 79, 72-83.

Baret, F., Jacquemoud, S., Guyot, G., and Leprieur, C., 1992: Modelled analysis of the biophysical nature of spectral shifts and comparison with information content of broad bands; Remote Sensing of Environment, 41, 133-142.

Bonham-Carter, G., F., 1988: Numerical procedures and computer program for fitting an inverted gaussian model to vegetation reflectance data; Computers & Geosciences, 14 (3), 339-356.

Clevers, J., G., P., W., 1989: The application of a weighted infrared-red vegetation index for estimating Leaf Area Index by correcting for soil moisture; Remote Sensing of Environment, 29, 25-37.

Clevers, J., G., P., W., 1994: Imaging spectrometry in agriculture – plant vitality and yield indicators; In Hill, J., Mégier, J., (eds.): Imaging Spectrometry – a tool for environmental observations; Kluwer Academic Publishers, Dordrecht/Boston/London, p. 193-219.

Clevers, J., G., P., W., 2001: Atmospheric correction of optical remote sensing data; Laboratory of Geo-information Science and Remote Sensing, Centre for Geo-Information, Wageningen University, Wageningen, 30 pp.

Clevers, J., G., P., W., Büker, C., 1991: Feasibility of the red edge index for the detection of nitrogen deficiency; In Proceedings of 5th Int. Coll. on Physical Measurements and Signatures in Remote Sensing, Courchevel, France, ESA SP-319, 165-168.

Clevers, J., G., P., W., and Verhoef, W., 1993: LAI estimation by means of the WDVI: A sensitivity analysis with a combined PROSPECT-SAIL mode; Remote Sensing Reviews, 7, 43-64.

Clevers, J., G., P., W., Van Leeuwen, H., J., C., Verhoef, W., 1994: Estimating the fraction APAR by means of vegetation indices: A sensitivity analysis with a combined PROSPECT-SAIL model; Remote Sensing Reviews, 9, 203-220.

Commission of the European Communities and Directorate-General for Agriculture, 1991: Remote sensing applications for forest health status assessment; Manual, Walphot S.A., Belgium.

Cudlín, P., Novotný, R., Moravec, I., Chmelíková, E., 2001: Retrospective evaluation of the response of montane forest ecosystems to multiple stress; Ekológia, Bratislava, Vol. 20, No. 1.

Curran, P., J., 1994: Attempts to drive ecosystems simulation models at local to regional scales; In Dawson, T., P., Curran, P., J., Plummer, S., E., 1998: LIBERTY – Modeling the effects of leaf biochemical concentration on reflectance spectra; Remote Sensing of Environment, 65, 50-60.

Dawson, T., P., Curran, P., J., Plummer, S., E., 1998: LIBERTY – Modeling the effects of leaf biochemical concentration on reflectance spectra; Remote Sensing of Environment, 65, 50-60.

Demarez, V., and Gastellu-Etchegorry, J., P., 2000: A modeling approach for studying forest chlorophyll content; Remote Sensing of Environment, 71: 226-238.

Dickson, R. E., Isebrands, J. G., 1991: Leaves as regulators of stress response. In Mooney, H. A., Winner, W. E., Pell, E. J., Chu, E. (eds): Response of plants to multiple stress. Academic Press, London, p. 4-34.

Entcheva, P., K., 2000: Remote sensing of forest damage in the Czech Republic using hyperspectral methods; Dissertation, University of New Hampshire, New Hampshire, 225 pp.

ENVI User's Guide, 2000: ENVI Version 3.4; Research Systems, Inc., 930 pp.

Fish, A., K., Peart, R., A., Franklin, S., E., 1995: Mapping montane forest structure using high spatial resolution casi data; In Proceedings of the 17th Canadian Symposium on Remote Sensing, Saskatoon, Saskatchewan, Vol. II, pp. 558-561.

Gobron, N., Pinty, B., Verstraete, M., M., and Govaerts, Y., 1997: A semidiscrete model for the scattering of lights by vegetation; J. Geophys. Res. Atmosph., 102(D8), 9431-9446.

Gruber, F., 1994: Morphology of coniferous trees: possible effects of soil acidification on the morphology of Norway spruce and Silver fir; In Godbold, D.L., Hüttermann, A. (eds), Effects of acid rain on forest processes, Wiley-Liss, New York, p. 265-324.

Guyot, G., and Baret, F., 1988: Utilisation de la haute resolution spectrale pour suivre l'etat des couverts vegetaux; In Proceedings of 4th Int. Coll. on Spectral Signatures of Objects in Remote Sensing, Ausoirs, France, ESA SP-287, 279-286.

Guyot, G., Baret, F., Major, D., J., 1988: High spectral resolution: Determination of spectral shifts between the red and near infrared; Int. Arch. of Photogr. and Rem. Sensing, 27 (11), 750-760.

Hare, E., W., Miller, J., R., and Edwards, G., R., 1984: Studies of the vegetation red reflectance edge in geobotanical remote sensing; In Proceedings of 9th Canadian Symposium on Remote Sensing, St. Johns, Newfoundland, 433-440.

Horler, D., N., H., Dockray, M., Barber, J., Barringer, A., R., 1983: Red edge measurement for remotely sensing plant chlorophyll content; Advances in Space Research, 3, 273-277.

Hoshizaki, T., Rock, B., N., Wong, S., K., S., 1988: Pigment analysis and spectral assessment of spruce trees undergoing forest decline in the NE Unites States and Germany; GeoJournal, 17, 173-178.

Hykš, P., Hraška, J., 1990: Slnečné žiarenie a budovy; Vydavateľstvo Alfa, Bratislava, p. 26-28.

Iaquinta, J., and Pinty, B., 1994: Adaptation of a bidirectional reflectance model including the hot-spot to an optically thin canopy; In: Jacquemoud, S., Bacour, C., Poilvé, H., Frangi, J., P., 2000: Comparison of four radiative transfer models to simulate plant canopies reflectance: direct and inverse mode; Remote Sensing of Environment, 74: 471-481.

Innes, J., L., 1987: Air pollution and forestry. Forestry Commission, Bulletin, 70, p. 40.

Jacquemoud, S., Baret, F., 1990: Prospect: A Model of Leaf Optical Properties Spectra; Remote Sensing of Environment, 34, 75-91.

Johnson, L., F., Hlavka, C., A., and Peterson, D., L., 1994: Multivariate analysis od AVIRIS data for canopy biochemical estimation along the Oregon transect; Remote Sensing of Environment, 47, 216-230.

Kimes, D., Gastellu-Etchegorry, J., Esteve, P., 2002: Recovery of forest canopy characteristics through inversion of a complex 3D model; Remote Sensing of Environment, 79, 320-328.

Kokaly, R., F., and Clark, R., N, 1999: Spectroscopic determination of leaf biochemistry using band-depth analysis of absorption features and stepwise multiple linear regression; Remote Sensing of Environment, 67, 267-287.

Kruse, F., A., Kierein-Young, K., S., Boardman, J., W., 1990: Mineral mapping at Cuprite, Nevada with a 63 channel imaging spectrometer; Photogrammetric Engineering and Remote Sensing, 56, 83-92.

Kruse, F., A., Lefkoff, A., B., Boardman, J., W., Heidebrecht, K., B., Shapiro, A., T., Barloon, P., J., and Goetz, A., F., H., 1993: The Spectral Image Processing System (SIPS) – Interactive Visualization and Analysis of Imaging Spectrometer Data; Remote Sensing of Enviroment, 44, 145-163.

Kuusk, A., 1985: The hot spot effect of a uniform vegetative cover; Sov. J. Remote Sensing, 3, 645-658.

Kuusk, A, 1991: The hot spot effect in plant canopy reflectance; In Ross, R., and Myneni, R., (Eds.): Photon vegetation interactions – Application in optical remote sensing and plant ecology; Springer, Berlin, p. 139-159.

Kuusk, A., 1995: A Markov chain model of canopy reflectance; Agric. For. Meteorol., 76, 221-236.

Lambert, N., J., Ardö, J., Rock, B., N., Vogelmann, J., E., 1995: Spectral characterization and regression-based classification of forest damage in Norway spruce stands in the Czech Republic using Landsat Thematic Mapper data; Int. J. of Remote Sensing, 16, 1261-1287.

Lillesand, T., M., Kiefer, R., W., 2000: Remote Sensing and Image Interpretation, Fourth Edition; John Wiley & Sons, Inc., New York, Chichester, Weinheim, Brisbane, Singapore, Toronto, 724 pp.

Malenovský, Z., 2001: Possibilities of using satellite data for mapping the vegetation formation types in the forested area of Mediterranean region; Journal of Forest Science, 47, 114-123.

Meunier-Caldairou, V., 1999: Analyse des transformations de l'information dans des images satellitales classées au cours de procédures de généralisation de leur contenu: Influence de différents niveaux de précision cartographique et de nomenclatures de type "occupation du sol", "utilisation du sol", et "motif paysager"; Thèse de doctorat, ESA Purpan, Toulouse, 135 pp.

Miller, J., R., Hare, E., W., Neville, R., A., Gauthier, R., P., McColl, W., D., and Till, S., M., 1985: Correlation of metal concentrations with anomales in narrow band multispectral imagery; In Proceedings of 4th Thematic Conference, Remote Sensing for Exploration Geology, San Francisco, California, 143-154.

Moos, D., M., and Rock, B., N., 1991: Analysis of red edge spectral characteristics and total chlorophyll values for red spruce (*Picea rubens*) branch segments from Mt. Moosilauke, NH, USA; Proceedings IGARSS '91, Helsinki (June 3-6, 1991), Finland.

O'Neil, A., L., Kupiec, J., A., Currain, P., J., 2002: Biochemical and reflectance variation throughout a Sitka spruce canopy; Remote Sensing of Environment, 80, 134-142.

Robbez-Masson, J., M., 1994: Reconnaissance et délimitation de motifs d'organisation spatiale. Application à la cartographie des pédopaysages; Thèse de doctorat, ENSA, Montpellier, 161pp.

Robbez-Masson, J., M., Borne, F., Girard, M., C., 1996: Description et Segmentation de Motifs d'Organisations Spatiale: Aplication à l'obtention d'esquisses paysagères; Actes du Colloque INRA "Phenomènes Spatiaux en Agriculture", La Rochelle, 65-79.

Rock, B., N., Hoshizaki, T., Miller, J., R., 1988: Comparison of in situ and airborne spectral measurements of the blue shift associated with forest decline; Remote Sensing of Environment, 24, 109-127.

Schowengerdt, R., A., 1983: Techniques for image processing and classification in remote sensing; Academic press, Inc., Orlando, London, 235 pp.

Ulrich, B., 1994: Process hierarchy in forest ecosystems: an integrative ecosystem theory. In Godbold, D., L., Hüttermann, A. (eds): Effects of acid rain on forest processes, Wiley-Liss, New York, p. 353 – 397.

Verhoef, W., 1984: Light Scattering by Leaf Layers with Application to Canopy Reflectance Modeling: The SAIL Model; Remote Sensing of Environment, 16, 125-141.

Verhoef, W., 1998: Theory of radiative transfer models applied in optical remote rensing of vegetation canopies; Thesis Landbouwuniversiteit Wageningen, Wageningen, 310 pp.

Verhoef, W., Bunnik, N., J., J., 1981: Influence of crop geometry on multispectral reflectance determined by the use of canopy reflectance models; In Proceeding Int. Coll. on Signatures of Remotely Sensed Objects, Avignon, France, 273-290.

Vogelmann, J., E., and Rock, B., N., 1988: Assessing forest damage in high elevation coniferous forests in Vermont and New Hampshire using Thematic Mapper data; Remote Sensing of Environment, 24, 227-246.

Vogelmann, J., E., and Rock, B., N., Moos, D., M., 1993: Red edge spectral measurements from sugar maple leaves; Int. J. Remote Sensing, 14, 1563-1575.

Wessman, C., A., Aber, J.,D., and Peterson, D., L., 1989 : An evaluation of imaging spectrometry for estimating forest canopy chemistry; International Journal od Remote Sensing, 10, 1293-1316.

Zarco-Tejada, P., J., Miller, J., R., Mohammed, G., H., Noland, T., L., Sampson, P., H., 2000: Chlorophyll fluorescence effects on vegetation apparent reflectance: II. Laboratory and airborne canopy-level measurements with hyperspectral data; Remote Sensing of Environment, 74, 596-608.

Appendices

- **Appendix 1** – Spatial specification of functional parts of Norway spruce crown
- **Appendix 2** – "East" AISA image classification – land use and forest categories
- **Appendix 3** – Spatial separation of juvenile and production spruce crown parts from the remote-sensed data at a spatial resolution of 1.1 metre
- **Appendix 4** – Results of one-sample T – test for disparity of juvenile and production spruce crown parts through the REIP values of selected trees on the "East" AISA image
- **Appendix 5** – Results of one-sample T – test for disparity of juvenile and production crown parts through the REIP values of selected trees on the "West" AISA image
- **Appendix 6** – Results of the simple linear regression test of the REIP dependence on North-East to South-West direction for selected trees on the "East" AISA image
- **Appendix 7** – Results of the simple linear regression test of the REIP dependence on North-East to South-West direction for selected trees on the "West" AISA image
- **Appendix 8** – The REIP-WDVI nomograms from PROSAIL simulation with the values of Norway spruce crowns of three RPs established on the "East" AISA image
- **Appendix 9** – "East" AISA image – Evaluation of status of Norway spruce crowns
- **Appendix 10** – "West" AISA image with the Norway spruce forest stands of interest
- **Appendix 11** – The REIP-WDVI nomograms from PROSAIL simulation with the values of Norway spruce crowns of three FSs established on the "West" AISA image
- **Appendix 12** – Map of estimated chlorophyll content for Norway spruce crowns and map of assumed health–state (covering the AISA image in natural colours) for seven chosen forest stands

Spatial specification of functional parts of Norway spruce crown

Norway spruce crown parts - vertical projection:
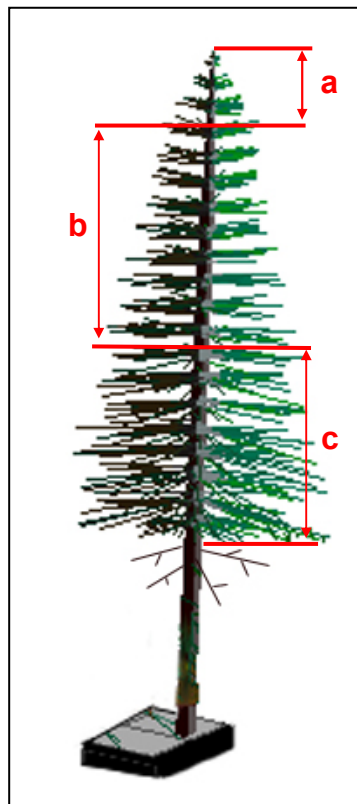
a/ **juvenile part** – upper part of the crown includes growing top. It defines a vertical increment of the tree and a colonisation of around space (positive heliotropism).

b/ **production part** – main part of the crown with high photosynthetic activity. It provides assimilates to the other part of tree and participates on a thickness increment.

c/ **saturation part** – is the part of shadowy crown with low photosynthetic activity. After the improvement of light income it can change again into the production part of the crown.

Norway spruce crown parts - horizontal projection:

Photo is RGB colour composition in unnatural colours captured by the multispectral hand camera Dycam from tower of permanent research plot Načetín at the Krušné Hory mountains (Czech Republic) - April 2000 (R = red, G = NIR, B = empty).

Vertical projection of stressed Norway spruce tree:
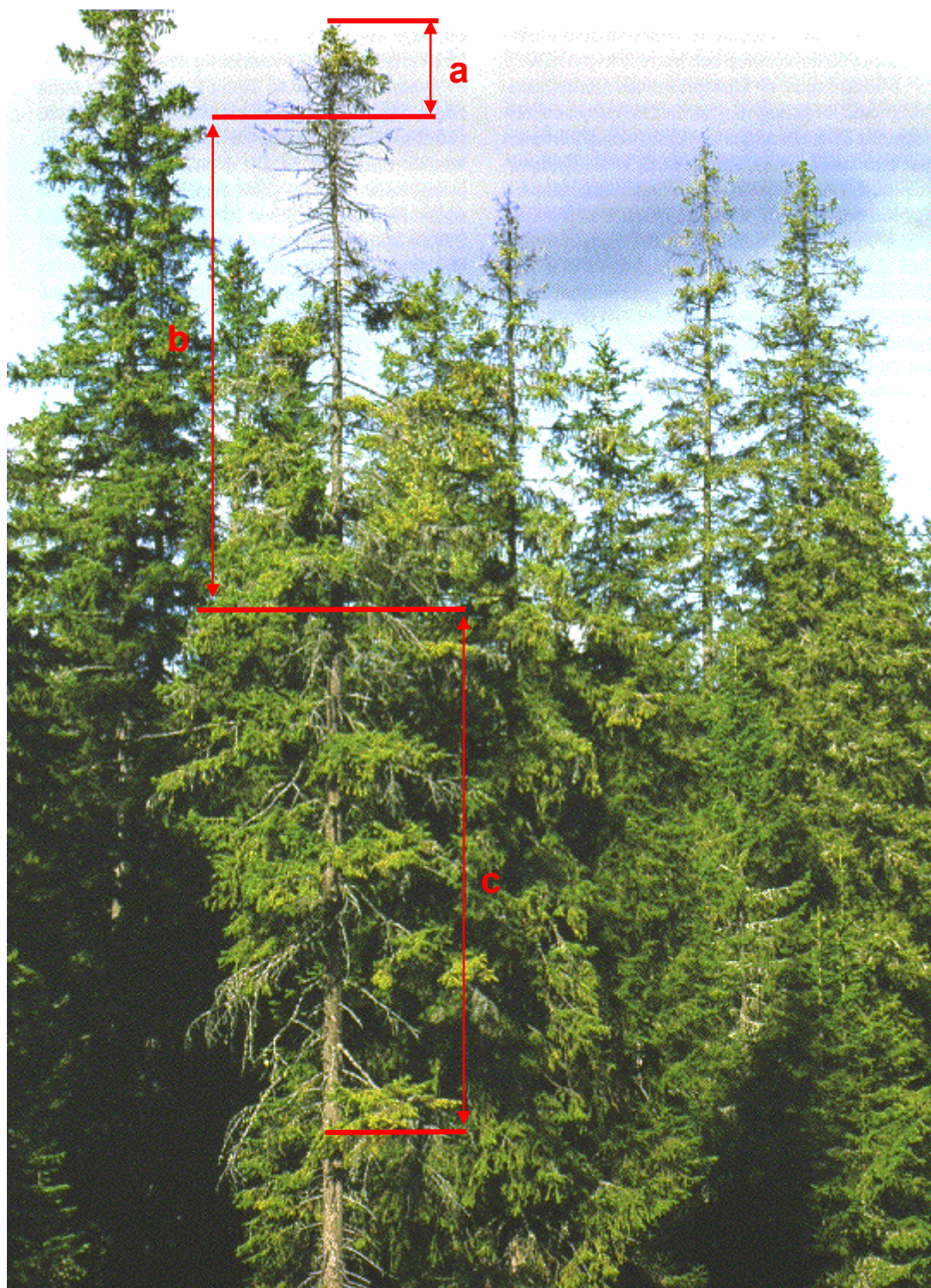
Photo source: The condition of Norway spruce (Picea abies) stands in the Straits of the Gulf of Bothnia between Finland and Sweden;
http://www.metla.fi/hanke/3194/mkurkku/e12.htm

„East" AISA image classification
- land use and forest categories -

Legend:

Land use categories

- Main roads
- River
- No data
- Urban area
- Agriculture area
- Open water

Forest categories

- Clear cut
- Forest break
- Tree plantation
- Young trees

- Deciduous forest
- Coniferous forest
- Mixed forest
- Bare soil & low vegetation

Scale: 1 : 10,000

Map projection: Finnish KKJ (Zone 3)

Overview map of the „East" AISA image classification segments

N

PART I.

PART II.

PART III.

0   500   1000   1500 Meters
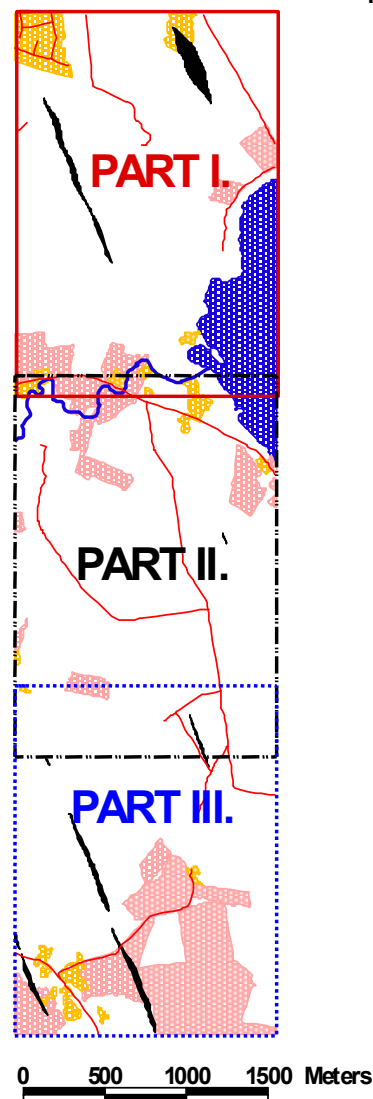
Result of the classification procedure over transformed „East" AISA image no.1.

© Zbyněk Malenovský
Laboratory of Geo-information
Science and Remote Sensing
Wageningen University - 2002

Land use and forest categories
- AISA image classification -
PART I.
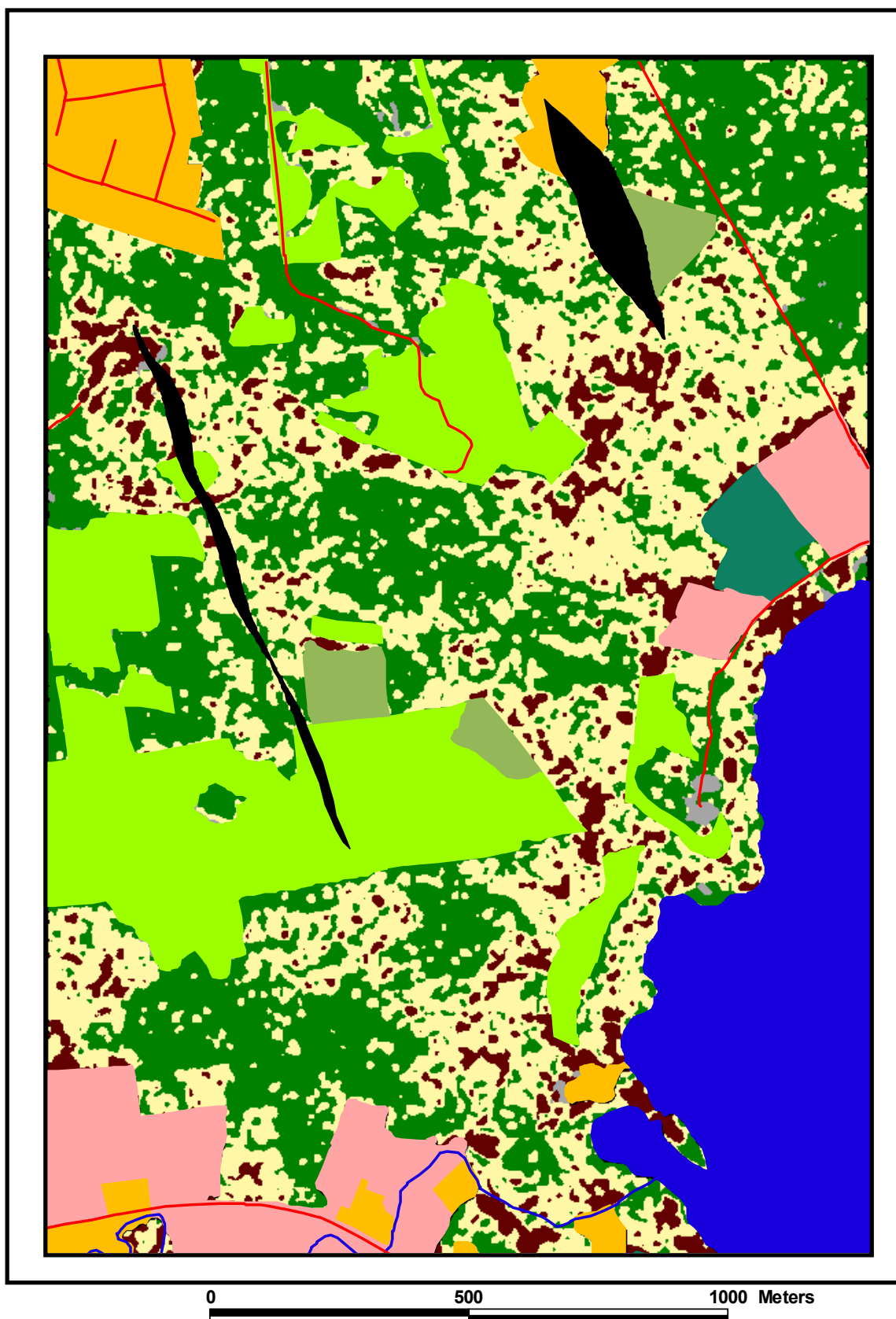
N

0   500   1000   Meters

Land use and forest categories
- AISA image classification -
PART II.

N
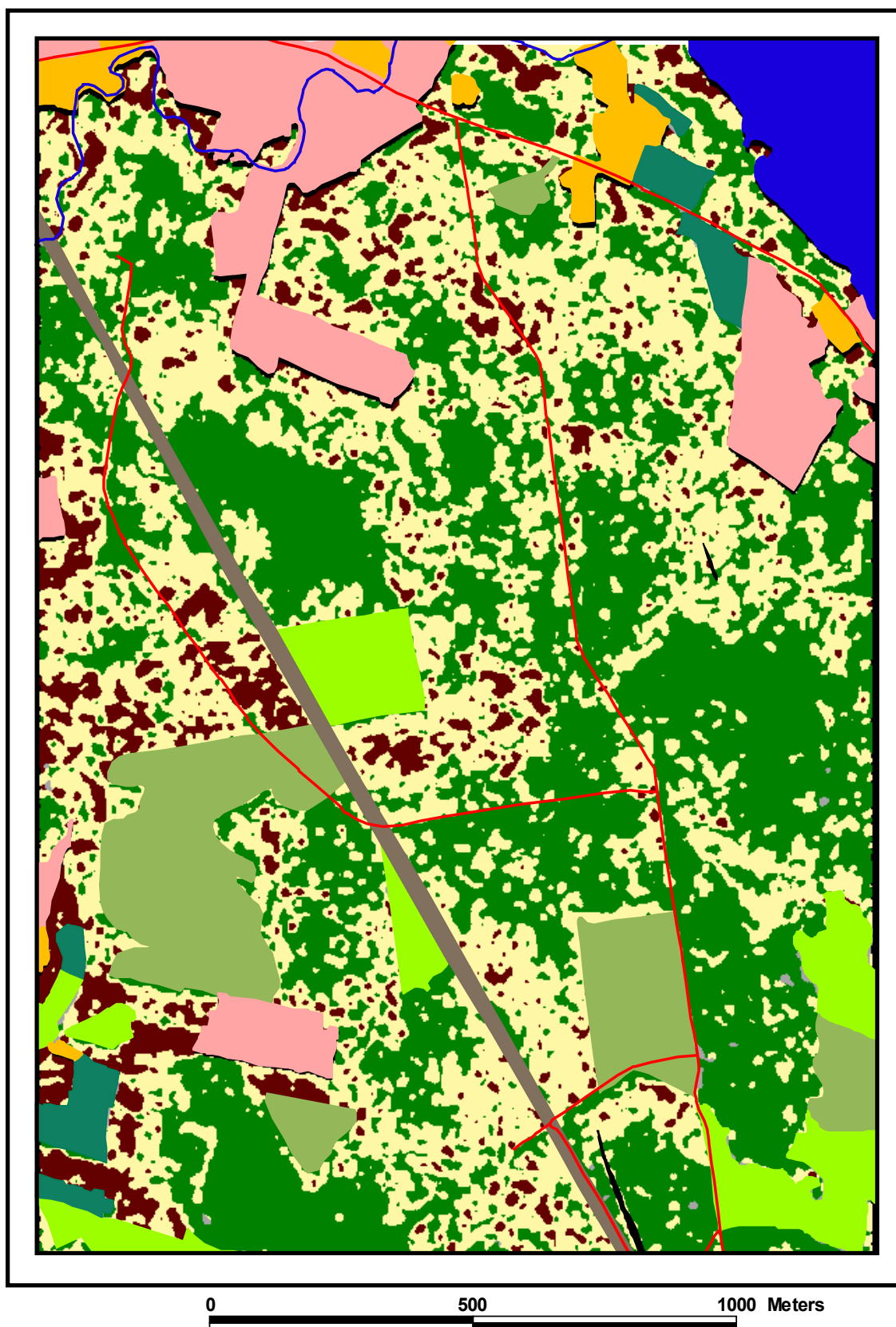
0   500   1000 Meters

Land use and forest categories
- AISA image classification -
PART III.

N
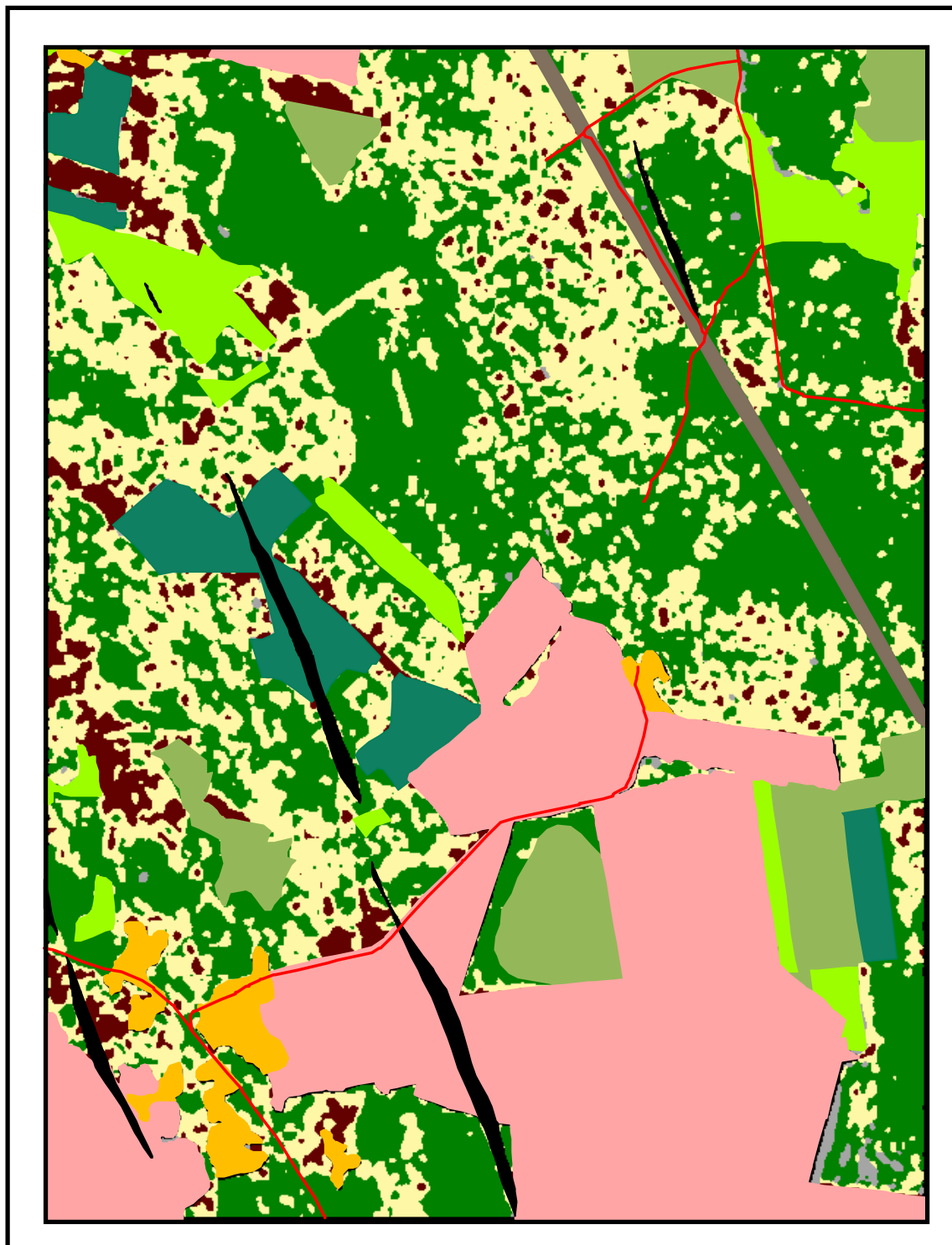
| 0 | 500 | 1000 Meters |

Spatial separation of juvenile and production spruce crown parts from the remote-sensed data at a spatial resolution of 1.1 metre

Cut window - RGB colour composition of AISA channels 12, 10, 7:

N

25 m

Inner matrix of crown

Inner matrix of juvenile part

Horizontal crown projection

5.5 m

Inner image matrix of crown or juvenile part

Horizontal projection of crown or juvenile part

a .... side of an inner image matrix
c .... diameter of crown or juvenile part
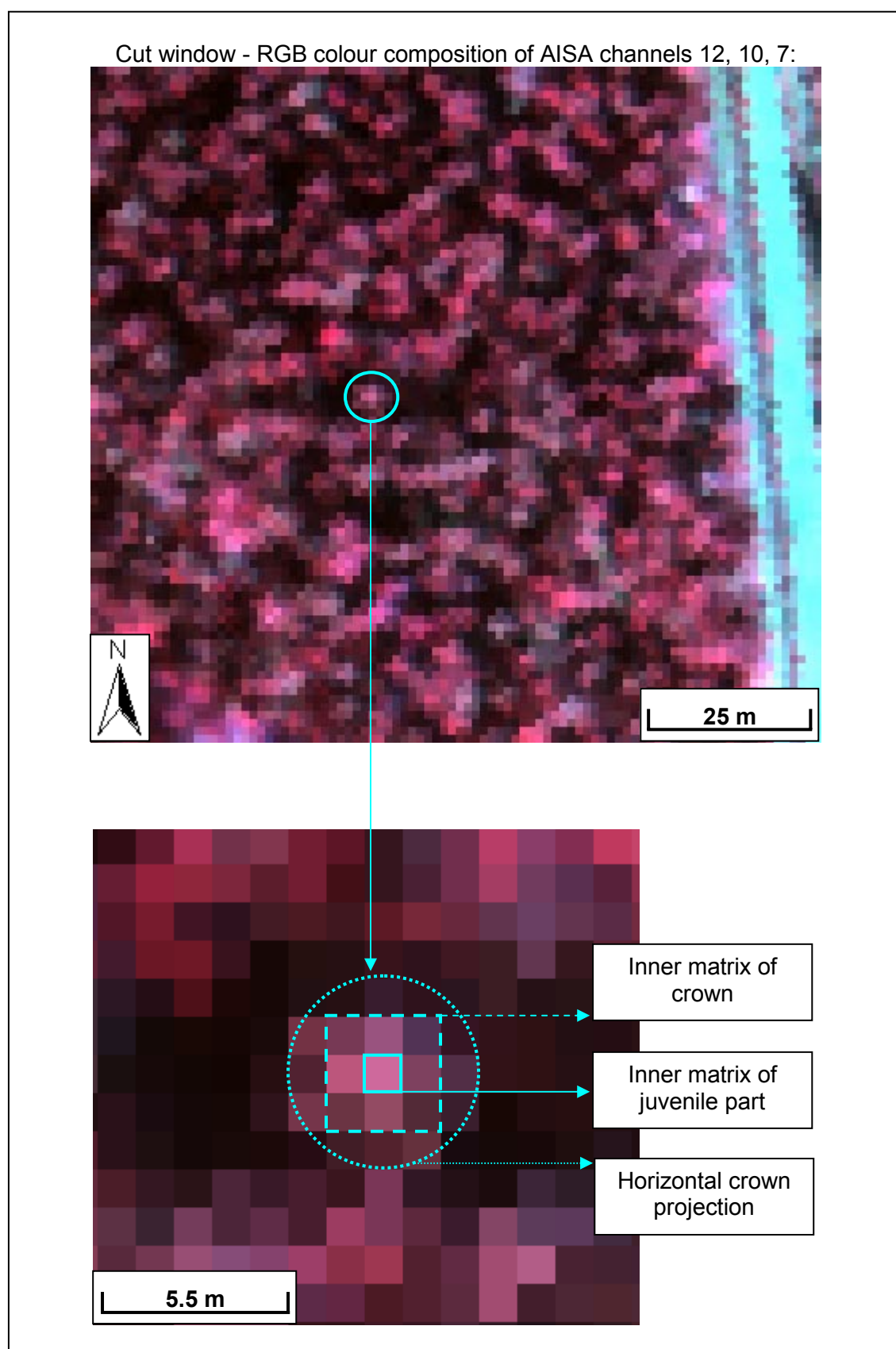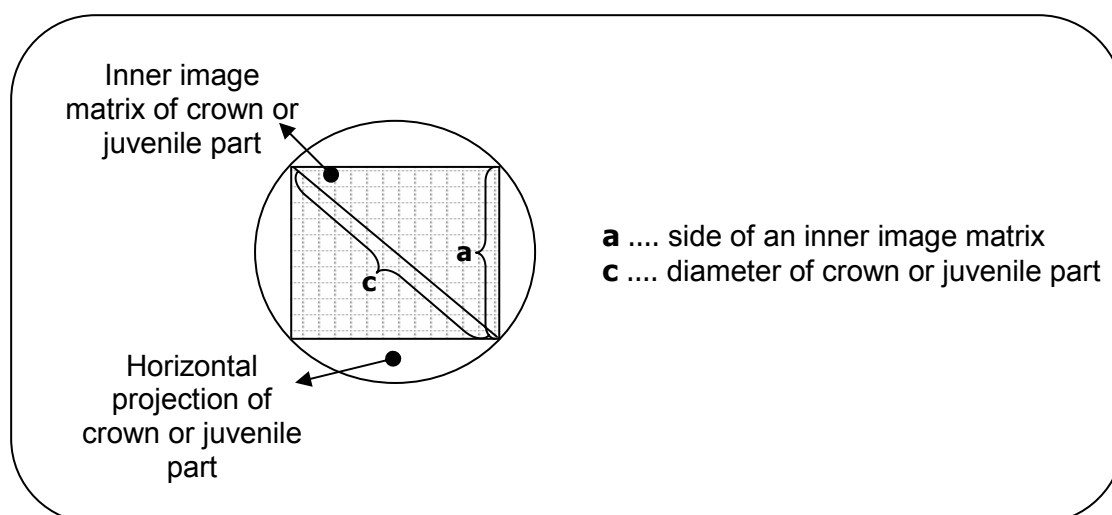
Spatial resolution of AISA image .... **1.1** m
Diameter of crown projection .... c_c
Diameter of juvenile part of crown .... c_j
Side of inner matrix of crown, production part respectively ..... a_c
Side of inner matrix of juvenile part .... a_j

Norway spruce crown of the medium size:
- Production part: c_c = 5 m => a_c = 3.54 m ~ the inner matrix = **3.2 x 3.2** pixels.
- Juvenile part: c_j = 1.5 m => a_j = 1.06 m ~ the inner matrix = **1 x 1** pixels.

Norway spruce crown of the large size:
- Production part: c_c = 7 m => a_c = 4.95 m ~ the inner matrix = **4.5 x 4.5** pixels.
- Juvenile part: c_j = 2.5 m => a_j = 1.77 m ~ the inner matrix = **1.6 x 1.6** pixels.

Results of one-sample T – test for disparity of juvenile and production crown parts through the REIP values of selected trees on the "East" AISA image

RP	Tree ID	Ho Mean	Mean	Std Error	t	df	Prob. level
1	1	718.555	719.495	2.951	0.900	7	0.398
1	2	718.067	718.889	1.405	1.655	7	0.142
1	3	719.112	718.472	1.648	-1.098	7	0.308
1	4	718.357	719.791	1.496	2.711	7	0.030
1	5	719.481	720.540	0.365	8.210	7	0.000
1	6	721.063	720.353	1.026	-1.958	7	0.091
1	7	717.208	717.925	2.037	0.995	7	0.353
1	8	719.545	720.404	1.179	2.061	7	0.078
1	9	720.149	719.878	1.592	-0.482	7	0.645
1	10	719.248	720.171	2.807	0.931	7	0.383
1	11	720.278	720.677	3.230	0.349	7	0.737
1	12	720.396	719.742	2.475	-0.748	7	0.479
1	13	720.384	720.477	1.696	0.154	7	0.882
1	14	718.015	719.034	1.456	1.978	7	0.088
1	15	717.683	719.362	2.382	1.994	7	0.086
1	46	720.519	721.161	1.511	1.202	7	0.268
1	47	721.566	721.980	1.790	0.654	7	0.534
1	48	721.430	721.071	1.525	-0.665	7	0.527
1	49	718.533	719.456	2.826	0.924	7	0.386
1	50	721.051	720.272	2.161	-1.020	7	0.342
1	51	720.343	720.227	1.554	-0.211	7	0.839
1	52	718.129	718.943	1.497	1.538	7	0.168
1	53	715.840	716.774	1.738	1.521	7	0.172
1	54	720.419	719.346	0.792	-3.832	7	0.006
1	55	717.804	718.500	2.540	0.775	7	0.464
2	16	718.315	717.916	2.357	-0.478	7	0.647
2	17	720.629	719.810	1.770	-1.309	7	0.232
2	18	718.109	718.391	2.176	0.367	7	0.724
2	19	718.862	719.319	2.045	0.632	7	0.548
2	20	719.697	719.494	2.663	-0.216	7	0.835
2	21	719.014	720.158	1.267	2.554	7	0.038
2	22	718.594	719.209	2.483	0.701	7	0.506
2	23	717.211	717.137	3.044	-0.069	7	0.947
2	24	721.771	720.703	2.652	-1.139	7	0.292
2	25	719.553	718.819	2.996	-0.693	7	0.510
2	26	719.071	719.981	0.843	3.054	7	0.018
2	27	719.230	720.089	1.773	1.371	7	0.213

RP	Tree ID	Ho Mean	Mean	Std Error	t	df	Prob. level
2	28	721.512	719.087	3.918	-1.751	7	0.123
2	29	717.748	718.725	2.278	1.214	7	0.264
2	30	714.921	718.061	2.881	3.083	7	0.018
2	56	717.286	718.312	1.191	2.438	7	0.045
2	57	719.326	720.159	2.010	1.172	7	0.280
2	58	721.723	720.517	1.175	-2.902	7	0.023
2	59	718.940	719.570	1.669	1.069	7	0.321
2	60	719.838	720.261	1.405	0.854	7	0.422
2	61	719.570	720.405	1.040	2.271	7	0.057
2	62	718.285	719.533	1.365	2.585	7	0.036
2	63	718.260	718.255	2.569	-0.005	7	0.996
2	64	719.229	718.503	2.217	-0.927	7	0.385
2	65	718.333	718.239	2.580	-0.104	7	0.920
3	31	720.613	721.117	1.893	0.753	7	0.476
3	32	717.721	719.260	2.667	1.632	7	0.147
3	33	720.497	720.770	1.883	0.410	7	0.694
3	34	716.150	717.900	2.086	2.372	7	0.049
3	35	720.818	720.304	2.102	-0.692	7	0.511
3	36	720.362	720.450	1.238	0.201	7	0.847
3	37	721.011	720.785	1.770	-0.362	7	0.728
3	38	719.958	719.774	1.508	-0.344	7	0.741
3	39	719.045	719.442	2.243	0.501	7	0.632
3	40	720.255	719.143	3.876	-0.811	7	0.444
3	41	719.870	720.809	3.031	0.876	7	0.410
3	42	717.870	718.730	2.854	0.852	7	0.422
3	43	718.189	716.959	4.679	-0.744	7	0.481
3	44	719.249	718.793	1.644	-0.784	7	0.459
3	45	721.457	720.141	2.205	-1.688	7	0.135
3	66	722.348	722.304	0.563	-0.221	7	0.832
3	67	720.735	720.741	1.183	0.014	7	0.989
3	68	721.001	721.694	0.603	3.252	7	0.014
3	69	721.365	721.835	0.539	2.471	7	0.043
3	70	720.294	721.541	0.858	4.111	7	0.005
3	71	720.568	720.731	0.762	0.605	7	0.564
3	72	721.028	721.020	0.626	-0.038	7	0.971
3	73	721.810	721.575	0.524	-1.267	7	0.246
3	74	718.783	719.318	0.518	2.917	7	0.022
3	75	718.801	718.960	0.874	0.515	7	0.622

Results of one-sample T – test for disparity of juvenile and production crown parts through the REIP values of selected trees on the "West" AISA image

FS	Tree ID	Ho Mean	Mean	Std Error	t	df	Prob. level
1	76	713.924	715.642	1.775	2.738	7	0.029
1	77	711.227	714.031	1.538	5.158	7	0.001
1	78	717.291	717.067	1.388	-0.456	7	0.662
1	79	713.703	714.999	0.927	3.954	7	0.006
1	80	717.557	717.800	1.380	0.498	7	0.634
1	81	715.680	716.741	0.869	3.452	7	0.011
1	82	717.230	717.564	1.180	0.800	7	0.450
1	83	717.101	717.875	1.709	1.280	7	0.241
1	84	715.338	717.025	1.887	2.528	7	0.039
1	85	713.669	715.925	1.636	3.899	7	0.006
1	86	715.102	715.682	1.852	0.886	7	0.405
1	87	713.592	715.364	1.877	2.669	7	0.032
1	88	715.085	715.887	1.852	1.225	7	0.260
1	89	718.301	717.725	1.664	-0.980	7	0.360
1	90	717.901	718.120	2.236	0.276	7	0.790
1	91	713.377	715.604	1.928	3.268	7	0.014
1	92	716.658	717.850	1.289	2.616	7	0.035
1	93	715.435	716.899	1.934	2.141	7	0.070
1	94	716.120	716.164	2.312	0.054	7	0.959
1	95	716.587	716.853	1.663	0.453	7	0.664
1	96	714.707	715.194	1.856	0.742	7	0.482
1	97	717.490	717.708	0.820	0.751	7	0.477
1	98	717.262	717.526	1.389	0.537	7	0.608
1	99	717.299	715.372	4.569	-1.193	7	0.272
1	100	718.169	718.046	2.042	-0.170	7	0.870
2	101	714.488	715.095	1.958	0.877	7	0.409
2	102	715.590	716.069	0.997	1.358	7	0.216
2	103	715.229	716.830	1.904	2.377	7	0.049
2	104	717.262	716.833	1.193	-1.017	7	0.343
2	105	714.804	715.740	1.186	2.233	7	0.061
2	106	711.924	713.588	1.733	2.716	7	0.030
2	107	717.023	717.441	1.148	1.029	7	0.338
2	108	716.745	716.667	1.814	-0.122	7	0.906
2	109	714.745	715.662	0.937	2.769	7	0.028
2	110	712.357	713.610	1.667	2.126	7	0.071
2	111	715.946	716.814	1.025	2.394	7	0.048
2	112	715.099	714.908	0.657	-0.820	7	0.439

FS	Tree ID	Ho Mean	Mean	Std Error	t	df	Prob. level
2	113	715.748	716.375	1.224	1.448	7	0.191
2	114	713.677	714.224	1.981	0.781	7	0.460
2	115	714.776	715.728	0.979	2.750	7	0.028
2	116	713.995	714.055	1.121	0.152	7	0.884
2	117	715.553	715.983	1.085	1.121	7	0.299
2	118	714.499	716.235	0.985	4.984	7	0.002
2	119	712.922	714.437	0.995	4.307	7	0.004
2	120	713.477	714.174	1.239	1.591	7	0.156
2	121	715.295	716.574	1.616	2.238	7	0.060
2	122	714.582	715.282	0.637	3.106	7	0.017
2	123	714.847	715.750	1.308	1.951	7	0.092
2	124	716.640	716.712	1.167	0.173	7	0.867
2	125	714.404	715.495	0.624	4.944	7	0.002

APPENDIX 6

Results of the simple linear regression test of the REIP dependence on North-East to South-West direction for selected trees on the "East" AISA image

RP	Tree ID	Multiple R	SQR Mult. R	α	β	T (β)	Prob. level
1	1	0.609	0.371	715.245	1.382	2.032	0.082
1	2	0.553	0.305	716.981	0.606	1.754	0.123
1	3	0.707	0.500	715.848	0.899	2.645	0.033
1	4	0.854	0.729	716.538	1.031	4.343	0.003
1	5	0.069	0.005	720.339	0.028	0.184	0.859
1	6	0.726	0.527	718.674	0.586	2.794	0.027
1	7	0.805	0.649	714.057	1.263	3.594	0.009
1	8	0.620	0.385	718.577	0.577	2.093	0.075
1	9	0.599	0.359	717.718	0.730	1.981	0.088
1	10	0.880	0.775	714.369	1.900	4.911	0.002
1	11	0.963	0.928	713.498	2.378	9.480	0.000
1	12	0.849	0.721	714.976	1.613	4.258	0.004
1	13	0.940	0.883	716.813	1.218	7.271	0.000
1	14	0.739	0.546	716.380	0.847	2.904	0.023
1	15	0.876	0.768	714.243	1.644	4.817	0.002
1	46	0.878	0.770	718.016	1.024	4.842	0.002
1	47	0.707	0.500	719.025	0.969	2.644	0.033
1	48	0.715	0.511	718.603	0.836	2.707	0.030
1	49	0.020	0.000	719.486	-0.044	-0.054	0.958
1	50	0.677	0.458	716.980	1.126	2.431	0.045
1	51	0.798	0.637	717.397	0.948	3.502	0.010
1	52	0.487	0.238	717.150	0.568	1.477	0.183
1	53	0.762	0.581	713.580	1.030	3.114	0.017
1	54	0.454	0.206	718.549	0.305	1.349	0.219
1	55	0.881	0.776	713.272	1.717	4.922	0.002
2	16	0.765	0.585	713.822	1.380	3.143	0.016
2	17	0.529	0.280	717.726	0.725	1.650	0.143
2	18	0.756	0.571	714.588	1.257	3.053	0.019
2	19	0.843	0.710	715.307	1.321	4.141	0.004
2	20	0.986	0.971	713.500	2.005	15.388	0.000
2	21	0.820	0.672	717.532	0.833	3.785	0.007
2	22	0.788	0.620	714.643	1.499	3.381	0.012
2	23	0.951	0.905	710.509	2.212	8.169	0.000
2	24	0.961	0.923	714.925	1.966	9.148	0.000
2	25	0.945	0.893	712.389	2.170	7.647	0.000
2	26	0.785	0.616	718.255	0.541	3.350	0.012
2	27	0.763	0.582	716.850	1.048	3.120	0.017

| RP	Tree ID	Multiple R	SQR Mult. R	α	β	T (β)	Prob. level
2	28	0.905	0.820	711.032	2.775	5.644	0.001
2	29	0.948	0.898	713.614	1.668	7.856	0.000
2	30	0.810	0.656	711.975	1.913	3.657	0.008
2	56	0.611	0.374	716.453	0.582	2.044	0.080
2	57	0.882	0.778	715.958	1.369	4.956	0.002
2	58	0.881	0.777	718.123	0.843	4.938	0.002
2	59	0.733	0.537	716.672	0.943	2.850	0.025
2	60	0.747	0.558	717.796	0.806	2.975	0.021
2	61	0.766	0.587	718.412	0.633	3.156	0.016
2	62	0.757	0.573	716.904	0.830	3.066	0.018
2	63	0.970	0.941	712.544	1.904	10.611	0.000
2	64	0.842	0.709	714.276	1.436	4.134	0.004
2	65	0.909	0.827	712.874	1.792	5.781	0.001
3	31	0.898	0.807	717.146	1.305	5.415	0.001
3	32	0.797	0.635	714.119	1.657	3.488	0.010
3	33	0.710	0.505	717.671	1.023	2.671	0.032
3	34	0.774	0.599	713.844	1.287	3.234	0.014
3	35	0.915	0.838	715.936	1.475	6.016	0.001
3	36	0.775	0.600	718.242	0.733	3.243	0.014
3	37	0.905	0.818	717.138	1.224	5.617	0.001
3	38	0.784	0.614	717.083	0.904	3.339	0.012
3	39	0.805	0.648	715.253	1.382	3.588	0.009
3	40	0.919	0.845	711.059	2.736	6.178	0.000
3	41	0.869	0.756	714.630	2.025	4.655	0.002
3	42	0.874	0.765	712.883	1.917	4.769	0.002
3	43	0.985	0.969	706.493	3.534	14.886	0.000
3	44	0.904	0.817	715.423	1.140	5.592	0.001
3	45	0.876	0.767	715.762	1.508	4.803	0.002
3	66	0.117	0.014	722.157	0.050	0.313	0.764
3	67	0.757	0.573	718.690	0.683	3.062	0.018
3	68	0.136	0.019	721.414	0.068	0.364	0.727
3	69	0.666	0.444	720.922	0.287	2.364	0.050
3	70	0.566	0.320	720.150	0.418	1.815	0.112
3	71	0.542	0.294	719.763	0.317	1.708	0.131
3	72	0.579	0.336	720.190	0.277	1.881	0.102
3	73	0.841	0.707	720.580	0.341	4.113	0.005
3	74	0.256	0.066	718.934	0.108	0.701	0.506
3	75	0.544	0.295	717.851	0.364	1.713	0.130

Results of the simple linear regression test of the REIP dependence on North-East to South-West direction for selected trees on the "West"AISA image

FS	Tree ID	Multiple R	SQR Mult. R	α	β	T (β)	Prob. level
1	76	0.888	0.788	711.632	1.273	5.101	0.001
1	77	0.303	0.092	712.445	0.425	0.842	0.428
1	78	0.664	0.441	714.976	0.705	2.350	0.051
1	79	0.206	0.042	714.367	0.163	0.556	0.595
1	80	0.866	0.751	715.029	0.915	4.590	0.003
1	81	0.164	0.027	716.267	0.119	0.439	0.674
1	82	0.540	0.291	716.060	0.489	1.697	0.134
1	83	0.833	0.694	714.483	1.102	3.987	0.005
1	84	0.881	0.777	712.837	1.333	4.937	0.002
1	85	0.692	0.479	712.782	0.964	2.538	0.039
1	86	0.715	0.511	712.567	1.017	2.703	0.031
1	87	0.815	0.665	711.467	1.233	3.724	0.007
1	88	0.779	0.607	712.452	1.115	3.290	0.013
1	89	0.701	0.492	715.094	0.898	2.603	0.035
1	90	0.921	0.848	713.373	1.574	6.257	0.000
1	91	0.783	0.614	711.615	1.247	3.336	0.012
1	92	0.616	0.379	715.802	0.639	2.068	0.077
1	93	0.742	0.551	713.329	1.136	2.932	0.022
1	94	0.784	0.615	712.007	1.384	3.341	0.012
1	95	0.750	0.563	713.961	0.954	3.002	0.020
1	96	0.196	0.039	714.302	0.279	0.530	0.613
1	97	0.676	0.457	716.408	0.425	2.426	0.046
1	98	0.922	0.849	714.557	0.980	6.279	0.000
1	99	0.939	0.882	705.645	3.314	7.232	0.000
1	100	0.929	0.862	713.715	1.448	6.626	0.000
2	101	0.883	0.779	711.043	1.328	4.969	0.002
2	102	0.655	0.429	714.497	0.506	2.295	0.055
2	103	0.786	0.618	713.071	1.194	3.365	0.012
2	104	0.612	0.375	715.194	0.562	2.048	0.080
2	105	0.497	0.247	714.233	0.468	1.516	0.173
2	106	0.895	0.801	709.647	1.252	5.310	0.001
2	107	0.919	0.844	714.957	0.812	6.155	0.000
2	108	0.814	0.662	713.293	1.127	3.702	0.008
2	109	0.614	0.377	714.165	0.465	2.058	0.079
2	110	0.443	0.197	711.717	0.584	1.309	0.232
2	111	0.790	0.625	714.778	0.646	3.415	0.011
2	112	0.587	0.344	714.042	0.296	1.916	0.097

FS	Tree ID	Multiple R	SQR Mult. R	α	β	T (β)	Prob. level
2	113	0.732	0.536	714.218	0.696	2.843	0.025
2	114	0.776	0.602	710.625	1.180	3.254	0.014
2	115	0.831	0.691	713.649	0.658	3.954	0.006
2	116	0.823	0.678	711.934	0.705	3.840	0.006
2	117	0.881	0.776	713.724	0.737	4.923	0.002
2	118	0.048	0.002	715.913	0.043	0.128	0.901
2	119	0.239	0.057	713.650	0.206	0.650	0.536
2	120	0.476	0.226	712.720	0.459	1.430	0.196
2	121	0.410	0.168	714.855	0.526	1.189	0.273
2	122	0.166	0.028	714.944	0.087	0.446	0.669
2	123	0.875	0.766	712.948	0.901	4.783	0.002
2	124	0.793	0.629	714.584	0.707	3.442	0.011
2	125	0.724	0.525	714.154	0.407	2.779	0.027

The REIP-WDVI nomograms from PROSAIL simulation with the values of Norway spruce crowns of three RPs established on the "East" AISA image
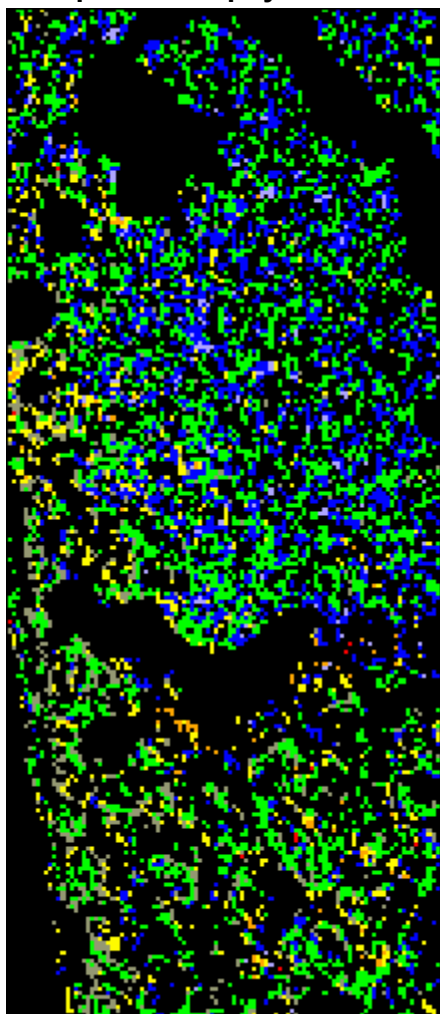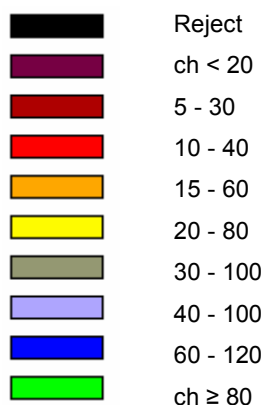
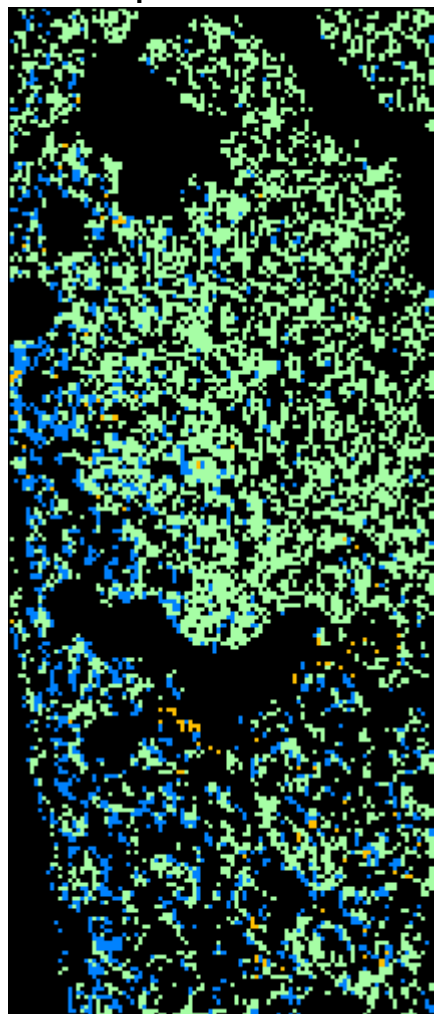**Research place no. 1**
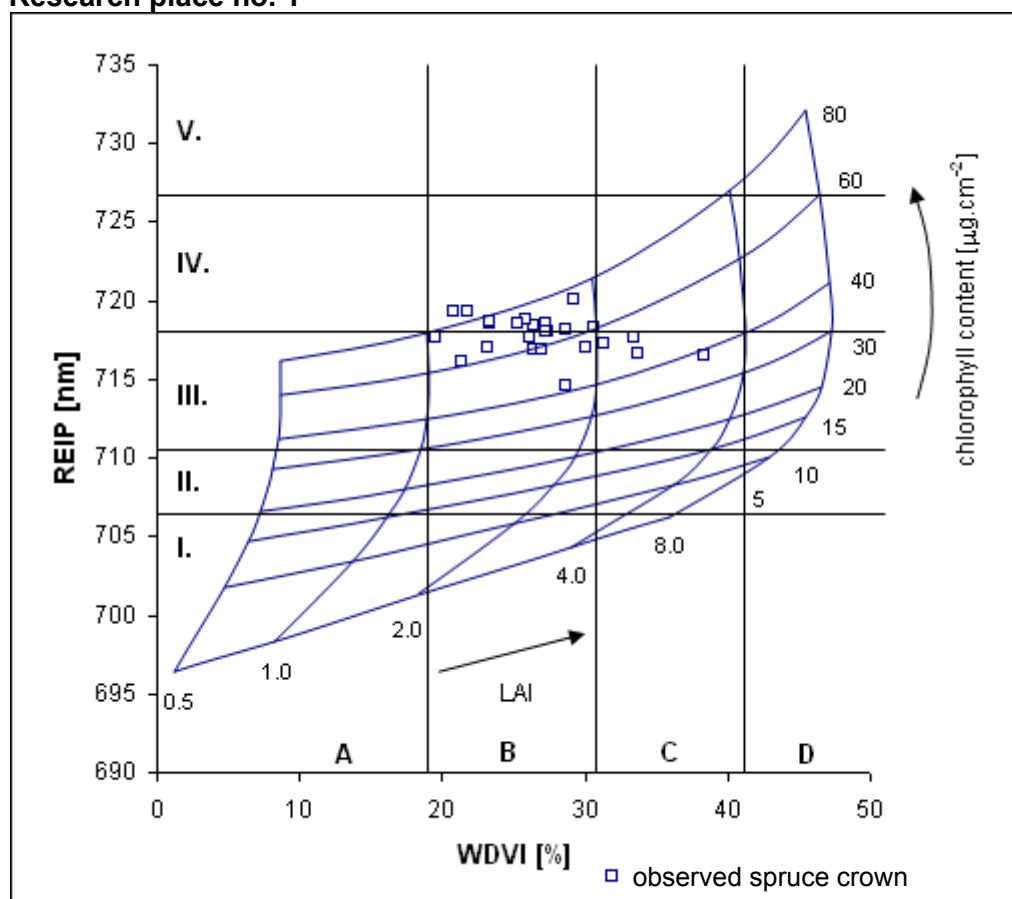
Brief statistical overview:

Damage	Crowns	Freq. [%]
Moderate	4	16
Low	9	36
None	12	48

Research place no. 2
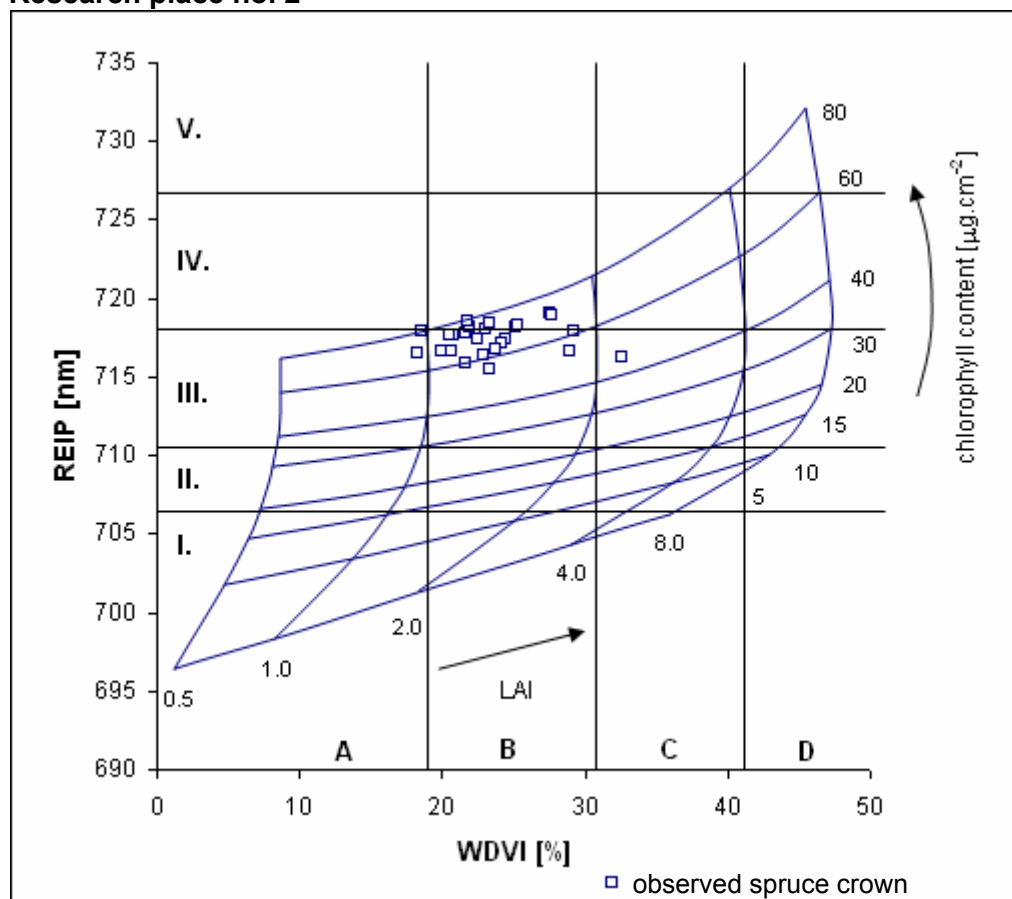
Brief statistical overview:

Damage	Crowns	Freq. [%]
Moderate	1	4
Low	16	64
None	8	32

Research place no. 3
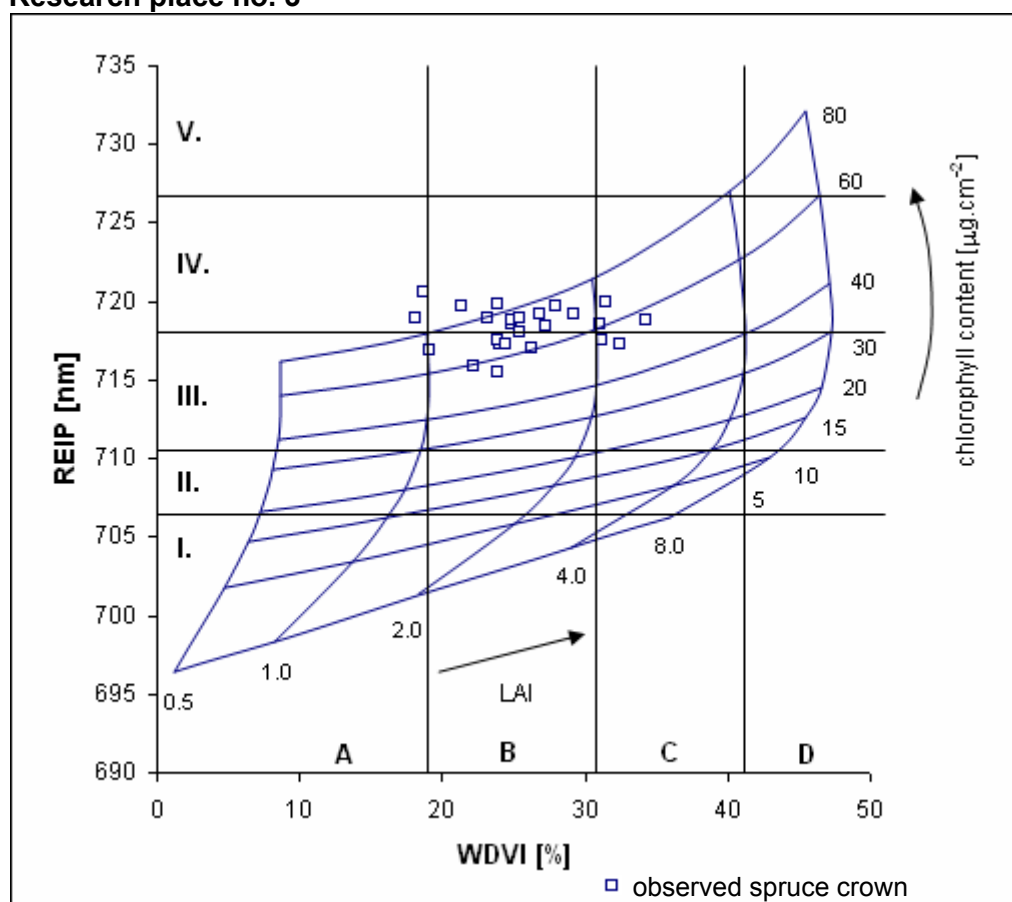
Brief statistical overview:

Damage	Crowns	Freq. [%]
Moderate	2	8
Low	7	28
None	16	64

"East" AISA image – Evaluation of status of Norway spruce crowns

Map of chlorophyll content

Map of health-state

Chlorophyll content – ch [$\mu g.cm^{-2}$]

■ (black)	Reject
■ (dark maroon)	ch < 20
■ (dark red)	5 - 30
■ (red)	10 - 40
■ (orange)	15 - 60
■ (yellow)	20 - 80
■ (olive)	30 - 100
■ (light purple)	40 - 100
■ (blue)	60 - 120
■ (green)	ch ≥ 80

Health-state

|	
■ (black)	Reject
■ (red)	High damage
■ (orange)	Moderate damage
■ (blue)	Low damage
■ (light green)	Very low or none damage

50 m

1: 2,000

North
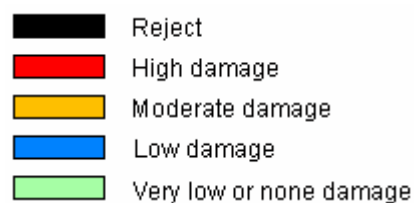
The results of chlorophyll content and health-state estimation for a slit of AISA image no. 1 – "East".

Source: Zbyněk Malenovský
Laboratory of Geo-information
Science and Remote Sensing
Wageningen University - 2002

"West" AISA image with the Norway spruce forest stands of interest
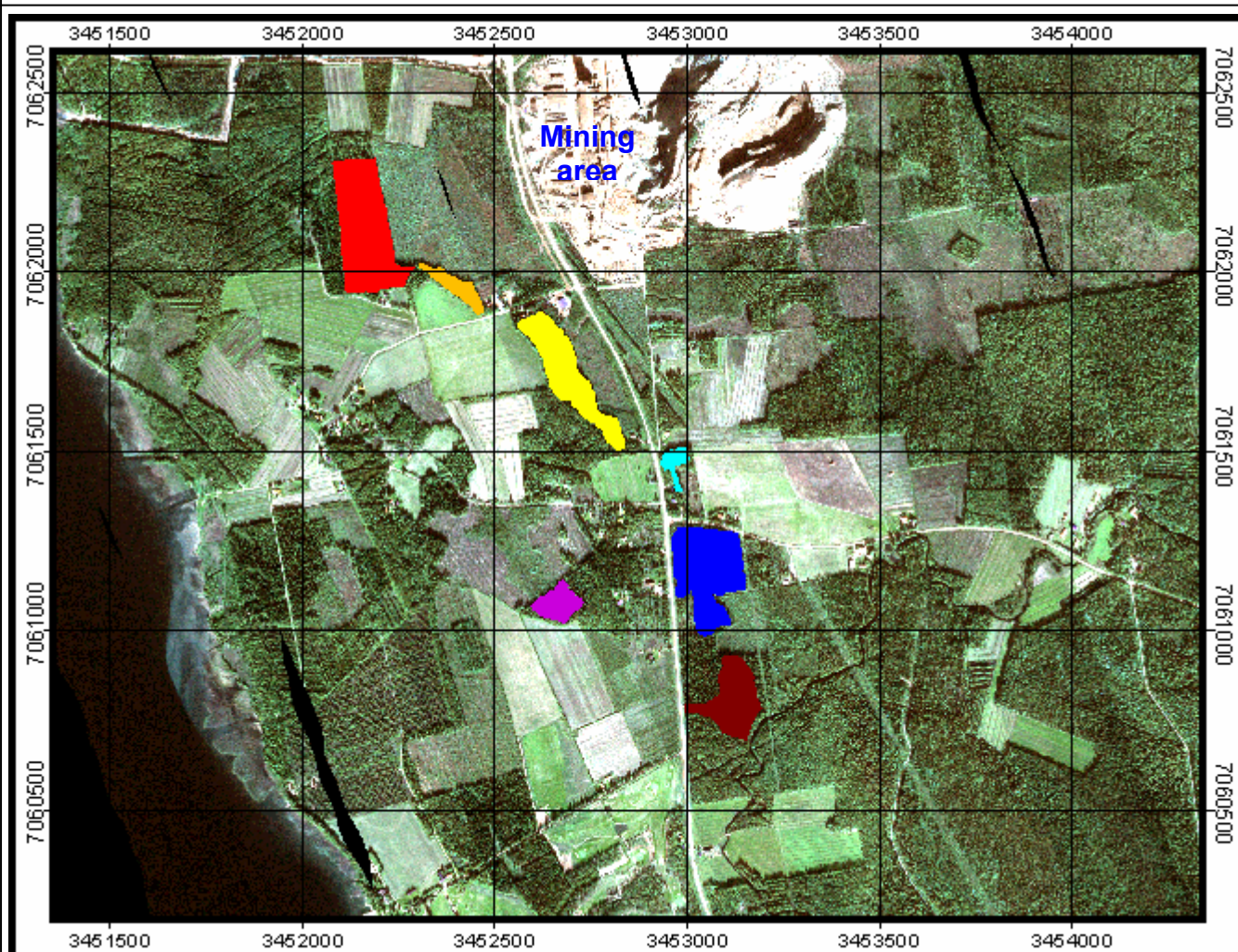
Forest stand No. 1
Forest stand No. 2
Forest stand No. 3
Forest stand No. 4
Forest stand No. 5
Forest stand No. 6
Forest stand No. 7

Scale: 1:14,000
Map Projection: Finnish KKJ
(Uniform Zone [27° E])

The RGB composition in natural colours of 7,5,3
"West" AISA bands with selected spruce forest
stands.

Source: Zbyněk Malenovský
GIRS Laboratory – WUR 2002

Polygons of the Norway spruce forest stands of interest covering the "West" AISA image in natural colours.
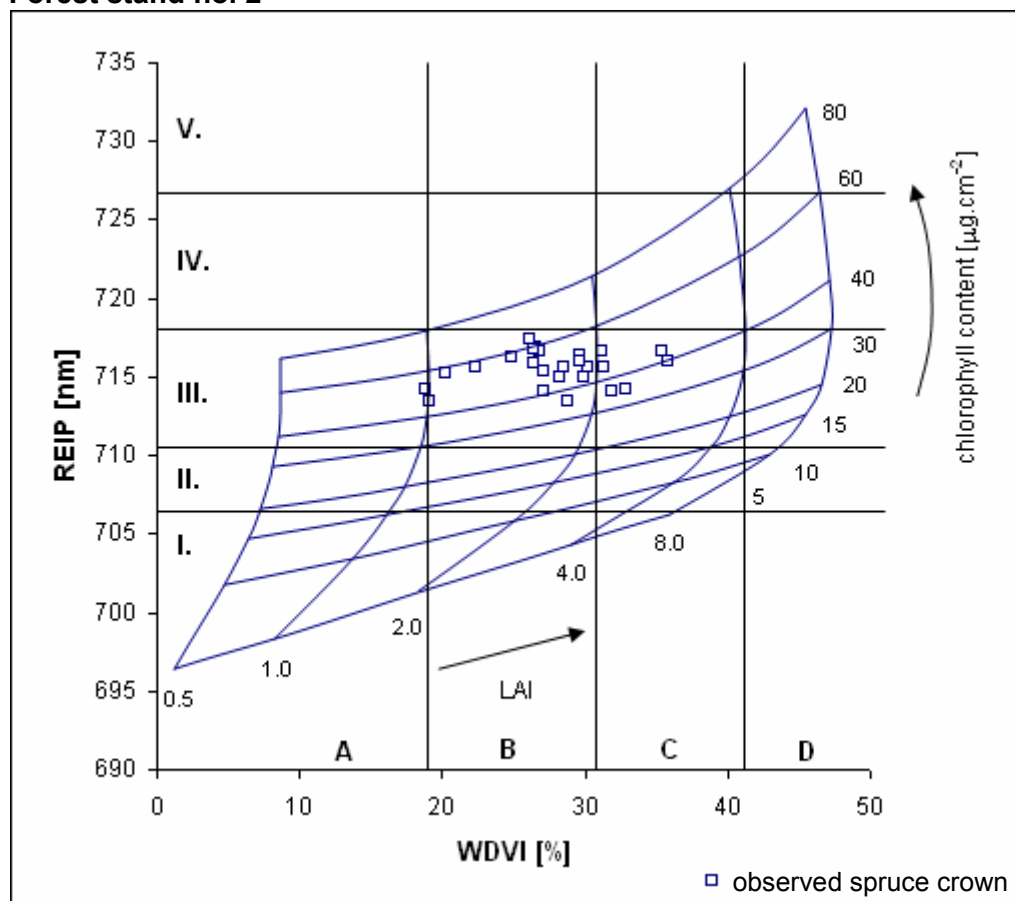
The REIP-WDVI nomograms from PROSAIL simulation with the values of Norway spruce crowns of three FSs established on the "West" AISA image
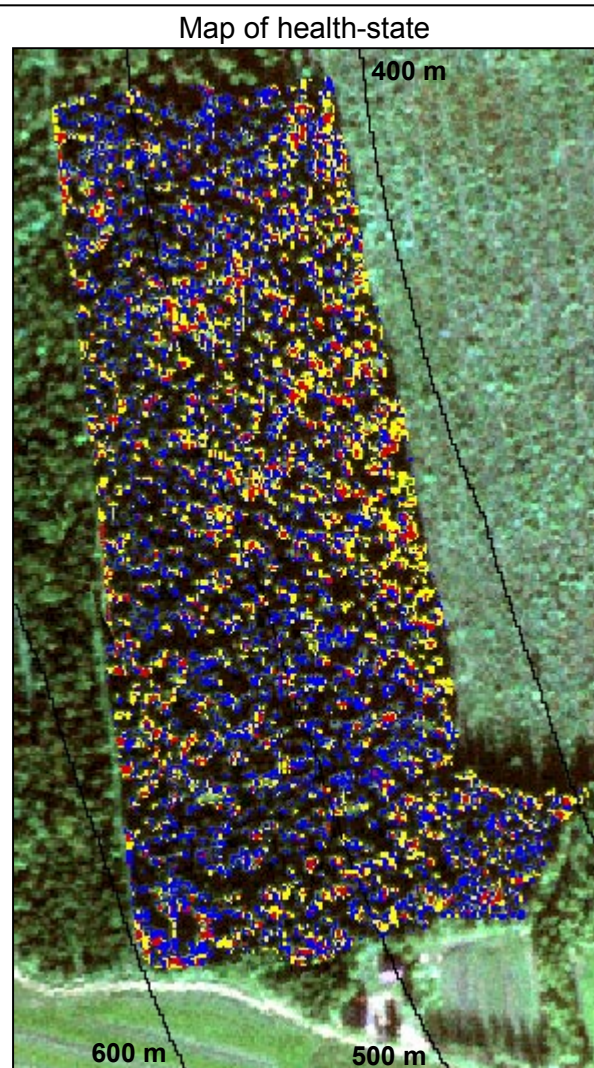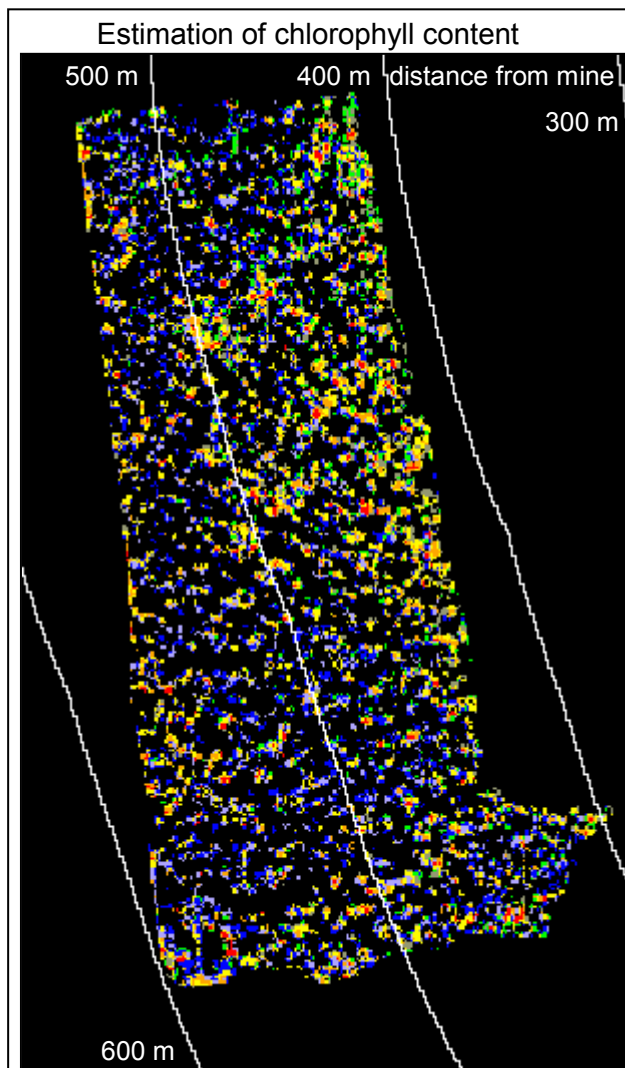
Forest stand no. 1
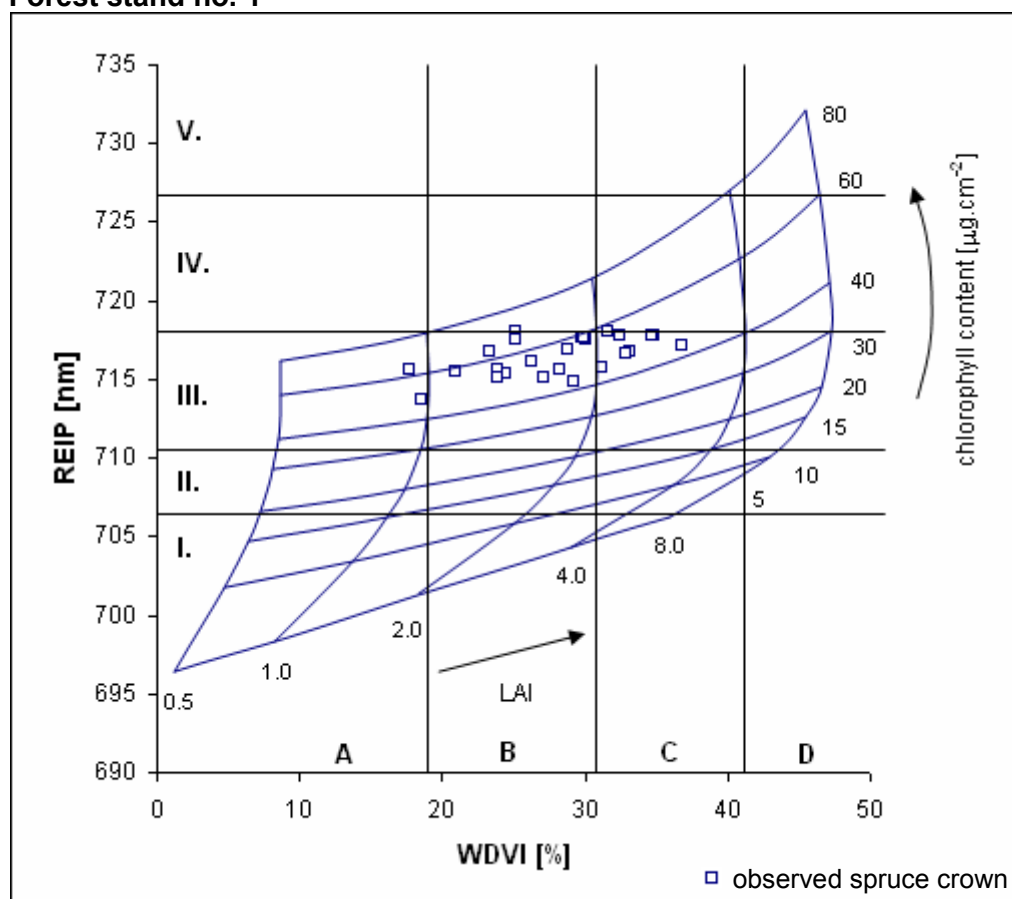
Brief statistical overview:

Damage	Crowns	Freq. [%]
Moderate	8	32
Low	16	64
None	1	4

Forest stand no. 2

Brief statistical overview:

Damage	Crowns	Freq. [%]
Moderate	6	24
Low	19	76
None	0	0

APPENDIX 12

Map of estimated chlorophyll content for Norway spruce crowns and map of assumed health-state (covering the AISA image in natural colours) for seven chosen forest stands

Forest stand No. 1

Estimation of chlorophyll content

500 m 400 m distance from mine

300 m

600 m

Map of health-state

400 m

600 m 500 m

Chlorophyll content - ch - [$\mu g.cm^{-2}$]	Number of pixels	Frequency [%]
Reject	-	-
10 - 40	541	3.5
15 - 60	1760	11.4
20 - 80	3794	24.6
30 - 100	1436	9.3
40 - 100	2349	15.3
60 - 120	4358	28.3
ch $\geq$ 80	1163	7.6
SUM	15401	100.0

Health-state	Number of pixels	Freq. [%]
Moderate damage	2301	14.9
Low damage	5230	34.0
Very low or no damage	7870	51.1
SUM	15401	100.0

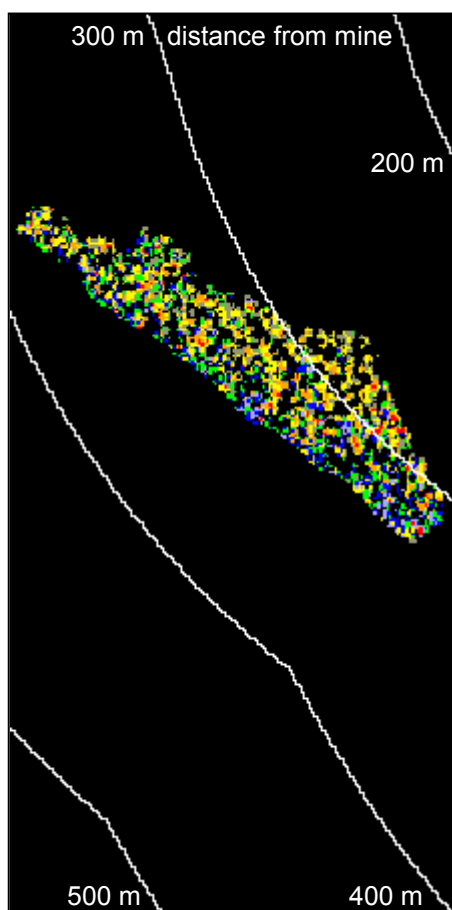| Distance from the Cu–Zn sulphide mine [m]	
min	max
383	598

0 100 200 Meters
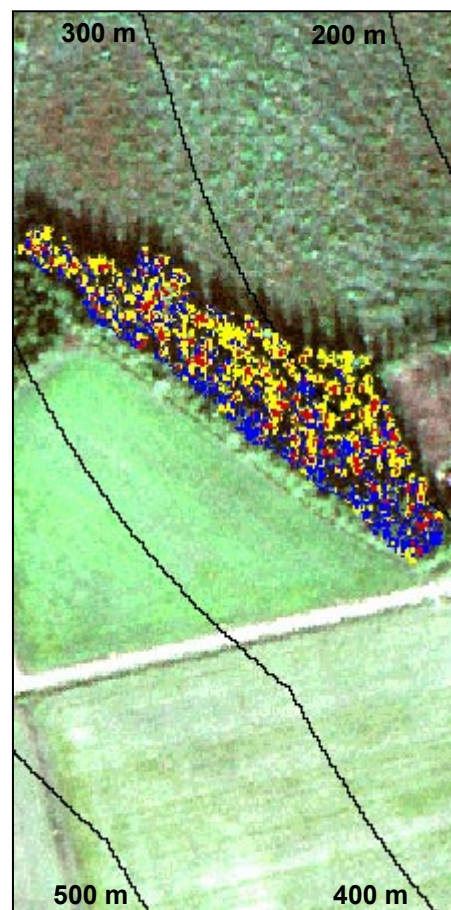
Source: Zbyněk Malenovský; GIRS Laboratory – WUR 2002

Forest stand No. 2
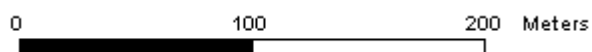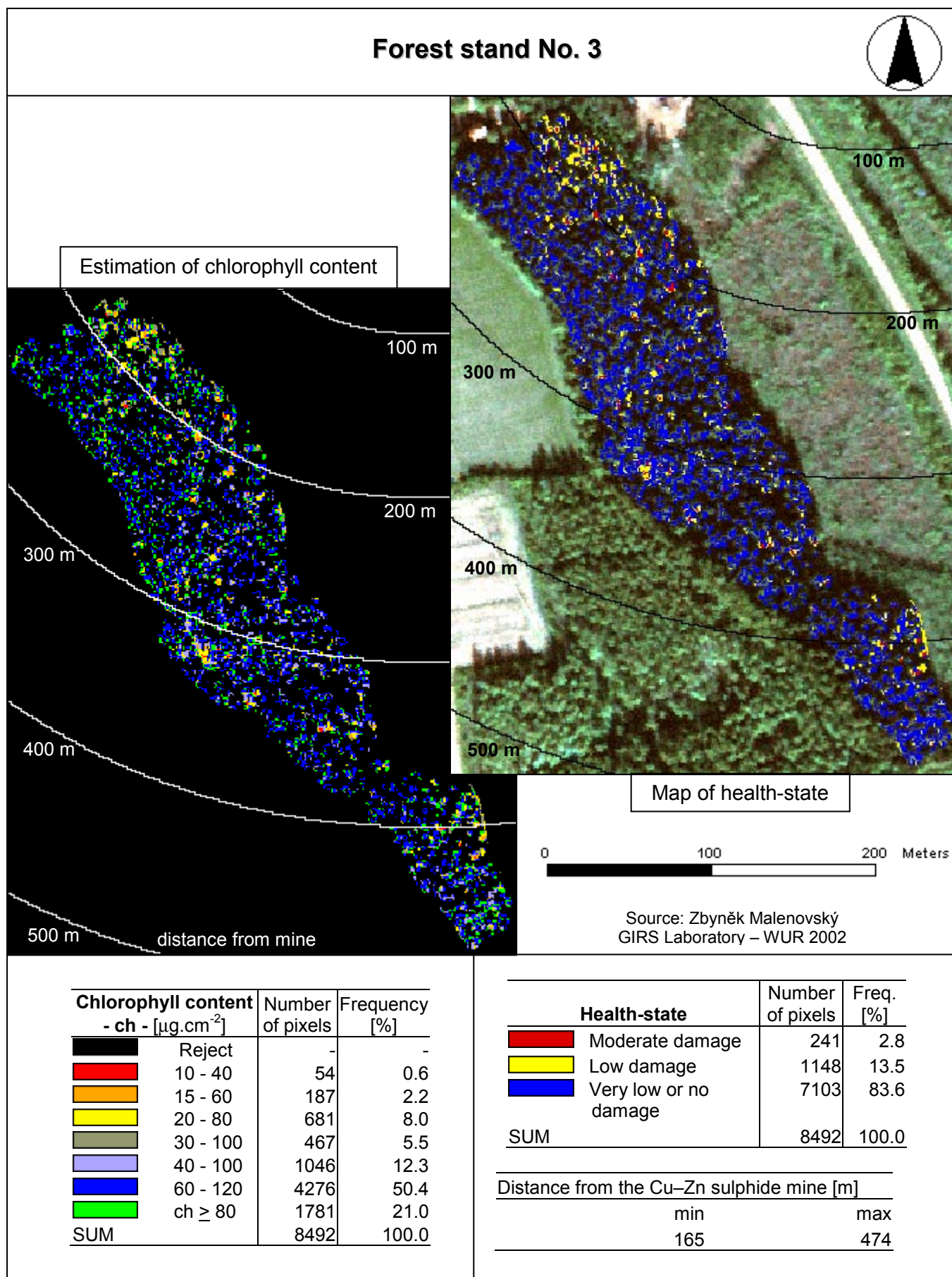
Estimation of chlorophyll content

Map of health-state

Chlorophyll content - ch - [µg.cm^{-2}]		Number of pixels	Frequency [%]
	Reject	-	-
	10 - 40	115	3.1
	15 - 60	528	14.3
	20 - 80	969	26.2
	30 - 100	708	19.1
	40 - 100	214	5.8
	60 - 120	554	15.0
	ch $\geq$ 80	613	16.6
SUM		3701	100.0

Health-state		Number of pixels	Freq. [%]
	Moderate damage	643	17.4
	Low damage	1677	45.3
	Very low or no damage	1381	37.3
SUM		3701	100.0

Distance from the Cu–Zn sulphide mine [m]

min	max
273	383

0   100   200   Meters

Source: Zbyněk Malenovský
GIRS Laboratory – WUR 2002

Forest stand No. 3

Estimation of chlorophyll content

100 m

200 m

300 m

400 m

500 m   distance from mine

100 m

200 m

300 m

400 m

500 m

Map of health-state

0   100   200   Meters

Source: Zbyněk Malenovský
GIRS Laboratory – WUR 2002

Chlorophyll content - ch - [$\mu g.cm^{-2}$]	Number of pixels	Frequency [%]
Reject	-	-
10 - 40	54	0.6
15 - 60	187	2.2
20 - 80	681	8.0
30 - 100	467	5.5
40 - 100	1046	12.3
60 - 120	4276	50.4
ch $\geq$ 80	1781	21.0
SUM	8492	100.0

Health-state	Number of pixels	Freq. [%]
Moderate damage	241	2.8
Low damage	1148	13.5
Very low or no damage	7103	83.6
SUM	8492	100.0

Distance from the Cu–Zn sulphide mine [m]

min	max
165	474

Forest stand No. 4

Estimation of chlorophyll content

distance from mine

400 m

500 m

600 m

Map of health-state

400 m

500 m

600 m
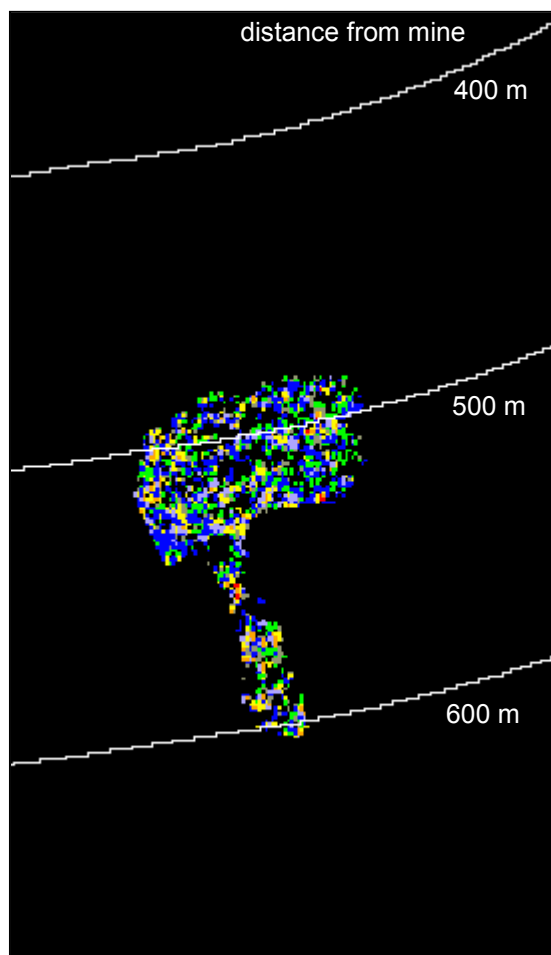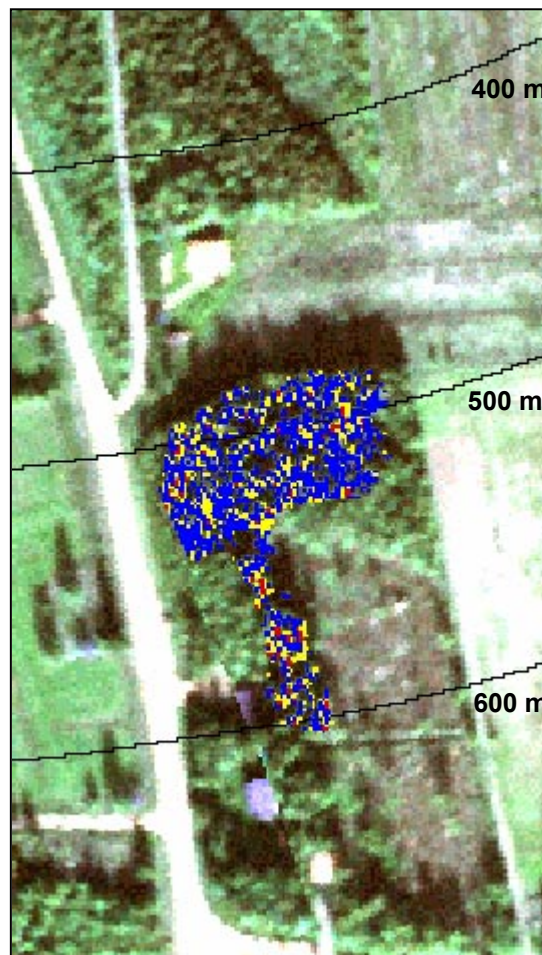
Chlorophyll content - ch - [$\mu g.cm^{-2}$]	Number of pixels	Frequency [%]
Reject	-	-
10 - 40	10	0.4
15 - 60	97	4.3
20 - 80	344	15.4
30 - 100	229	10.3
40 - 100	259	11.6
60 - 120	814	36.5
ch $\geq$ 80	478	21.4
SUM	2231	100.0

Health-state	Number of pixels	Freq. [%]
Moderate damage	107	4.8
Low damage	573	25.7
Very low or no damage	1551	69.5
SUM	2231	100.0

Distance from the Cu–Zn sulphide mine [m]	
min	max
482	606

0   80   160   Meters

Source: Zbyněk Malenovský
GIRS Laboratory – WUR 2002

Forest stand No. 5

Estimation of chlorophyll content

distance from mine
700 m
800 m
900 m
1000 m

Map of health-state

700 m
800 m
900 m
1000 m
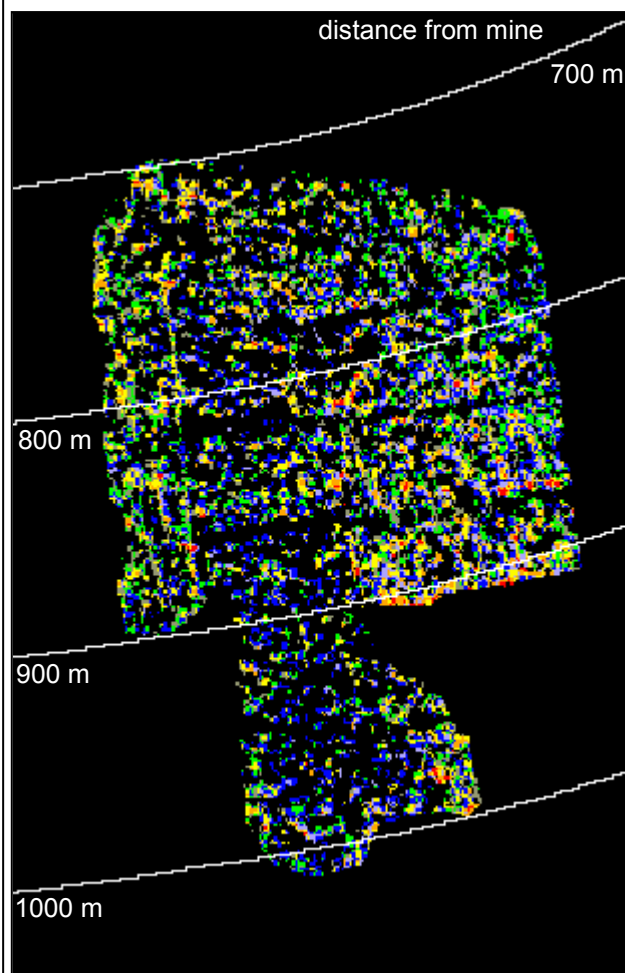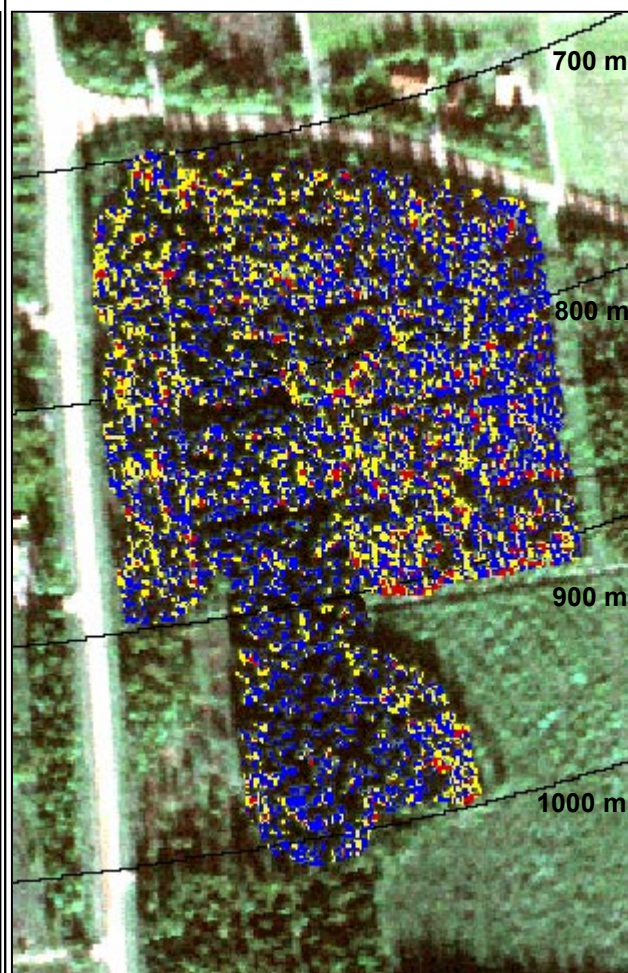
Chlorophyll content - ch - [µg.cm^{-2}]	Number of pixels	Frequency [%]
Reject	-	-
10 - 40	223	1.4
15 - 60	1107	6.9
20 - 80	3201	20.0
30 - 100	2366	14.8
40 - 100	1593	9.9
60 - 120	4785	29.9
ch $\geq$ 80	2749	17.2
SUM	16024	100.0

Health-state	Number of pixels	Freq. [%]
Moderate damage	1330	8.3
Low damage	5567	34.7
Very low or no damage	9127	57.0
SUM	16024	100.0

Distance from the Cu–Zn sulphide mine [m]

min	max
696	1010

0   100   200 Meters
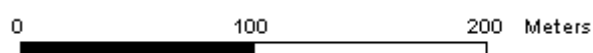
Source: Zbyněk Malenovský
GIRS Laboratory – WUR 2002

Forest stand No. 6

Estimation of chlorophyll content

distance from mine

800 m

900 m

1000 m

Map of health-state

800 m

900 m

1000 m
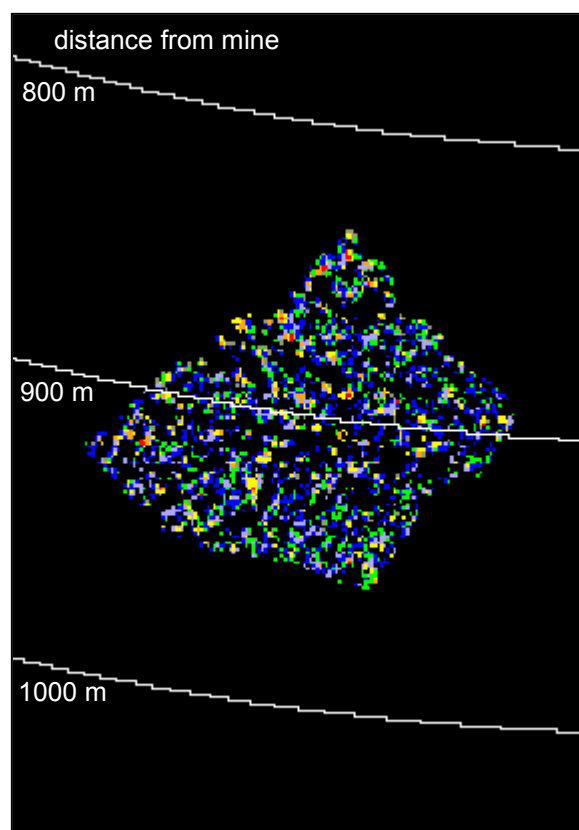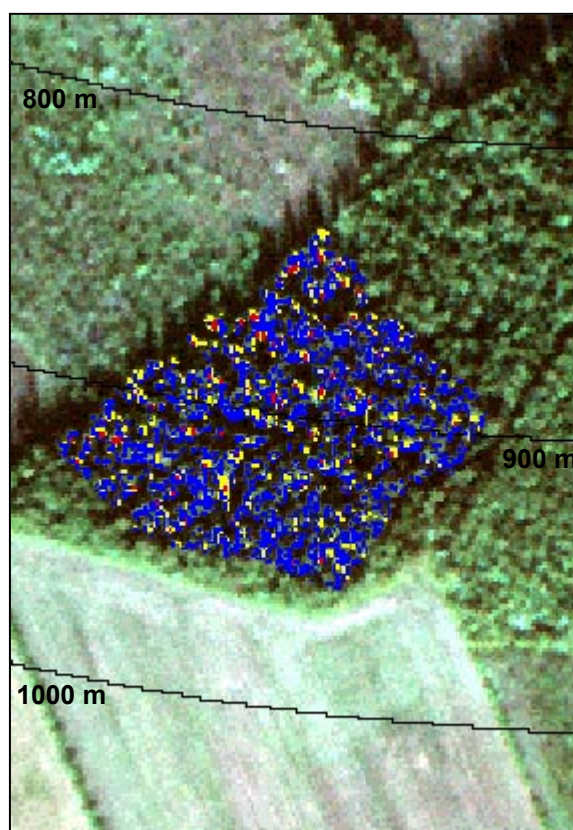
Chlorophyll content - ch - [$\mu g.cm^{-2}$]	Number of pixels	Frequency [%]
Reject	-	-
10 - 40	23	0.7
15 - 60	119	3.8
20 - 80	371	11.9
30 - 100	174	5.6
40 - 100	557	17.8
60 - 120	1233	39.4
ch $\geq$ 80	649	20.8
SUM	3126	100.0

Health-state	Number of pixels	Freq. [%]
Moderate damage	142	4.5
Low damage	545	17.4
Very low or no damage	2439	78.0
SUM	3126	100.0

Distance from the Cu–Zn sulphide mine [m]	
min	max
833	956

0   80   160   Meters
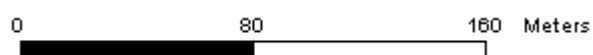
Source: Zbyněk Malenovský
GIRS Laboratory – WUR 2002

Forest stand No. 7

Estimation of chlorophyll content

1100 m

1200 m

1300 m

1400 m

distance from mine

Map of health-state

1100 m

1300 m

1400 m
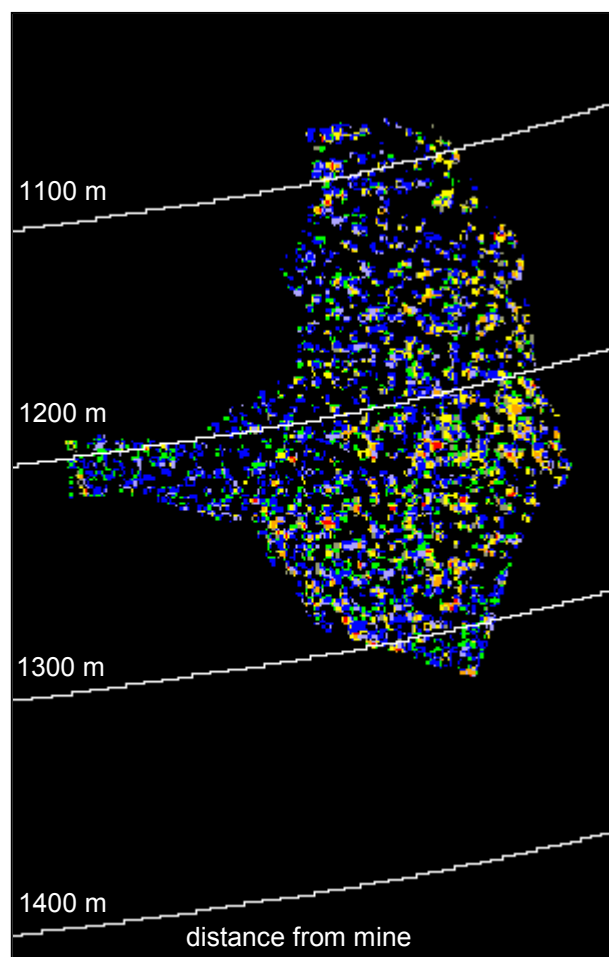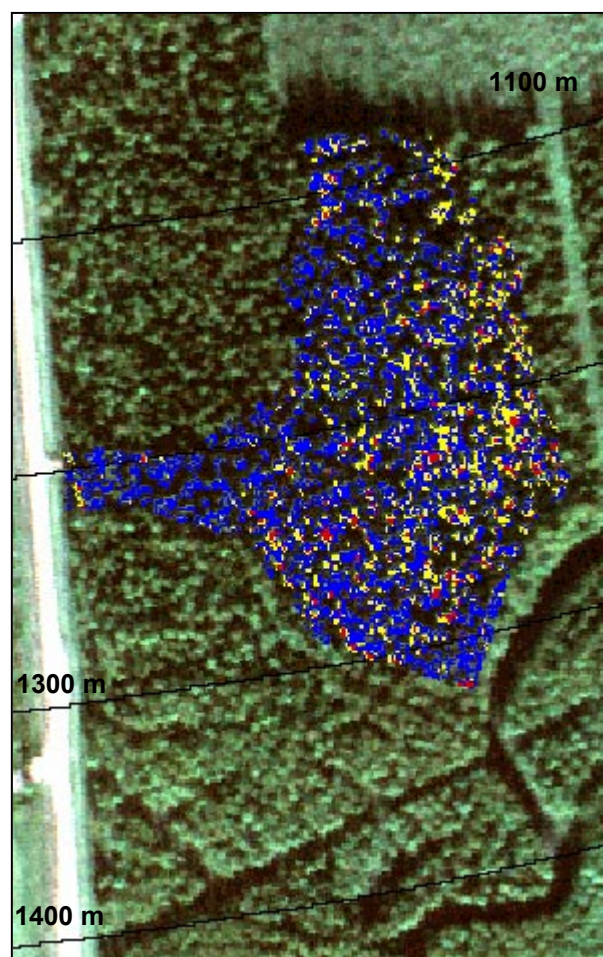
Chlorophyll content - ch - [$\mu g.cm^{-2}$]	Number of pixels	Frequency [%]
Reject	-	-
10 - 40	92	1.1
15 - 60	436	5.4
20 - 80	1277	15.8
30 - 100	612	7.6
40 - 100	982	12.2
60 - 120	3473	43.1
ch $\geq$ 80	1194	14.8
SUM	8066	100.0

Health-state	Number of pixels	Freq. [%]
Moderate damage	528	6.5
Low damage	1889	23.4
Very low or no damage	5649	70.0
SUM	8066	100.0

Distance from the Cu–Zn sulphide mine [m]	
min	max
1074	1320

0   100   200 Meters